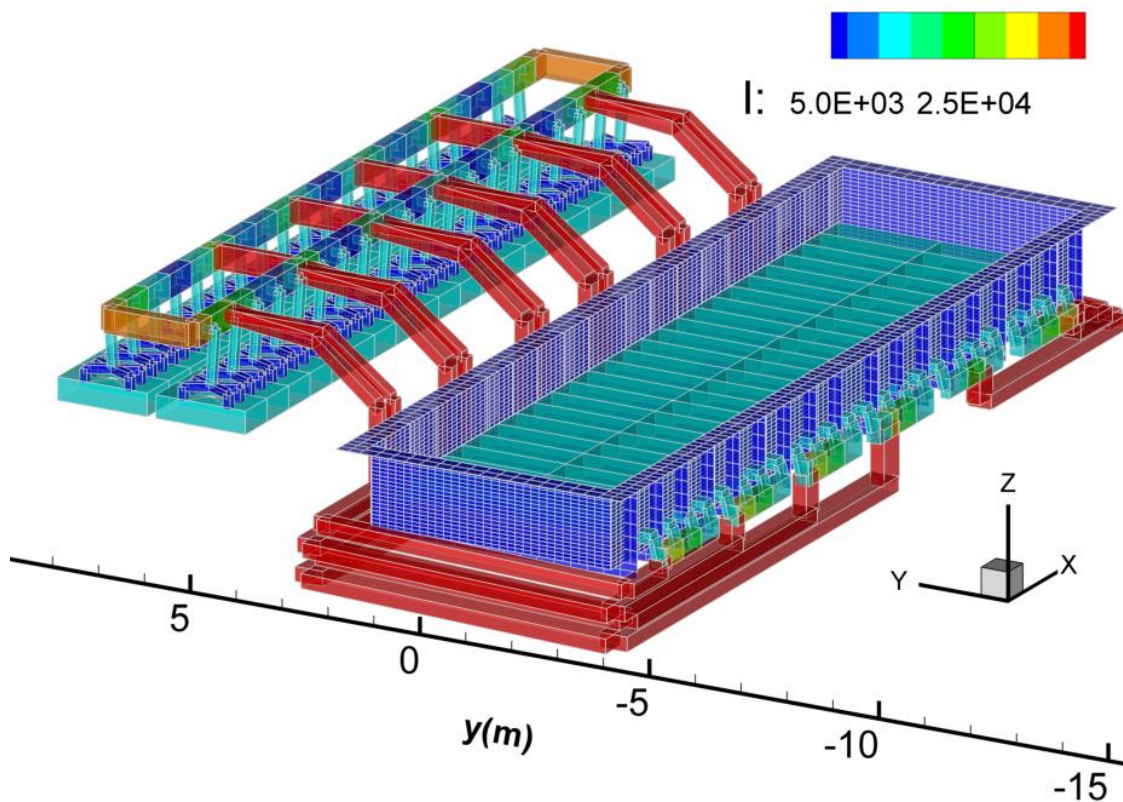


MHD-VALDIS
(Magneto-Hydro-Dynamic Versatile Aluminium
pad Displacement Instability Solver)

Reference Manual

Version 2023/07/29



© University of Greenwich

Dr. Valdis Bojarevics
University of Greenwich
London, SE10 9LS, UK
E-mail: v.bojarevics@gre.ac.uk
Phone: +44 (0)20 83318565

Purpose

- **User oriented** package to design MHD stable **aluminium reduction cells**, to retrofit older pot lines and analyze operation problems
- Allows **interactively** to construct busbar network for optimum (magnetic and thermal) electric current distribution and add steel construction elements
- The model **couples** the **electromagnetic field** distribution and the **waves** at aluminum-bath interface; both, electric and magnetic fields are recalculated continuously as the wave shape changes
- The model calculates **turbulent flows** in the two liquid layers and their effects on the non-linear waves; the flow turbulent energy distribution identifies **mixing rates** and **the ledge/lining risk** zones
- The fluid flow and wave model is **transient** and effectively **three-dimensional**, using for the metal and bath flow the 3-d derivation of the shallow-layer approximation accounting for the large electrolyte channels and the bottom profile
- The electric current distribution in the bus bars is calculated by coupling the electric current in the fluid zone to the **complete resistance network** representing individual anodes and cathode collector bars as well as the **whole bus-bar circuit** between the cells
- The Kirchhoff equations for the bus bar network are generated automatically and solved at each time step in order to simulate the effect of waves on electrical current redistribution in the whole electrical circuit
- The efficient non-linear calculation of the magnetic field from **steel** construction elements is performed continuously during the wave and flow evolution
- Possibilities to reuse the previously computed magnetic fields
- Ledge profile and bottom protrusion effects
- Anode change effects on the MHD stability
- Tool to design the cathode collector inserts

Post processing

The MHD-VALDIS runs under Windows OS Intel® 64 architecture-based systems. If older 32 bit version is required, it can be generated on request. The computed results are output in the format for post processing using the supplied layout files for the graphical presentation tool Tecplot (Tecplot 360 at the time of release); the Licensee must acquire a Tecplot license from Tecplot, Inc. <http://www.tecplot.com> independently of the MHD-VALDIS license.

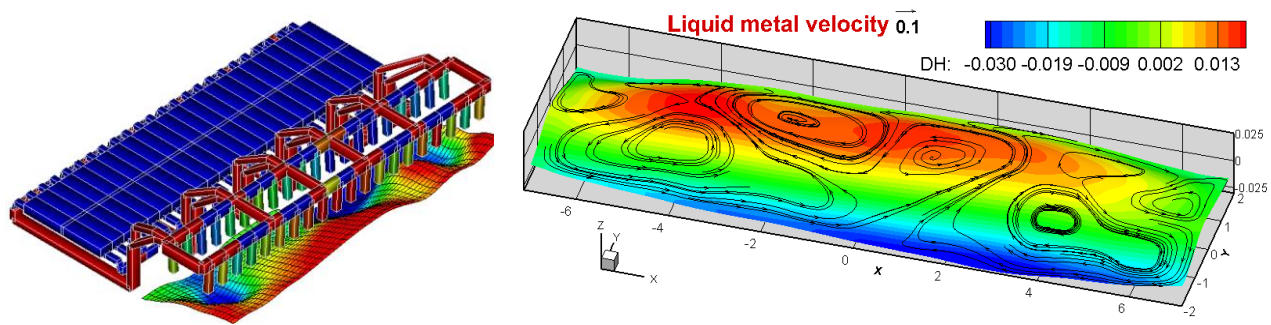


Figure 1. Demonstration of the bath-metal interface correlation to electric currents in a simplified bus bar case and the real interface affected by the turbulent velocity distribution.

GENERAL DESCRIPTION OF THE MHD MODEL

“I hear and I forget, I see and I remember, I do and I understand” (Chinese proverb)

The electric current in an aluminium electrolysis cell drives the essential electrochemical reactions and produces Joule heating to maintain the necessary thermal balance. At the same time the current generates a volume force distribution within the liquid aluminium and the electrolyte. The force distribution is rather non-uniform and therefore drives fluid flow and can easily produce waves at the interface between the liquid layers. The force results from the magnetic field, which is created by integral action of all the currents in the cell, in the complex bus-bar arrangement around the cell, in the neighbor cells and the return line, and, additionally, by the effect of cell steel parts magnetization. The control of the magnetic field is of prime importance for maintaining a desirable gentle mixing in the fluid volumes, avoiding

unstable wave growth and the wall erosion associated with the intense flow. The complexity of any practically usable Magneto-Hydro-Dynamic (MHD) model for the cell arises from the complete coupling of the various physical effects: fluid dynamics, electric current distribution (depending on the electrochemical reactions rate), magnetic field and thermal field. The MHD model presented here accounts for the first three couplings, only partly accounting for the temperatures of the busbars on the resistivity, leaving the full thermal coupling to be achieved when using in conjunction with the companion thermoelectric software from GENISIM.

The MHD model is a generalization of the previous non-linear wave models [1-9] by accounting for the turbulence model for flow in the two fluid layers [10-13]. The simulation of the cell's electromagnetic field is extended to include individual anode and cathode collector connections to the fluid layers, and also the whole bus bar circuit with the specific path of electrical connections between the bus bars between two adjacent cells [13-15]. All the necessary Kirchhoff equations [17] in the MHD-VALDIS are generated automatically and solved at each time step, which permits to simulate the wave effect on the electric current redistribution in the whole circuit including the liquid metal and bath with locally varying ACD, ledge effect, etc., as shown in the instructive demonstration in the Figure 1, where the actual anodes have been removed from the picture in order to have a clear view. The electrical network can be periodically continued to include more neighboring cells for the magnetic field computation. In addition to this, the full magnetic field is computed accounting for the effect of the ferromagnetic construction parts of the test cell as it is influenced by all the current carrying bars and liquid layers at all time moments [15, 16].

A user defined cell data input starts by filling in the specific cell material properties and general dimensions in the file 'DATA', and the bus network geometry data in a specially designed compact table in the file 'BUSNET'. The input is simplified for the user yet gives a full 3-dimensional representation of the cell and the supply busbar network. The created bus network can be visualized in a 3-d view using the widely used commercial package Tecplot (<https://www.tecplot.com>) permitting a publication and presentation quality printouts and animated views (for instance rotating and/or zooming in the details).

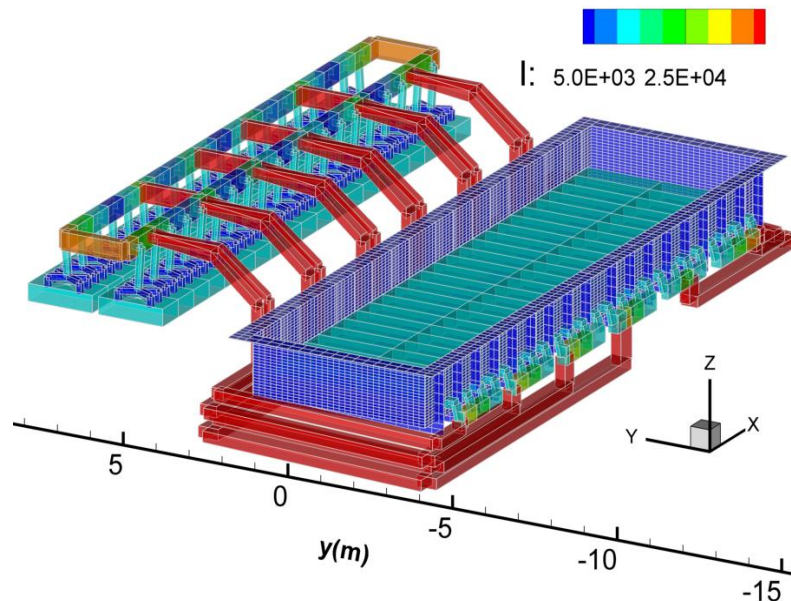


Figure 2. Asymmetric bus-bar network and the steel shell used for the 500 kA MHD model. The current I (A) distribution in the network is shown by the color identified in the top floating legend.

The user has complete freedom to experiment and optimize the network by adding connections, changing bus locations and their cross-sections. As an example the bus arrangement for the demonstration 500 kA cell and the steel shell are shown in Figure 2. The on-screen view can be arbitrary rotated, shifted and zoomed to inspect the details, as the Figure 3 showing a bottom view for the cell. The currents, their time dependent deviations from a stationary state and the temperature of the bars can be shown in color flooded levels at different time moments.

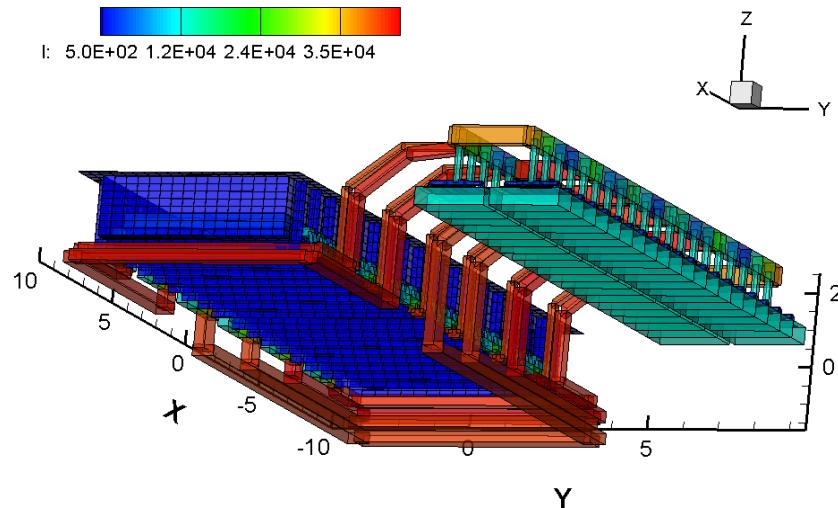


Figure 3. The 500 kA bus network view from the cell bottom.

The asymmetric bus arrangement for this cell partly compensates the return line on the left (see Figure 12). All the electrically independent cathode collectors are connected in 12 sections taking current from 4 collector bars each, and then the upstream and downstream counterparts are connected at 6 risers to the anode ring. The almost ideal 50 – 50 per cent upstream and downstream current division is achieved by the adjusted cross-sections for the individual sections (see file 'BUSNET'). The fine adjustment of the collector currents can be achieved by prescribing individual cross-sections to each collector flex connection.

The electric current distribution in the fluid layers is shown in Figure 4, as computed for the bath-metal interface at each time moment, usually starting the first time step with the initial flat interface (for reference). At the second time step the initial interface is adjusted to the assumed stationary interface shape for the currents and magnetic field as computed at the first time step (flat interface). Then the dynamic process is initiated for the interface wave development recomputing the actual electromagnetic field distribution at each time step.

The cathode collector currents are not exactly equal because of the bus connections, unequal lengths and cross-sections for the respective connecting bus elements. The horizontal current in liquid metal arises even in the case of the flat aluminium surface because of the anode and collector bar geometrical differences and the tendency for the cathode current to find the path of the least resistivity (with the effect of ledge and contact resistance).

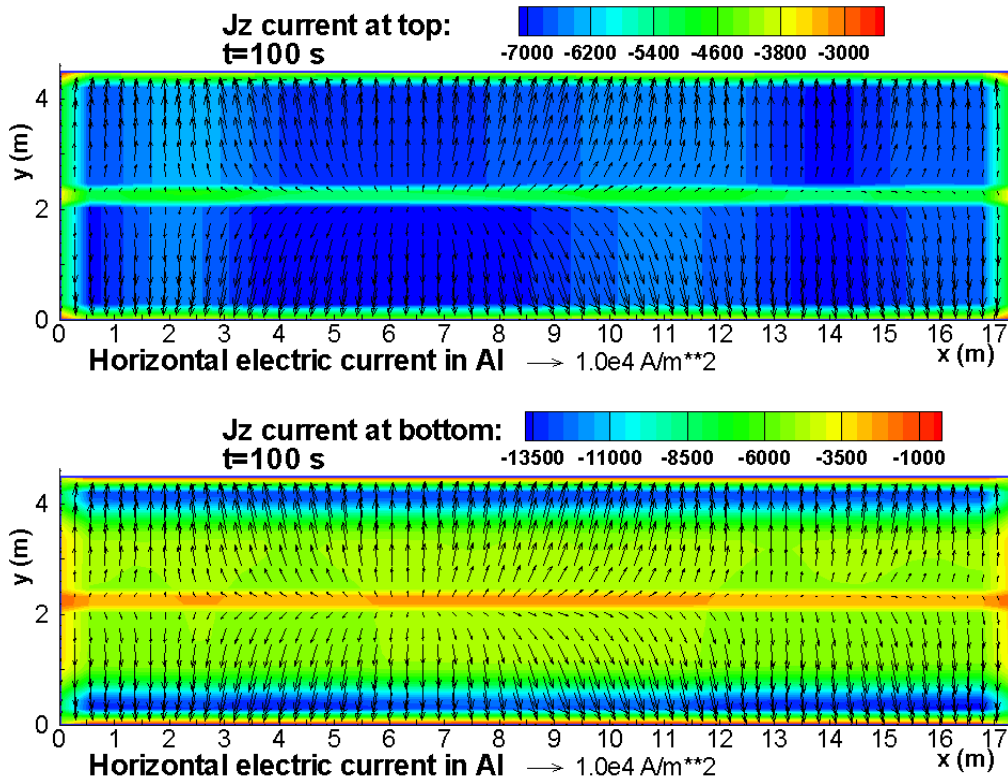


Figure 4. The electric current distribution in the 500 kA cell including the effects of the whole connecting bus network. Top – color flood contours show the dominant vertical current $J_z = J_E$ in the electrolyte entering the liquid metal, arrows – the depth averaged horizontal current in the liquid aluminium, bottom – the vertical current $J_z = J_B$ leaving to the carbon cathode at the bottom of the cell.

MATHEMATICAL MODELS USED IN MHD-VALDIS

Introduction

Historically one of the first modeling attempts for the aluminum electrolysis cells were devoted to the current supplying bus bar system, how to organize it, and what cross-sections to assign to the different bars in the rather complex network [17]. The purpose was to distribute current as evenly as possible over the cell and to avoid excessive heating of individual bars. The task seemed relatively simple since the ordinary linear Kirchhoff equations are readily applicable for this purpose. However, with the growing amperage and the size of the cells, the typical networks were growing in complexity and in the number of elements. Thus computer programs were growing in complexity, yet the worst was that the data input difficulties for the large networks were taking many days and weeks of strenuous labor.

In addition to the thermo-electric optimization, the bus network design for high amperage reduction cells must be optimized for the magnetic field to be reduced and made of a special distribution ensuring for a stable melt interface, and to avoid vigorous velocities within the liquid melt. This means that the very

similar data inputs both for the magnetohydrodynamic simulations and for the thermo-electric current modeling in the bus network are in fact used. Moreover, a deeper physical and engineering insight in this problem suggests that these problems are mutually interconnected and should be solved interactively. This means that a realistic computer program must use the same data input and eventually compute from this the electric current, voltages, temperatures in the bus network, and the magnetic field. Finally, the program needs to iterate back to account for the variation of the local interpolar distance to couple the current distribution in the liquid media to the supplying bus network. The time dependent results affect the magnetic field distribution, the hydrodynamic velocities and the wave development. The neighbor cells are affected as well, because of the interconnection to the test cell varying properties.

Electric current distribution modelling in the bus bar network

As the first task in this multiphysics coupled computer simulation we attempted to unify the data input for the network electric current modelling and the magnetohydrodynamic programs. The MHD package generates the very large set of Kirchhoff equations automatically from the relatively simple unified data input. When the temperatures of the electrically heated bars are computed, the resistivity changes are updated accordingly. The unified input gives a flexibility to simulate, for instance, the anode changes, disconnected cathode bars, various branching of the current path between the cells, compensating bus lines, etc.

During the development of the program the previous experience in the electric current simulation programming was taken into account: NEWBUS from Hydro Aluminum [17], reports from Reynolds Metals Company, and Russian program TOK from the VAMI institute.

Current distribution in a bus bar network can be described to a good approximation accuracy by linear resistance elements. The electric currents and voltages in such a circuit are governed by the Kirchhoff laws. The two Kirchhoff laws are:

- 1) the **voltage law**: The algebraic sum of the potential differences taken around a loop (or 'mesh') of a circuit is zero;
- 2) the **current law**: The algebraic sum of the currents into a node of a circuit is zero.

If these laws are directly applied, they contain unknown potential differences for each resistance and unknown currents for each mesh of a given circuit. There are two methods to reduce the number of independent unknowns and the equations respectively. These are based on combining the two laws and are referred to as either mesh analysis or nodal analysis.

The mesh analysis is based on currents as unknowns. A set of mesh currents I_n are chosen to traverse all complete loops of the circuit. Since each mesh current flows right through any junction (node) in its path, the current law is automatically satisfied. Then it is left to apply the voltage law for each of the meshes by replacing the potential differences with the algebraic sums of currents through the particular resistance multiplied by the resistance (Ohms law). For the reduction cell situation this procedure was used in the previously referenced programs and involves a tedious job of locating all possible meshes of the circuit, what is difficult to make automatic. Therefore this approach involves an intelligent input from the program user and results in long labor days with a possibility of potential errors. Principal changes in the circuit, such as anode or cathode element disconnection or new branching, require significant reconsideration of the equation set.

For the automatic circuit analysis purpose the nodal analysis is found to be more convenient. According to this method the potentials at the nodes are the independent unknowns. The use of node potentials rather than mesh currents makes for greater efficiency in the analysis of circuits that are predominantly parallel in character, since the number of simultaneous equations that have to be solved is significantly

smaller. The following equation set arises for M nodes each of which have N directly connected neighbor resistances:

$$\sum_{n=1}^N \frac{U_m - U_n + E_n}{R_n} = I_m; \quad m = 1, 2, \dots, M, \quad (1a)$$

$$\text{or} \quad U_m \sum_{n=1}^N \frac{1}{R_n} - \sum_{n=1}^N \frac{U_n}{R_n} = I_m, \quad (1b)$$

where U_m is potential at the m -th node, U_n - for nodes at other ends of neighbor bars, R_n - resistances of neighbor bars, I_m - external current entering the node, and E_n - optional irreversible part of the electrochemical potential drop (see file 'DATA' for the user options). The constraint needs to be imposed that the total current ' I ' enters the reference nodes in the liquid metal of previous cell and ' $-I$ ' current leaves the nodes at the liquid metal of the downstream cell. For all other nodes the external current - right side of the equation - is zero.

This is just another statement of the current law, and the voltage law is satisfied because the sum of the potential differences, with U_m expressed from (1), over the closed mesh is identically zero. Formally this law can be applied even for two resistances connected in series, and this property is essential in order to generate automatically the set of equations to solve.

After finding the potentials at nodes, the potential difference between two neighbor nodes multiplied by the connecting resistance gives the current in each resistance. The main task of the present program is to find the current distribution in the bar network, yet a further improvement in accuracy can be achieved when accounting for the temperature change due to the Joule heating of the resistance elements: $R_m I_m^2$.

Knowing the Joule heating, it is possible to estimate the temperature of a bar. For this purpose we integrate the heat conduction equation over an individual bar volume, which yields:

$$k \cdot \frac{\partial T}{\partial n} \Big|_s \cdot S = -RI^2, \quad (2)$$

where T is the temperature, k is the thermal conductivity, $\frac{\partial T}{\partial n} \Big|_s$ - the temperature gradient at the surface

S . The equation (2) is replaced by a discretised approximation over the bar, giving the equation set for discretized variables:

$$\sum_n \frac{k_m \cdot (T_m - T_n) \cdot S_m}{L_m} + h_m \cdot S_m \cdot (T_m - T_{air}) = R_m I_m^2 \quad (3)$$

where k_m is the thermal conductivity of the m -th bar, summation is over n neighbor bars, S_m is the cross section area, L_m - length, and h_m is the global (convective and radiative) heat transfer coefficient for the bus bar external surface to the surrounding environment. According to [13] the heat transfer coefficient can be approximated as

$$h_m = h_0(1 + \alpha T_m), \quad h_0 = 4 \cdot \left(\frac{W}{K \cdot m^2} \right), \quad \alpha = 0.0096 \left(\frac{1}{K} \right),$$

which gives good comparisons with the ANSYS 3-d simulations. Optionally, the values for these constants can be supplied by the user in the file 'DATA'.

When the temperatures for all bars of the total number M are calculated, the electrical resistances $R_m(T)$ can be updated taking into account the linear temperature dependence for the resistivity ρ_T :

$$\rho_T = \rho_0 \cdot (1 + \alpha_R T), \quad (4)$$

where α_R is the linear temperature coefficient, ρ_0 – the resistivity at 0 deg C. The new resistances are calculated, and the full electric circuit equation set (1) solved again to iterate the whole procedure while the convergence is achieved. The convergence is easily established for bars with reasonable cross sections and sufficiently effective heat transfer to the ambient air and to the neighbor bars. For the sake of completeness we incorporate in the program also the heating at the ends of first and last bars connected to the anodes and the cathode carbon, respectively, by assigning the user defined temperatures at these ends.

Electric current distribution in the fluid layers

The previous section described the first calculation step needed for the MHD model by obtaining the electric current distribution in the bus bars representing the element division of the whole bus-bar circuit between two adjacent cells with the addition of the individual anodes and cathode collector bars. This step is coupled to the electric current in the continuum fluid zones. The electric current in the fluid zones must be computed from the continuous media equations governing the DC current (which can change in time with the waves and the optional anode burnout process):

$$\mathbf{j} = -\sigma \nabla \varphi + \sigma \mathbf{v} \times \mathbf{B}, \quad (5)$$

where the flow and magnetic field interaction induced currents in the highly conducting liquid metal are accounted for. The electric potential in the fluid is governed by the equation resulting from the continuity condition for the electric current, $\text{div } \mathbf{j} = 0$:

$$\nabla^2 \varphi = \nabla \cdot (\mathbf{v} \times \mathbf{B}). \quad (6)$$

The boundary conditions are the zero normal current at the insulating walls, given current distribution j_a at the anodes, j_c at cathode carbon. $j_a(x,y,t)$ and $j_c(x,y,t)$ are supplied from the finite element resistivity network solution of (1), which in turn is coupled to the computed potential distribution from (6). At the interface between the liquid metal and the electrolyte the continuity of the potential and the electric current normal component must be satisfied.

Since the depths of the liquid layers are extremely small if compared to their horizontal extension, the shallow layer approximation is very efficient to solve this 3-dimensional problem. It can be shown, see the detailed derivation in [1-4, 19] that the solution can be obtained from the following equation for the liquid layer:

$$j_{za}(x, y, t) - j_{zc}(x, y, t) = \sigma_{Al} \partial_k ((H_{Al}(x, y, t) - H_c(x, y)) \partial_k \varphi), \quad (7)$$

where $j_{za}(x, y, t)$ is the given vertical current density distribution at the bottom of anodes from the finite element resistivity network solution, $j_{zc}(x, y, t)$ - at the top of the cathode carbon. The aluminium-bath surface $z = H_{Al}(x, y, t)$ is recalculated at each time step from the hydrodynamic problem, and the bottom

of the cell profile $z = H_c(x,y)$ corresponds to the individual cell. The bottom profile $H_c(x,y)$ can be prescribed by the user in the file 'BOTTOM', permitting to input concave or convex shapes, or/and carbon 'ridges' of specialised cathodes (Figure 5). The electric current calculation can be updated to include the variable carbon bottom depth at the cell bottom above the cathode collectors.

The equation (7) is solved numerically by the fast spectral solver, using the Fourier decomposition and inversion. This permits efficiently to update the full electric current distribution for the cell and the network at thousands of time steps typically used when solving the full MHD stability problem.

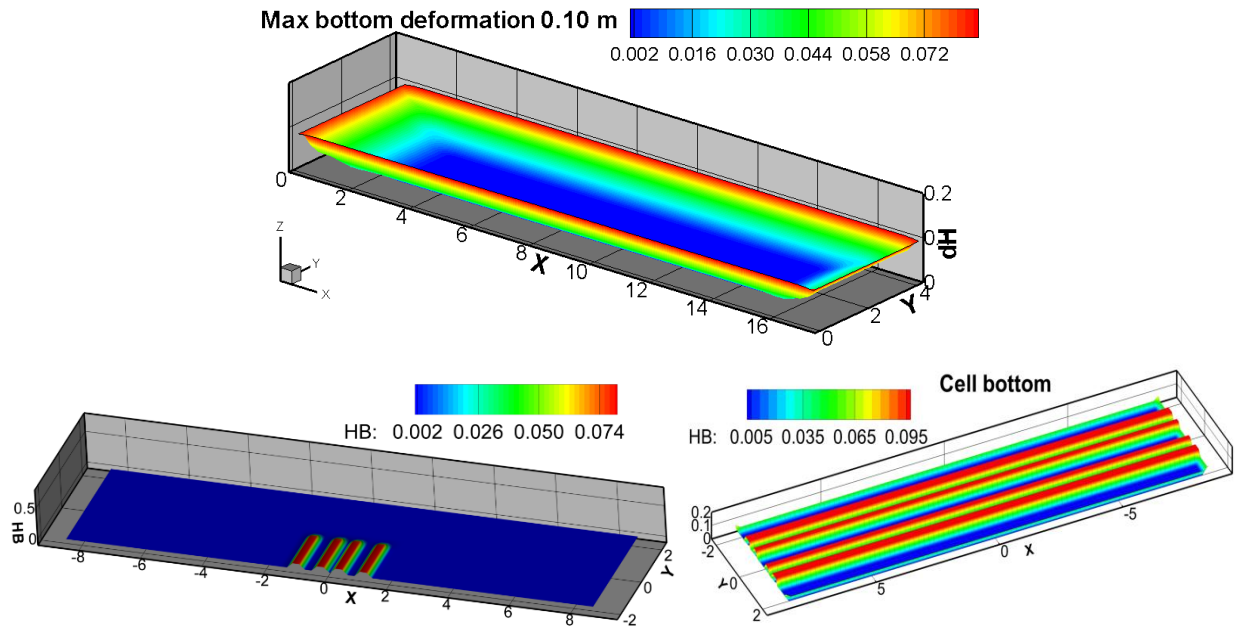


Figure 5. Examples of the bottom profiles to model cathode shape and 'ridges' in the 500 kA cell.

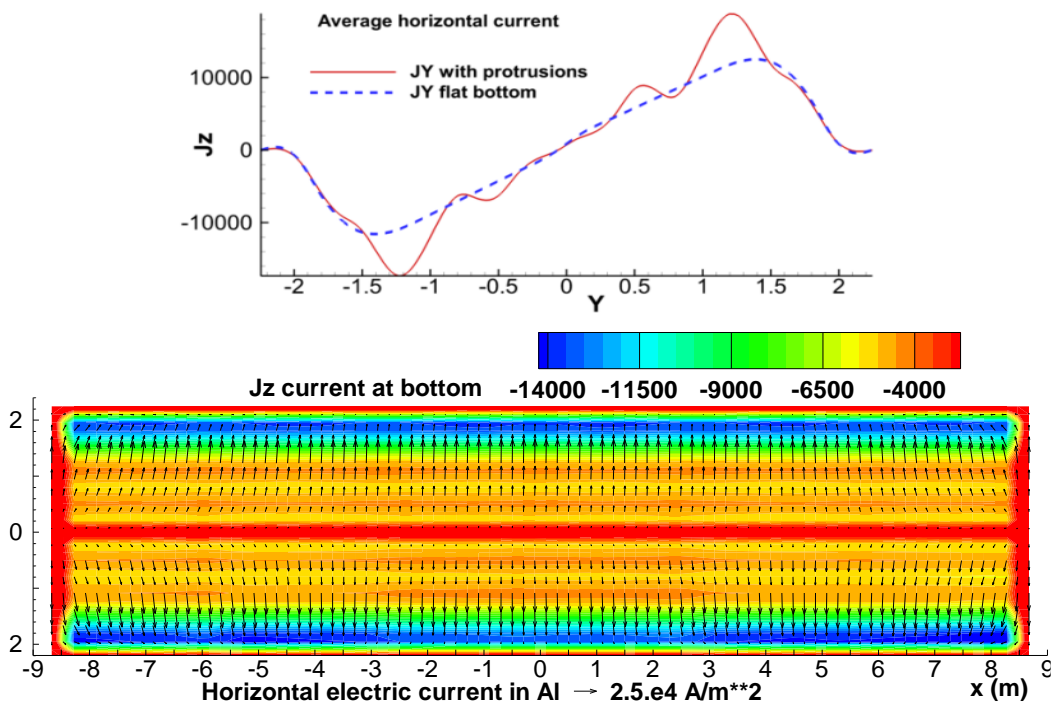


Figure 5a. The bottom profile effect on the horizontal current modification in the aluminium layer.

The electrical conductivity is assumed constant, but the effective resistivity of the discretized carbon layer is made proportional to the respective height of the element. The Figure 5a illustrates this effect for the 500 kA cell test case when the bottom profile is modified by adding two symmetric ridges at upstream and downstream sides of the cell.

In recent years a lot of innovative ideas around the cathode assembly of Al electrolytic cells have been published. For investigation of these ideas by using MHD-Valdis, a more general set-up of the cathode assembly is provided as extension of the software.

Two options are available: either 1) use of externally supplied current distribution over the cathode bottom, or 2) compute general current path from the cathode carbon via arbitrary connected collector bars to the overall electrical network.

Option 1.

Allows to specify the vertical current distribution on top of the carbon cathode block (e. g. derived from a FE-modelling of a cathode assembly) as an alternative to the internally calculated one. This profile can be a user specification given in the special input file Jcat_in.dat (where an arbitrary mesh division can be used of a similar structure as the automatically generated file Jcat_out.dat (provided as an example). The file structure is illustrated in the example below:

```

      88          32 ! 'Nx Ny'    ! number of x-nodes, y-nodes
-0.86700E+01 -0.22450E+01 0.00000E+00
-0.84707E+01 -0.22450E+01 0.00000E+00
-0.82714E+01 -0.22450E+01 0.00000E+00
-0.80721E+01 -0.22450E+01 0.00000E+00
-0.78728E+01 -0.22450E+01 0.00000E+00
-0.76734E+01 -0.22450E+01 0.00000E+00
-0.74741E+01 -0.22450E+01 0.00000E+00
-0.72748E+01 -0.22450E+01 0.00000E+00
-0.70755E+01 -0.22450E+01 0.00000E+00
-0.68762E+01 -0.22450E+01 0.00000E+00
.....
-0.84707E+01 -0.21002E+01 -0.30958E+04
-0.82714E+01 -0.21002E+01 -0.61915E+04
-0.80721E+01 -0.21002E+01 -0.61907E+04
-0.78728E+01 -0.21002E+01 -0.61814E+04
-0.76734E+01 -0.21002E+01 -0.61602E+04
-0.74741E+01 -0.21002E+01 -0.61356E+04
-0.72748E+01 -0.21002E+01 -0.61162E+04
-0.70755E+01 -0.21002E+01 -0.61021E+04
-0.68762E+01 -0.21002E+01 -0.60883E+04
.....
X coordinate      Y coordinate      J density in arbitrary relative units (or A/m2)

```

This input permits to impose whatever Jz distribution needed (in relative units) and then rescaled to satisfy the total current conservation. The Jz distribution is interpolated to the computational mesh and used as the boundary condition in the electric current model calculation within the liquid layers.

If the ledge position is given, this will have priority to mask the portion of the Jz distribution on the bottom of the cell to restrict the current outflow.

The magnetic field calculation will account for the new current distribution in the liquid zone, but will continue to use the bar current from the total busbar arrangement. The busbar settings can be rearranged

to match closely the supposed current path. For this purpose the 'option N2' can be supplemented or used independently as described in the following.

Option 2.

Allows for a more general current path from the cathode carbon via collector bars to the busbars. As in the previous model for the cathode, the linear elements (resistors) are used. This means a unidirectional vertical current path in the carbon, connected via the contact resistances to the horizontal steel collector elements. The carbon elements are strictly above the steel elements. The cross section sizes can be different for the carbon and the steel connected elements.

The mesh division of the collectors under the cell corresponds to the internal liquid mesh size in the y direction (as used in the liquid metal). The mesh compatibility permits maximum sensitivity to the vertical current distribution in dependence of the cathode properties for a given liquid volume discretization.

The option for the electrical connection between the upstream and downstream collectors in the middle of the cell is available by setting ' 0.0' for the collector bar start position in the input file BUSNET. The following example shows unconnected collector setup:

```
0.2          !collector bar starts at (|Y|>=0, m) from cell central axis (0.- connected)
```

In the longitudinal x direction the mesh is adjusted to the actual number of the collector bars. There is one element per collector x-width and an additional refinement at the boundaries. If the double collector cathode blocks are used, the mesh is refined accordingly and becomes non-uniform to accommodate the jump in the collector spacing. The double collector option is activated giving a nonzero value to the parameter in the respective line in BUSNET file:

```
0.0          !distance between double collector bar axes in a cathode block
```

Comparing the new cathode discretization and the old style cathode, the electric current distribution is not qualitatively different, yet the current distribution for the new cathode model is 'smoother' due to more accurate representation of the transition approaching the cell edge.

The overall view of the cell bottom gives some visual impression of the differences in the cathode models (Figure 5aa).

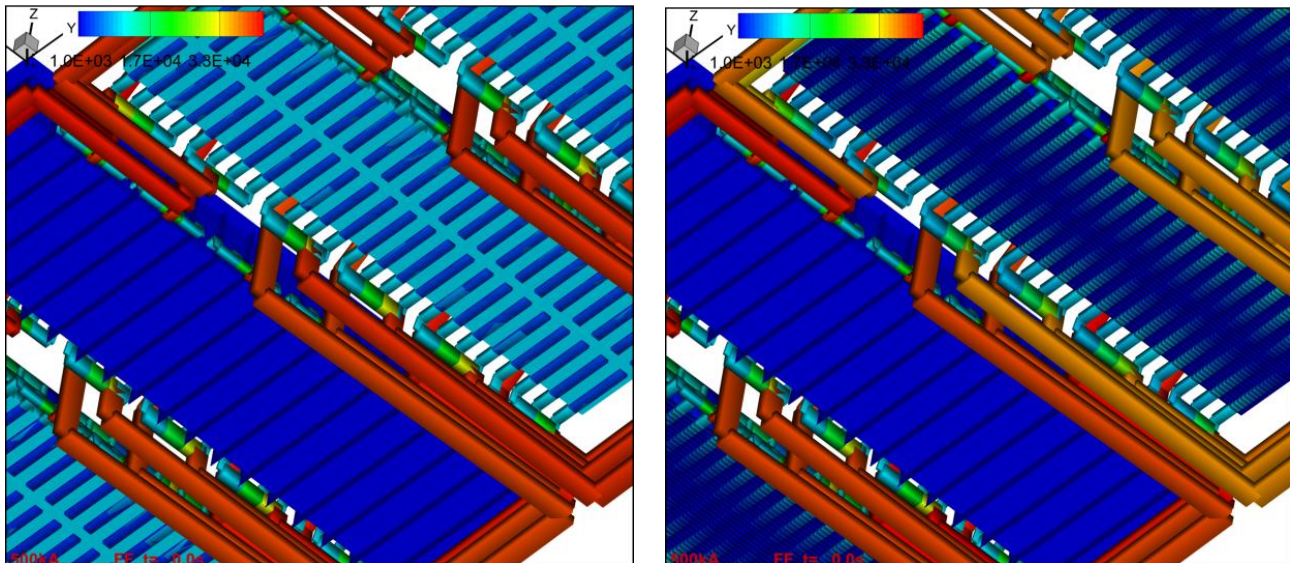


Figure 5aa (left). Option 1 version: view to the cell bottom. (Steel elements are obscuring the view to the test cell, leaving the neighbour cells free to view).

Figure 5aa (right). Option 2 version view to the cell bottom.

In the new Option 2 version each of the mesh nodes of the steel collectors can be used as an optional electrical connection to achieve the electric current withdrawal at desired locations at the cell bottom. The new connection can be arranged for each collector individually, even for the double collector blocks. A connection different to the normal flex connection (at the end of the collector bar) can be achieved if starting the section path at a position below the cell geometrical width. The new electrical connection will be created in the case if the section has the same bar number as the section start and the end numbers (one collector per section). For instance, the following line in the **BUSNET** will create the connection under the cell as shown in the Figure 5aaa:

```
|----X---|----Y---|----Z---||=====|-----|=====|-----|=====|Thc1|Thc2|
|-5.95 ! -0.01 ! -.85 !| Section| 28 !...to...| 28 ! bars | .3 ! .2 !
```

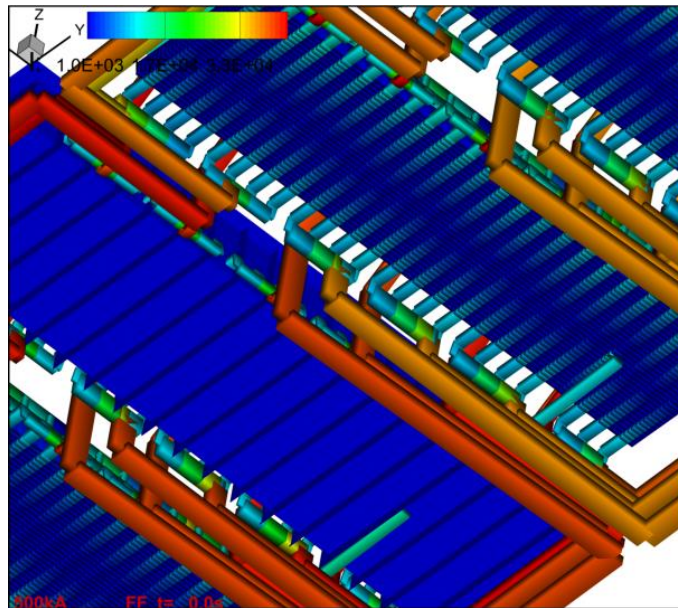


Figure 5aaa. Option 2 software version view to the cell bottom when the collector N 28 is connected at the middle position of the cell.

However the previous version of this line will retain the normal (end flex) connection (Figure 5aa):

```
| -5.95 ! -3.0 ! -.85 !| Section| 28 !...to...| 28 ! bars | .3 ! .2 !
```

The cathode path sections permit to compose new electrical arrangements in a similar or more complex patterns as prescribed in the file BUSNET. The connection nodes to the collectors are defined by the starting point of the specific section of the busbar path. In principle, the nodes can be connected in between collectors using the 'additional bars' option (at the end of BUSNET) to compose the full Kirchhoff equation set to be solved automatically and to ensure all conservation laws are satisfied.

This new cathode arrangement permits to preserve the existing structure of the overall solution. If the ledge position is prescribed, this has the priority, and results in masking the portion of the bottom of the cell to restrict the current outflow (the non-conducting film concept). The variable carbon height in the cathode is affecting the respective element resistance to change the associated vertical current J_z and the horizontal current distribution. The old cathode model is naturally overtaken by the new program structure, however preserving full compatibility of the results as shown in the Figures 1 and 3 for the normal flex connections.

The connection under the cell leads to the modification of the bus connection and the current distribution. The corresponding magnetic fields are recomputed as previously, leading to modified force distribution, velocities and the interface wave evolution.

Possibility for 1, 2, 3 and/or 4 anode changes

The following new style input file MENU should be used to invoke the options to test anode change effects on the MHD stability. Up to 4 arbitrary anode changes can be tested if choosing the input numbers for the test anodes different to 0.

```
IN| MENU: EXPLANATIONS and COMMENTS
==|=====
1 |Anode base burnout (2nd time step & continuous):Integer 1 means "yes", 0 - "no"
20|Create data for TECPLOT files with N*dt frequency .GE.1 (0 - no)
0 |0=Input from BUSNET only; 1=Input from BARSIN
0 | 'N' of anode to change at NTIME=3, 0 - no
1 |Recompute magnetic field at all time steps:Integer 1 means "yes", 0 - "no"
0 | 'N' of 2nd anode to change at NTIME=3, 0 - no
0 | 'N' of 3rd anode to change at NTIME=3, 0 - no
0 | 'N' of 4th anode to change at NTIME=3, 0 - no
0 |0=keep velocity fixed after initial 20s; 1=full nonlinear dynamics
==|=====
```

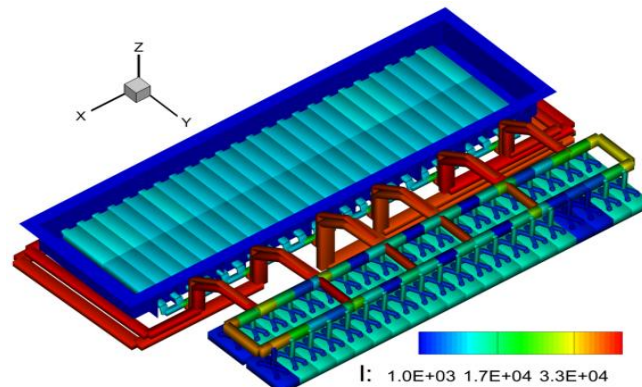


Figure 5b. The four anode change (Ns 3, 4, 20, 40) effect on the busbar current distribution.

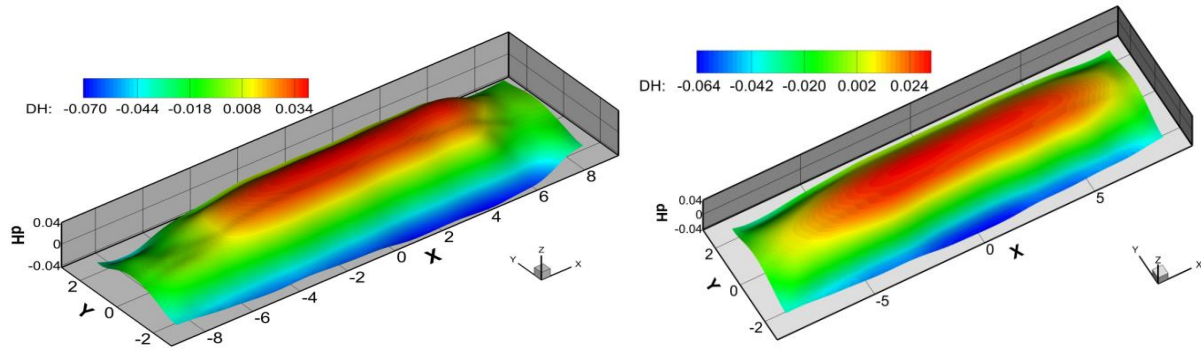


Figure5c. The four anode change (Ns 3, 4, 20, 40) effect on the interface (left) as compared to the normal reference case (right).

The use of optional input file CBARCONTR

The file CBARCONTR (or CBARCONTR.txt, or CBARCONTR.dat) gives an option to prescribe the contact resistance (at carbon/steel interface) distribution along the cathode collector bar in the y-direction. In addition, the file could be used to prescribe the temperature distribution along the steel collector bar. In the absence of the file, the generic inputs from the file DATA are used to define the total value of the collector contact resistance and the average temperature of the collector embedded in the cell (INBARS). An example of the file CBARCONTR is given below:

```

N<15|ContRes,Om| Ycoord,m | Tco1,Cdeg| Comments
-----
0|0.0 | 1.8750 | 930. | - carbon block end at |Y|>=0, <='half cell cavity width,m'
1|0.00002 | 0.060484 | 930. | - local contact resistance between carbon block/collector
2|0.00002 | 0.18145 | 930. | starting at (Y=0) from cell central axis
3|0.00002 | 0.30242 | 930. | - T deg C of steel collector bar
4|0.00002 | 0.42339 | 930. |
5|0.00002 | 0.54435 | 930. |
6|0.00002 | 0.66532 | 930. |
7|0.00022 | 0.78629 | 930. |
8|0.00022 | 0.90726 | 930. |
9|0.00022 | 1.0282 | 930. |
10|0.00022 | 1.1492 | 930. |
11|0.00022 | 1.2702 | 930. |
12|0.00022 | 1.3911 | 930. |
13|0.00022 | 1.5121 | 930. |
14|0.00022 | 1.6331 | 930. |
15|0.00022 | 1.7540 | 930. |
| finish reading with N=0 or an empty line

```

The ASCII file CBARCONTR formatting is fixed. The first two lines are not read in the input and serve to format file and give some information about the inputs. The following 3rd line defines the end position of the cathode carbon block (electrically conducting part).

The contact resistance (in Om) distribution along the defined elements in the steel collector bar is prescribed in the following lines. The input is limited by 15 node positions (or less) along the collector length (Y-coordinate) which can be at arbitrary Y starting always at the position closest to the cell axis Y=0 and ending at location close to the collector end at cell wall. The first column is an order number of the input, the second column prescribes the local contact resistance between the collector and carbon in Om units. The third column gives the Y-coordinate in growing order from the cell axis.

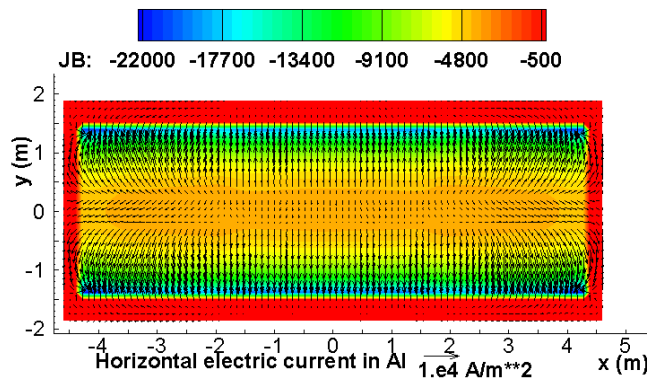
The fourth column permits to input the temperature distribution along the steel collector bar. If this input is not known, the fixed temperature can be prescribed for all lines (the same as given in the file DATA). The temperature will be used to compute the electrical resistivity of the collector steel.

The input reading will be stopped if an empty line is encountered, or N=0 is read, or the total number of N > 15.

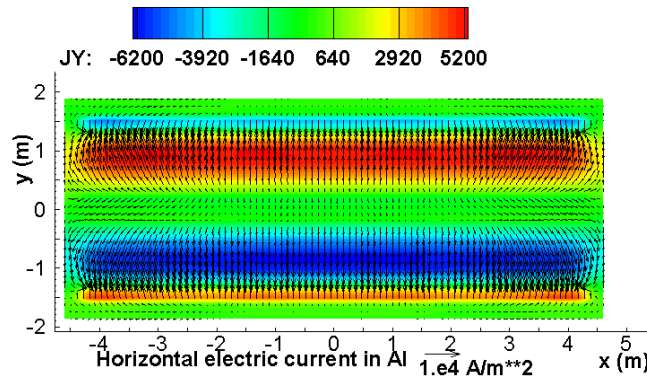
The program will perform interpolation of the input data to the computational mesh. In the present implementation the mesh size is 32 nodes along the full cell width, which means that there will be 15 mesh elements for each collector in Y direction.

Examples of the input CBARCONTR results

- 1) If the file CBARCONTR is absent (reference case), the inputs from DATA are used. The electric current distribution in the liquid metal is obtained:
Jz at bottom of cell (JB) and the horizontal current shown by arrows:



Jy in liquid metal and the horizontal current shown by arrows:



- 2) If the file CBARCONTR prescribes the contact resistances along the collector with low values in the central part of the cell and higher values at wall region. This could lead to reduced horizontal current density and a better MHD stability of the cell:

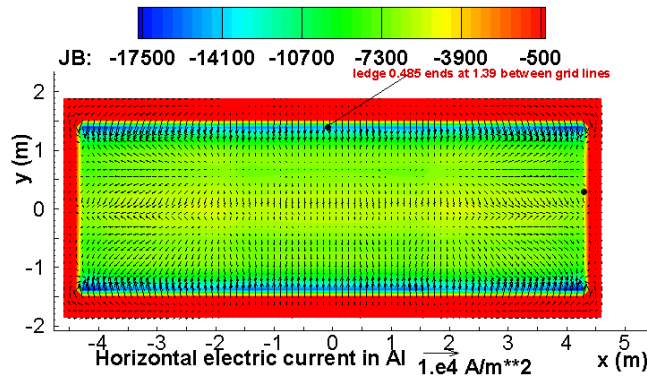
N<15	ContRes,0m	Ycoord,m	Tcol,Cdeg	Comments
0	0.0	1.8750	930.	- carbon block end at Y >=0, <= 'half cell cavity width,m
1	0.00002	0.060484	930.	- local contact resistance between carbon block/collector
2	0.00002	0.18145	930.	starting at (Y=0) from cell central axis
3	0.00002	0.30242	930.	- T deg C of steel collector bar
4	0.00002	0.42339	930.	

5	0.00002	0.54435	930.
6	0.00002	0.66532	930.
7	0.00022	0.78629	930.
8	0.00022	0.90726	930.
9	0.00022	1.0282	930.
10	0.00022	1.1492	930.
11	0.00022	1.2702	930.
12	0.00022	1.3911	930.
13	0.00022	1.5121	930.
14	0.00022	1.6331	930.
15	0.00022	1.7540	930.

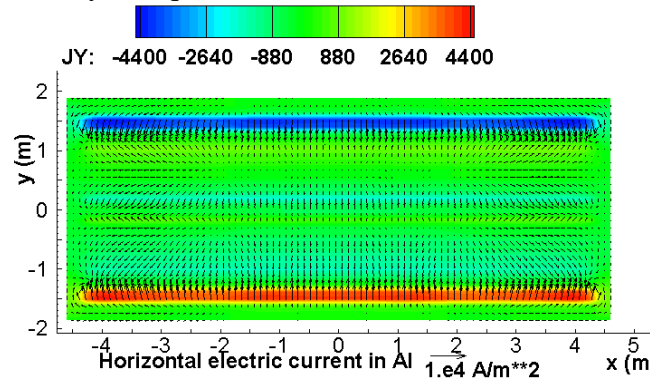
finish reading with N=0 or an empty line

The electric current distribution in the liquid metal is obtained:

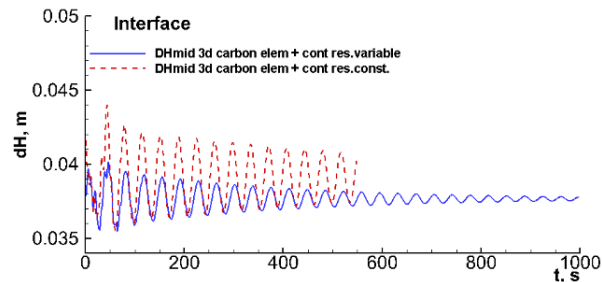
Lower J_z at bottom of cell (JB) and the reduced horizontal current shown by arrows:



The reduced horizontal current J_y in liquid metal



The MHD stability of the cell is significantly improved as shown by the long run of the program (the blue lines correspond to the prescribed new contact resistance distribution):

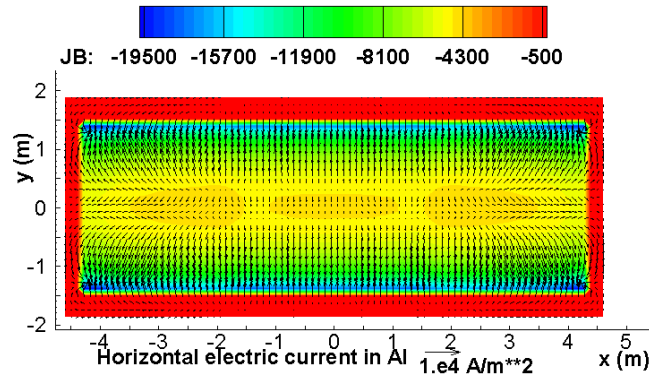


3) If the file CBARCONTR prescribes only the temperature variation along the steel collector bar as shown:

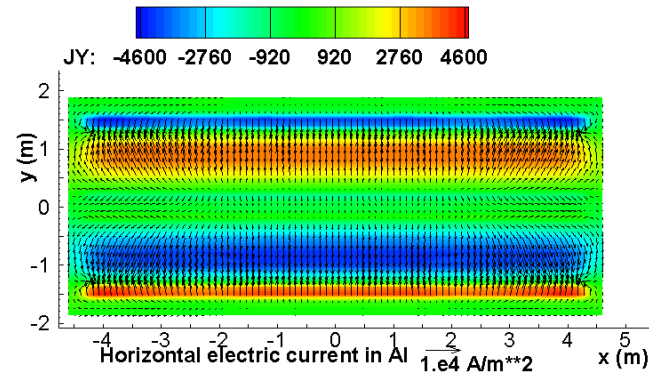
N<15	ContRes,Om	Ycoord,m	Tcol,Cdeg	Comments
0	0.0	1.8750	630.	- carbon block end at $ Y >=0$, $<=$ 'Cell cavity width,m
1	0.00022	0.060484	930.	- local contact resistance between carbon block/collector
2	0.00022	0.18145	930.	starting at (Y=0) from cell central axis
3	0.00022	0.30242	930.	- T deg C of steel collector bar
4	0.00022	0.42339	930.	
5	0.00022	0.54435	930.	
6	0.00022	0.66532	930.	
7	0.00022	0.78629	930.	
8	0.00022	0.90726	930.	
9	0.00022	1.0282	630.	
10	0.00022	1.1492	630.	
11	0.00022	1.2702	630.	
12	0.00022	1.3911	630.	
13	0.00022	1.5121	630.	
14	0.00022	1.6331	630.	
15	0.00022	1.7540	630.	

finish reading with N=0 or an empty line

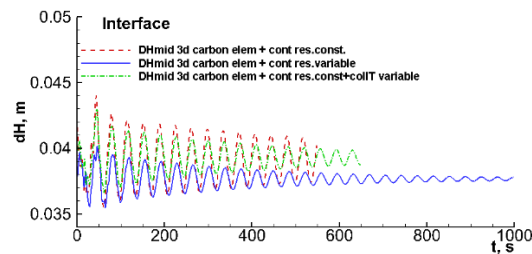
The electric current distribution in the liquid metal is obtained:



The horizontal current J_y in liquid metal:



The MHD stability of the cell is improved compared to the reference case as shown by the long run of the program (the green lines correspond to the prescribed case of the collector T distribution):



Magnetic field of aluminium reduction cells

Magnetic field in the aluminium reduction cell is created by the currents in the cell itself, from the complex bus-bar arrangement around the cell, from the currents of the neighboring cells and the return line, and by the magnetization effect of the cell construction steel. The present MHD model accounts for the time dependent coupling of the currents and magnetic fields with the bath-metal interface movement. Ledge profile at the bottom of the cell cavity is assumed to be given either uniform along edges or obtained from the coupled thermal model. The MHD model couples the interface waves and the electromagnetic field distribution: electric and magnetic fields are both recalculated as the wave shape changes.

After the electric current distribution is obtained the second step in the MHD model is to calculate the magnetic field \mathbf{B} (called more precisely, magnetic induction), which is necessary to determine the electromagnetic force distribution within the liquid zone,

$$\mathbf{f} = \mathbf{j} \times \mathbf{B}. \quad (8)$$

The magnetic field \mathbf{B} is the sum of two contributions:

$$\mathbf{B} = \mathbf{B}_I + \mathbf{B}_M; \quad (9)$$

\mathbf{B}_I is generated by all the currents and \mathbf{B}_M by the ferromagnetic steel material. The magnetic field \mathbf{B}_I from the currents in the full bus-bar network is recalculated at time steps in the dynamic simulation using the Biot-Savart law

$$\mathbf{B}_I = \frac{\mu_0}{4\pi} \int \frac{\mathbf{j} \times \mathbf{R}}{R^3} dV. \quad (10)$$

The equation (10) is used on the 3D grid within the cell fluid layers where a special analytical technique is applied to deal with the singularity in the Biot-Savart law in order to obtain a smooth, convergent solution when the field calculation position coincides to the electric current location [20]. The internal magnetic field calculation is optimized by switching between finite volume, line element and analytical representation of the Biot-Savart equation which describes the nearby element influence on the magnetic field in the liquid, and particularly on the steel elements where the very high intensity magnetic field is present.

The result is close to the previous, but more accurately describes the nearby element influence on the magnetic field in the liquid, and particularly on the steel elements where the very high intensity magnetic field is present.

The calculation of the magnetic field \mathbf{B}_M from the steel elements requires some more effort. The difficulty arises because the steel parts of the cell are made of ferromagnetic material, whose magnetization \mathbf{M} (\mathbf{H}) depends non-linearly on the local magnetic field intensity \mathbf{H} in the magnetic material. The local magnetic induction \mathbf{B} in the ferromagnetic material is orders of magnitude higher than for the non-magnetic material, like air, liquid aluminium, bath etc. Equation (11) gives the relationship between magnetic induction, magnetization and magnetic field intensity.

$$\mathbf{B} = \mu_0(\mathbf{M} + \mathbf{H}) \quad (11)$$

where μ_0 is the permeability of vacuum, equal to $4\pi \times 10^{-7}$ (H/m) in the International System of Units. In the non-magnetic material $\mathbf{M} = 0$ and $\mathbf{B} = \mu_0 \mathbf{H}$. In the magnetic material the unknown magnetic field

intensity \mathbf{H} is related to the magnetization $\mathbf{M}(\mathbf{H})$ by the material properties of a particular material (depending also on the temperature, carbon content in steel, previous magnetization, etc.). The typical curves used for the aluminium electrolysis cells are discussed in [16]. In order to find the unknown magnetic field intensity in the magnetized material, we need to solve the integral equation:

$$\mathbf{H}(\mathbf{r}) = \mathbf{H}_I(\mathbf{r}) - \frac{1}{4\pi} \int_{V_m} \left[\frac{\mathbf{M}(\mathbf{r}')}{|\mathbf{r} - \mathbf{r}'|^3} - \frac{3(\mathbf{r} - \mathbf{r}')}{|\mathbf{r} - \mathbf{r}'|^5} (\mathbf{r} - \mathbf{r}') \cdot \mathbf{M}(\mathbf{r}') \right] dV', \quad (12)$$

where the magnetic field \mathbf{H}_I is given by the Biot-Savart law (10) computed from all the external electric currents, the co-ordinate location \mathbf{r} is for the field calculation position (observation point), the integration point position \mathbf{r}' is in the element volume dV' running through all the ferromagnetic material in V_m . The iterative solution procedure for the equation (12) starts with an assumed distribution of \mathbf{M} in the ferromagnetic elements, calculates \mathbf{H} for these elements, then uses $\mathbf{M}(\mathbf{H})$ material property to obtain the updated magnetization. The procedure ends when convergence is achieved. The obvious complication is due to the singularity in (12) when the integration point coincides with the observation point. This is a very important contribution to the solution and can't be simply discarded; instead the analytical singularity elimination is used to give smooth results.

Once the magnetization of steel is known, the magnetic flux density $\mathbf{B} = \mu_0 \mathbf{H}$ for the fluid zones can be calculated from the equation (12) using the observation location \mathbf{r} on the computational grid where the electromagnetic force distribution is needed. This method for the magnetic field calculation was validated extensively against the physical models of real reduction cells (scaled 1:10) with and without steel parts [1].

When using the notation and the equations similar to the reference [21], the magnetization vector \mathbf{M} can be expressed as

$$\mathbf{M} = \mathbf{B}/\mu_0 - \mathbf{H}, \quad (\text{A/m}) \quad (13)$$

The standard formulation, used in the electrical engineering, relates the magnetic field flux density \mathbf{B} to the field intensity \mathbf{H} by the magnetic permeability μ :

$$\mathbf{B} = \mu \mathbf{H}, \quad (14)$$

where in the isotropic ferromagnetic material the permeability

$$\mu(\mathbf{H}) = \mu_0 \mu_r(\mathbf{H}), \quad \mathbf{H} = |\mathbf{H}|. \quad (15)$$

The advantage of using the magnetization vector \mathbf{M} is that it is nonzero only in the magnetized material; while $\mathbf{M} = 0$ in the air, carbon, aluminium, electrolyte, etc.

When using $M(\mathbf{H})$ or $\mu_r(\mathbf{H})$ curve obtained from literature some caution is needed, because the steel used in the electrolysis cells could have different magnetic properties depending on the 'aging' process in a working cell. The carbon content of the steel is changing with time, the temperature has pronounced effect resulting in the change of the $\mu(\mathbf{H})$ dependence. If no specifically measured data is available, our recommendation is to use the table supplied as default in the MHD-VALDIS package. The data used in the 'MH' file are obtained from direct measurements on steel samples cut out of the construction elements of several year old cell. The default table uses $M(\mathbf{H})$ relation. It must be arranged strictly in the way that \mathbf{H} is in a growing order, minimum 5, maximum 100 entry points are required in the 'MH' table:

```

-----
1 | 16000. | 8. | M and H in SI units (A/m), !
2 | 32000. | 16. | H in growing order;
3 | 80000. | 40. | minimum 5, maximum 100 points
4 |160000. | 80. |
5 |480000. | 400. |
6 |800000. | 800. |
7 |1280000. |4000. |
8 |1400000. |8000. |
9 |1500000. |40000. |
10 |1520000. |80000. |

```

Solving the integral equation (12), the iteration process requires smooth behaviour of the $\mu(H)$ curve, which is facilitated by internal cubic spline interpolation from the data given in the M(H) table.

If the user has access to an alternative given B(H) curve, note that the magnitudes of B and H are used for the typical isotropic material, for example, $H=|H|$. In order to obtain M(H) expression the relation is:

$$M = B/\mu_0 - H, \tag{16}$$

where M and H are in units Ampere/meter, $\mu_0 = 4\pi \cdot 10^{-7}$ (Henry/meter), B is in Tesla.

The program solution outputs are given in the Tecplot data file 'BFE.PLT' containing the discretised ferromagnetic element node co-ordinates (X,Y,Z) of the steel elements, the full magnetic field magnitude Bm (T), see Figure 5, the resulting magnetization M (A/m), magnetic permeability μ_r , and the external magnetic field Bex (T) from all macroscopic currents.

MHD-VALDIS update to use multiple ferromagnetic properties

The program permits input of up to 20 different magnetization M(H) curves supplied in the file 'MH'. The new input format maintains an option to use the old style 'MH' input file. The new format 'MH' input is given in the example below:

File 'MH' as used for the test cell '500 kA'

```

N | M,A/m | H,A/m | M2,A/m | M3...M20 columns; H in growing order, (5 - 100) points
4 |M(H):1 -----2-----3-----4-----5-----6-----7-----8-----
1 | 1591.5 | 10. | 1591.5 | 1591.5 | 1591.5 | 1591.5 | 1591.5 | 1591.5 | 1591.5 |
2 | 13528.2 | 78. | 13528.2 | 13528.2 | 13528.2 | 13528.2 | 13528.2 | 13528.2 | 13528.2 |
3 | 20292.3 | 100. | 20292.3 | 20292.3 | 20292.3 | 20292.3 | 20292.3 | 20292.3 | 20292.3 |
4 | 31035. | 150. | 31035. | 31035. | 31035. | 31035. | 31035. | 31035. | 31035. |
5 | 40585. | 195. | 40585. | 40585. | 40585. | 40585. | 40585. | 40585. | 40585. |
6 | 151197. | 400. | 151197. | 151197. | 151197. | 151197. | 151197. | 151197. | 151197. |
7 | 223613. | 500. | 223613. | 223613. | 223613. | 223613. | 223613. | 223613. | 223613. |
8 | 477465. | 830. | 477465. | 477465. | 477465. | 477465. | 477465. | 477465. | 477465. |
9 | 580916. | 1000. | 580916. | 580916. | 580916. | 580916. | 580916. | 580916. | 580916. |
10 | 795775. | 1470. | 795775. | 795775. | 795775. | 795775. | 795775. | 795775. | 795775. |
11 | 962887. | 2000. | 962887. | 962887. | 962887. | 962887. | 962887. | 962887. | 962887. |
12 | 1066338. | 2500. | 1066338. | 1066338. | 1066338. | 1066338. | 1066338. | 1066338. | 1066338. |
13 | 1145916. | 3000. | 1145916. | 1145916. | 1145916. | 1145916. | 1145916. | 1145916. | 1145916. |
14 | 1225493. | 4000. | 1225493. | 1225493. | 1225493. | 1225493. | 1225493. | 1225493. | 1225493. |
15 | 1273240. | 4800. | 1273240. | 1273240. | 1273240. | 1273240. | 1273240. | 1273240. | 1273240. |
16 | 1368733. | 7200. | 1368733. | 1368733. | 1368733. | 1368733. | 1368733. | 1368733. | 1368733. |
17 | 1432395. | 10000. | 1432395. | 1432395. | 1432395. | 1432395. | 1432395. | 1432395. | 1432395. |
18 | 1591549. | 23000. | 1591549. | 1591549. | 1591549. | 1591549. | 1591549. | 1591549. | 1591549. |
19 | 1710916. | 50000. | 1710916. | 1710916. | 1710916. | 1710916. | 1710916. | 1710916. | 1710916. |

```

The meaningful input starts at the 2nd line where an integer (1 – 20) gives an optional number of input columns for M values corresponding to the single H (A/m) values in the ferromagnetic plate. In the

example above only 4 columns of M values will be used. The properties given in the numbered columns will be applied to the ferromagnetic elements created from the input file ‘Steelplates’ where the last column indicates the corresponding number of the M(H) curve created from the ‘MH’ input:

File ‘Steelplates’ as used for the test cell ‘500 kA’

N	x1, m	y1, m	z1, m	x2, m	y2, m	z2, m	Nx or dx	Ny or dy	Nz or dz	M-type
1	-9.20	-2.60	-0.80	9.20	2.60	-0.79	54	16	1	4
2	-9.21	-2.60	-0.80	-9.20	2.60	0.80	1	16	8	1
R	18.41						1			1
4	-9.20	-2.61	-0.80	9.20	-2.60	0.80	54	1	8	1
R		5.21					1			1
6	-9.70	-3.10	0.80	9.70	-2.60	0.81	54	2	1	1
R		5.70					1			1
8	-9.70	-2.60	0.80	-9.20	2.60	0.81	2	16	1	1
R	18.90						1			1
10	-8.71	-2.90	-1.10	-8.70	2.90	-0.80	1	16	2	1
R	1.0						17			1
30	-8.71	-2.90	-0.80	-8.70	-2.60	0.80	1	2	6	2
R	1.0						17			2
48	-8.71	2.60	-0.80	-8.70	2.90	0.80	1	2	6	3
R	1.0						17			3

The new update of the program is supposed to be compatible with the old types of input files ‘MH’ and ‘Steelplates’. If the last column in ‘Steelplates’ is absent, then the first column of the M(H) will be used for all ferromagnetic elements. If the number given in the ‘M-type’ column exceeds the total number of the M(H) property columns, the M-type is set = 1.

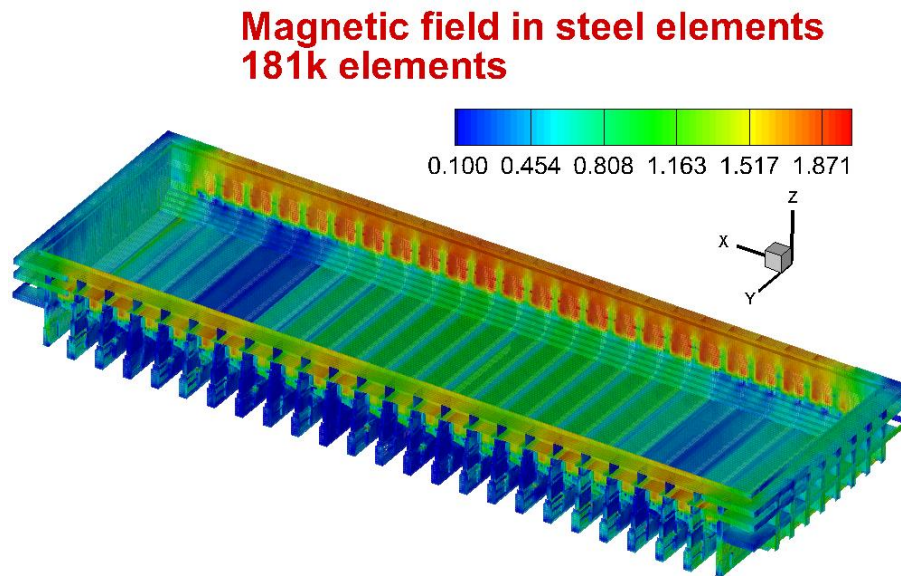


Figure 5. Cell steel construction geometry and the full magnetic field B in the ferromagnetic elements.

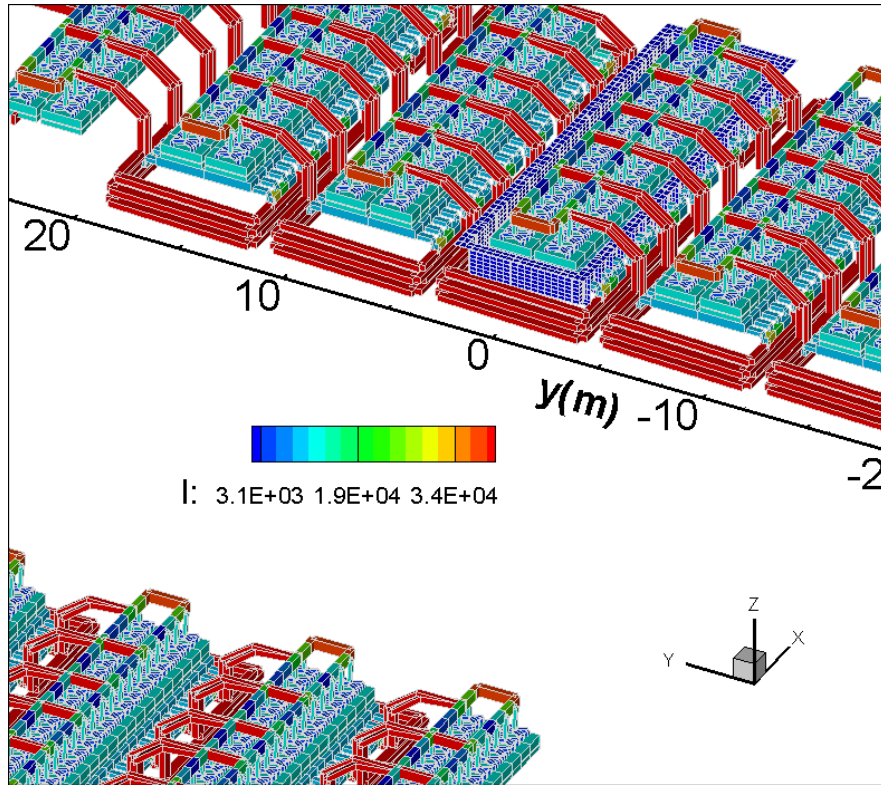
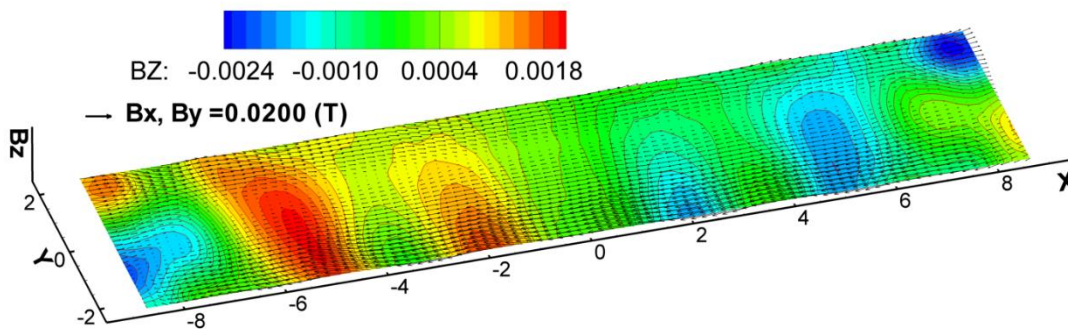


Figure 6. 500 kA cell example of bus bars, steel construction geometry and the optional cell position in the line (zoom-in and -out is available when viewing in Tecpot).

The MHD program for the complete magnetic field computation of an aluminium reduction cell permits to include the extended bus bar network of up to 8 neighboring cells in the same row and up to 6 cells in the return row, as shown for example in Figure 6. The steel construction elements are included for the test cell only (Figure 6). The steel parts are divided into up to 4000000 rectangular shape elements.

Figure 7 shows the total magnetic field in the liquid metal at the top and bottom levels respectively. The electromagnetic force, required for the fluid dynamics simulation, is constructed from the 3-dimensional magnetic field and electric current in the fluid layers. The inclusion of the steel parts is crucial for the optimization of the vertical magnetic field in order to design a stable cell.



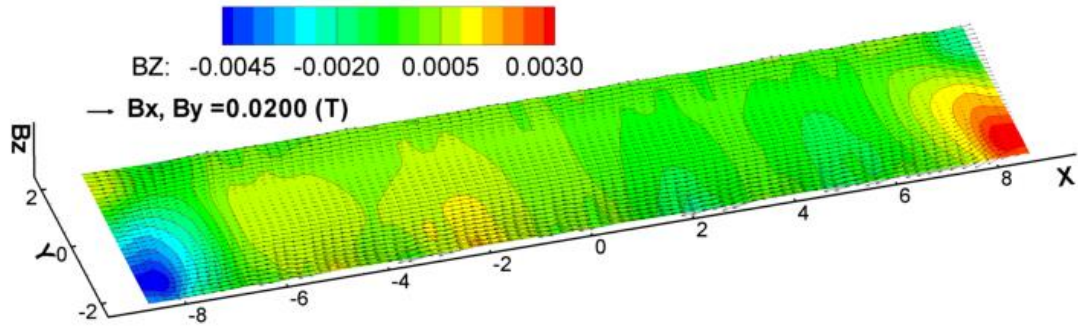


Figure 7. The total magnetic field distribution for the 500 kA cell (from all the current carrying elements and the steel shell shielding): horizontal field components shown as arrows, flooded contours for the vertical Bz component. The top figure shows the \mathbf{B} field at the top of the liquid metal and the bottom – at the bottom of liquid metal layer. The graphics are constructed with the tangent vector representation option in Tecplot for the 3-d magnetic field.

The MHD model uses a mesh for the fluid volume consisting of 88x32x2 elements in order to be able to re-compute the current distribution at each time step in a reasonable computational time. Nevertheless, the solution is sufficiently smooth and accurate because the approximation in space uses the global pseudo-spectral method, which permits much higher accuracy in comparison to finite element or finite volume approximations on the similar grid size [6-9].

The aluminium-electrolyte interface deformation makes the anode currents non-equal because of the local ACD change. The model includes an option to account for the time average gradual consumption of the anodes at the bottom, permitting to adjust the bath top to the anode burnout in a real cell. An artificially accelerated anode burn-out is permitted in order to achieve the result in a reasonable computational time interval (Figure 8). This effect often helps to stabilize the MHD of the cell, as it is observed in the cell operation.

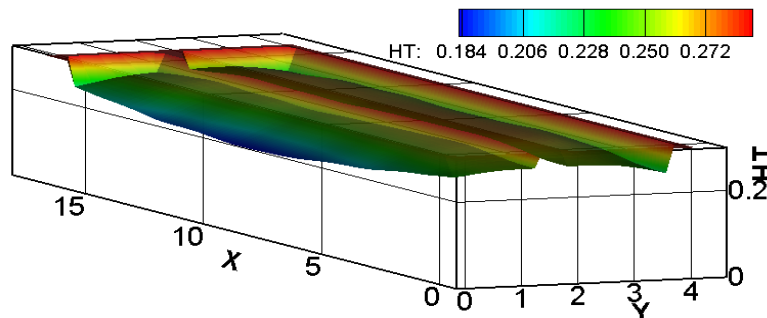


Figure 8. Anode bottom in contact to the liquid electrolyte after the burnout and the large channels in the centre and at the perimeter of the cell.

Hydrodynamics: interface deformation, velocities and waves

Statement of the “shallow water” problem

For the “shallow water” approximation the horizontal dimensions L_x and L_y are assumed to be much larger than the typical depth H of the fluid layers, and the interface wave typical amplitude A is also assumed to be small relative to the depth. Thus two small parameters of the mathematical problem are the nondimensional depth δ and the amplitude ε :

$$\begin{aligned}\delta &= \frac{H}{L} \ll 1, \\ \varepsilon &= \frac{A}{H} \ll 1.\end{aligned}\tag{17}$$

With the purpose to derive weakly nonlinear shallow layer approximation Boussinesq equations for the wave motion we will need to estimate the terms in the full three dimensional Navier-Stokes equations of motion. Therefore nondimensional variables are introduced using the following typical scales: the width of cell L for the coordinates x, y ; $u_0 = \sqrt{gH}$ for velocity \mathbf{v} , L/\sqrt{gH} for time t , $\rho_1 u_0^2$ for pressure p , IB_0/L^2 for the electromagnetic force \mathbf{f} (B_0 is typical magnetic field magnitude and I – the total electric current). According to the small depth assumption a stretched nondimensional vertical coordinate

$$\bar{z} = z/(L\delta)\tag{18}$$

is defined, and the nondimensional interface deformation of small amplitude is represented as

$$H_0/(L\delta) = \bar{H}_0 = \varepsilon\zeta(x, y, t).\tag{19}$$

With these definitions the nondimensional fluid flow equations: continuity, horizontal momentum and vertical momentum transport, are respectively:

$$\partial_k u_k + \delta^{-1} \partial_{\bar{z}} w = 0\tag{20}$$

$$\partial_t u_j + u_k \partial_k u_j + \delta^{-1} w \partial_{\bar{z}} u_j = -\partial_j p + \text{Re}^{-1} (\delta^{-2} \partial_{\bar{z}} \bar{\nu}_e \partial_{\bar{z}} u_j + \partial_k \bar{\nu}_e \partial_k u_j) + E f_j\tag{21}$$

$$\partial_t w + u_k \partial_k w + \delta^{-1} w \partial_{\bar{z}} w = -\delta^{-1} \partial_{\bar{z}} p + \text{Re}^{-1} (\delta^{-2} \partial_{\bar{z}} \bar{\nu}_e \partial_{\bar{z}} w + \partial_k \bar{\nu}_e \partial_k w) + E f_z - \delta^{-1},\tag{22}$$

where the summation convention is assumed over the repeating k indexes (equal to 1 or 2, respectively for x, y coordinates), $\bar{\nu}_e$ is the nondimensional effective turbulent viscosity, f_j are the components of electromagnetic force, and the last term in (22) represents the constant gravity in nondimensional form. The nondimensional governing parameters are the Reynolds number and the electromagnetic interaction parameter:

$$\text{Re} = Lu_0/\nu, \quad E = \frac{IB_o/L^2}{\rho u_0^2/L} = \frac{IB_o}{L^2 \rho g \delta}.\tag{23}$$

Formally the Boussinesq equations can be derived if assuming the leading terms of velocity expansion in the small amplitude parameter being given by

$$\mathbf{u}(x, y, z, t) = \mathbf{u}_o(x, y, t) + \varepsilon \mathbf{u}_\varepsilon(x, y, z, t) + o(\varepsilon), \quad (24)$$

where \mathbf{u}_o is the horizontal circulation, \mathbf{u}_ε is the wave related velocity. The leading accuracy $O(1, \varepsilon, \delta)$ pressure expression can be derived as

$$p(x, y, \bar{z}, t) = p(x, y, \bar{H}_0, t) - \bar{z} + \varepsilon \zeta + \delta E \int_{\bar{H}_0}^{\bar{z}} f_z d\bar{z}. \quad (25)$$

When the depth averaging procedure is applied to the horizontal momentum equations (21), the equations for the horizontal circulation \mathbf{u}_o plus ε -order $\hat{\mathbf{u}}_\varepsilon$ wave motion: $\hat{\mathbf{u}} = \hat{\mathbf{u}}_o + \hat{\mathbf{u}}_\varepsilon$ for each of the fluid layers are

$$\begin{aligned} \partial_t \hat{u}_j + \hat{u}_k \partial_k \hat{u}_j = \\ = -\partial_j p(\bar{H}_0) - \varepsilon \partial_j \zeta - \mu^* \hat{u}_j + \text{Re}^{-1} \partial_k \bar{v}_e \partial_k \hat{u}_{0j} + E \hat{f}_j - \frac{1}{2} \delta E \bar{H}_i \partial_j f_{0z} + O(\varepsilon^2, \delta^2, \varepsilon \delta) \end{aligned} \quad (26)$$

where the continuity of the pressure at the interface is satisfied by introducing $p(\bar{H}_0)$ - the pressure at the interface common to both layers. The term ' $-\mu^* \hat{u}_j$ ' accounts for the combined bottom and top friction in the shallow layer approximation. The nonlinear friction at the top and bottom of the fluid layers in (26) is defined similarly to general shallow water models [22]:

$$\mu \hat{u}_j = C_f |\hat{\mathbf{u}}| \hat{u}_j = \text{Re}^{-1} \delta^{-2} (\bar{H}_i - \bar{H}_o)^{-1} \int \partial_{\bar{z}} \bar{v}_e \partial_{\bar{z}} u_j d\bar{z}. \quad (27)$$

The appropriate boundary conditions to solve the equations (20),(26) are zero normal velocity and zero tangential horizontal circulation velocity components at the side walls:

$$\hat{u}_n = 0 \quad \text{and} \quad \hat{u}_{0\tau} = 0. \quad (28)$$

Then the velocity components and pressure are represented as series of Chebyshev polynomials $T_m(x)$ and $T_n(y)$:

$$\begin{aligned} \mathbf{u} &= \sum_{n=0}^N \sum_{m=0}^M u_{nm}(t) T_m(x) T_n(y), \\ \mathbf{v} &= \sum_{n=0}^N \sum_{m=0}^M v_{nm}(t) T_m(x) T_n(y), \end{aligned} \quad (29)$$

For the Navier-Stokes equations (26) the second order implicit time discretization and iterative linearization for the non-linear terms is implemented according to the following scheme:

$$\begin{aligned} \frac{3\mathbf{v}^k - 4\mathbf{v}^{k-1} + \mathbf{v}^{k-2}}{2\Delta t} - \mathbf{v}^{k-1/2} \times (\nabla \times \mathbf{v}^{k-1/2}) = \\ -\nabla(\rho^{-1} p^k + \frac{1}{2} \mathbf{v}^{k-1/2} \cdot \mathbf{v}^{k-1/2}) + \nabla \cdot (v_e^{k-1} (\nabla \mathbf{v}^k + \nabla \mathbf{v}^{kT})) + \rho^{-1} \mathbf{J}^{k-1} \times \mathbf{B}^{k-1}, \end{aligned} \quad (30)$$

where the 'k-1/2' denotes the iteration level. Typically just 2-4 iterations are necessary for the non-linear terms at each time step to reach convergence satisfying the relative maximum norm error < 0.0001 for the velocity components.

The effective viscosity as the sum of laminar and turbulent viscosity,

$$v_e(x,y,t) = \nu + \nu_T \quad (31)$$

is obtained by solving the time dependent k - ω two-equation model [10-12]. The k - ω model is a variant of low Re number turbulence models which permits to resolve the flow from laminar to developed turbulent states, and therefore is considered as suitable for the turbulent flow development simulations. The ω variable is related to the reciprocal turbulent time scale (frequency of vorticity fluctuations) and the k variable is turbulence kinetic energy. The k - ω model governing equations are:

$$\begin{aligned} \partial_t k + \mathbf{v} \cdot \nabla k &= \nabla \cdot [(\nu + \sigma_k \nu_T) \nabla k] + G - \beta^* \omega k + C_f |\mathbf{v}|^3 H_i^{-1} \\ \partial_t \omega + \mathbf{v} \cdot \nabla \omega &= \nabla \cdot [(\nu + \sigma_\omega \nu_T) \nabla \omega] + \alpha \frac{\omega}{k} G - \beta \omega^2 + 2C_f |\mathbf{v}|^4 H_i^{-2} \frac{1}{\beta^* k}, \end{aligned} \quad (32)$$

where the turbulent viscosity ν_T , turbulent kinetic energy generating term G , the mean velocity strain rate Δ , and different model constants and 'wall damping' functions are defined as (see [12] for details):

$$\begin{aligned} \nu_T &= \alpha^* \frac{k}{\omega} & G &= 2\nu_T (\Delta : \Delta) & \Delta &= \frac{1}{2} (\nabla \mathbf{v} + \nabla \mathbf{v}^*) \\ \sigma_k &= \frac{1}{2} & \sigma_\omega &= \frac{1}{2} & \alpha, \alpha^*, \beta, \beta^* & \text{- functions depending on } R_T = \frac{k}{\omega \cdot \nu} \\ \alpha &= \frac{5}{9} \frac{0.1 + R_T / 2.7}{1 + R_T / 2.7} (\alpha^*)^{-1}, & \alpha^* &= \frac{1}{40} + R_T / 6, & \beta^* &= 0.09 \frac{5}{18} + \frac{(R_T / 8)^4}{1 + (R_T / 8)^4}, & \beta &= \frac{3}{40}. \end{aligned} \quad (33)$$

The depth averaging in the shallow layer approximation adds the new terms ' $C_f |\mathbf{v}|^3 H_i^{-1}$ ' and ' $2C_f |\mathbf{v}|^4 H_i^{-2} \frac{1}{\beta^* k}$ ', in the equations (32) respectively.

The solution is sought with the boundary conditions:

$$\text{at solid wall: } k = 0, \quad \omega = \frac{6\nu}{\beta y^2}, \quad y\text{- distance to wall cell center.} \quad (34)$$

The numerical solution method uses similar spectral representation as in (29) for the turbulent quantities:

$$k = \sum_{n=0}^N \sum_{m=0}^M k_{nm} T_n(x) T_m(y), \quad \omega = \sum_{n=0}^N \sum_{m=0}^M \omega_{nm} T_n(x) T_m(y). \quad (35)$$

The time stepping scheme is similar to (30), and it is performed after the velocity time step. Additional two-layer (' ν_T ' and ' k - ω ') nested iterations are needed to obtain convergence for the non-linear terms in the k - ω equations.

The momentum (26) and continuity (20) equations for the two fluid layers can be combined in a single nonlinear wave equation for the metal-bath interface $\zeta(x,y,t)$ by taking the time derivative of (20), the horizontal divergence of (26) and finally the difference between the resulting equations for the layers with $i=1$ and $i=2$ to eliminate the common pressure at the interface $p(\bar{H}_0)$:

$$\begin{aligned} \varepsilon \left\langle \frac{\rho}{H} \right\rangle \partial_{tt} \zeta + \varepsilon \left\langle \frac{\mu \rho}{H} \right\rangle \partial_t \zeta + \varepsilon \langle \rho \rangle \partial_{jj} \zeta = \\ E \left\langle \partial_j \hat{f}_j \right\rangle - \delta E \left\langle \frac{1}{2} \bar{H} \partial_{jj} \hat{f}_z \right\rangle - \varepsilon \left\langle \frac{\rho}{H} \partial_{ij} (\zeta u_{jo}) + \frac{\mu \rho}{H} \partial_j (\zeta u_{jo}) \right\rangle - \langle \rho \partial_j (\hat{u}_k \partial_k \hat{u}_j) \rangle \end{aligned} \quad (36)$$

where $\langle F \rangle = F_1 - F_2$ denotes a difference of a variable in the two layers and the nondimensional density $\rho = \rho_i / \rho_1$. The equation (36) is used for the numerical solution of the interface waves development with coupling to the horizontal circulation obtained from the numerical solution of (26).

The nonlinear equation (36) can be further generalized for the waves in the cell with slowly varying top and bottom profiles [7]. The modified wave equation for the aluminium-electrolyte interface $H(x,y,t)$ with the variable bottom $H_b(x,y)$ and top $H_t(x,y)$ is

$$\begin{aligned} \left(\frac{\rho_1}{H - H_b} + \frac{\rho_2}{H_t - H} \right) \partial_{tt} H + \left(\frac{\rho_1 \mu_1}{H - H_b} + \frac{\rho_2 \mu_2}{H_t - H} \right) \partial_t H - (\rho_1 - \rho_2) g \partial_{jj} H = \\ = \partial_j (\hat{f}_{j2} - \hat{f}_{j1}) - \frac{1}{2} (H - H_b) \partial_{jj} \hat{f}_{z1} - [\rho_1 \partial_j (\hat{u}_{k1} \partial_k \hat{u}_{j1}) - \rho_2 \partial_j (\hat{u}_{k2} \partial_k \hat{u}_{j2})]. \end{aligned} \quad (37)$$

The most recent models using the variable top formulation permit to include the effect of the channels at the top of the electrolyte layer with additional effects of the pressure equalization at the top surface, similar to the 'connected vessels' principle, see more details in [8,9]. When the electrolyte channels are accounted in the pressure conditions, the electromagnetic force contribution in the electrolyte is negligible, reducing the wave equation to

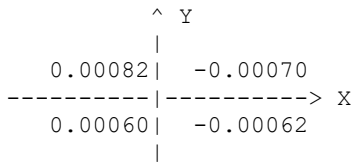
$$\begin{aligned} \left(\frac{\rho_1}{H - H_b} + \frac{\rho_2}{H_t - H} \right) \partial_{tt} H + \left(\frac{\rho_1 \mu_1}{H - H_b} + \frac{\rho_2 \mu_2}{H_t - H} \right) \partial_t H - (\rho_1 - \rho_2) g \partial_{jj} H = \\ = \partial_j (-\hat{f}_{j1}) - \frac{1}{2} (H - H_b) \partial_{jj} \hat{f}_{z1} - [\rho_1 \partial_j (\hat{u}_{k1} \partial_k \hat{u}_{j1}) - \rho_2 \partial_j (\hat{u}_{k2} \partial_k \hat{u}_{j2})]. \end{aligned} \quad (38)$$

Note that when accounting for the channels the electromagnetic force in the electrolyte \hat{f}_{j2} is retained for the solution of horizontal circulation velocities computed from the equation (26) in the electrolyte layer. The force distribution experiences significant change in the channels and their vicinity, contributing to the curl of the electromagnetic force, which drives the horizontal circulation in the large scale vortices. The solution using the equation (38) for the stationary interface is validated against the published 'benchmark' solution [23], see the extended validation results in [8].

Interpretation of the numerical solution results

When executing the program the output on-screen and in the file RESULTS is as shown in the example for the 500 kA test cell:

Quarter averages of BSZ in T



Additionally the magnetic field expansion in Fourier sinus-modes is given, which is useful for the linear MHD stability analysis according to Bojarevics&Romerio 1994 theoretical linear stability criteria. The most dangerous for the stability could be the modes in x and y directions interacting to give the resonance due to the magnetically induced shift of the gravity wave frequency. The easy to use criterion is the formula (4.20) in the paper, stating when the magnetic field first modes $B(N_x, N_y)$ give rise to the rotating wave over all the cell (as in the well known Sele or Urata theories).

For instance, setting in (4.20) $B(1,1)^2 = C11^2$ from the MHD-Valdis output, for the $m=1, n=1$, values for $L_x, L_y, H1, H2$, etc. the complex growth rate $OM = \pm \sqrt{OM^2}$ can be calculated. If the imaginary part of the '+' or '-' roots becomes negative, the linear stability criterion indicates a possible instability for the respective mode of the wave.

The computed first 4 expansion coefficients for the B_z field are output for each MHD-Valdis run. An example for the 500 kA standard test cell is reproduced below, where the imaginary parts of OM are remaining zero for the shifted gravity mode (1,1), indicating stability:

```
Amplitudes of BSZ expansion in sinuses:  
C11= 0.0022 C21= 0.0040 C12= 0.0001 C22= -0.0010  
  
Linear stability criterion is satisfied:  
OMP= 0.137 0.000  
OMM= 0.035 0.000
```

A transient MHD simulation is started with the flat metal-bath interface and zero velocity. There is an option, chosen in the file 'DATA' to start with the normal mode gravity wave (1,0) surface perturbation of a given amplitude, say 0.002 m. Normally this option is not required.

In the first time step the magneto-hydrostatic approximation of a stationary interface is used to compute the interface deformation, but using the electric currents computed for the flat interface. The resulting interface position for the 500 kA cell is shown in the Figure 9. At this stage the anode bottom surface is adjusted to the uniform interpolar distance ACD as prescribed numerically in the file DATA input. This precaution is required to avoid metal coming in contact to the anode and disrupting the program execution. See Figure 8 for the anode bottom surface acquired after the uniform ACD adjustment at this step.

At the second time step the electric currents and the magnetic field are computed for this interface and the modified anodes. This distribution, shown in Figure 10, is used as the actual initial state when investigating the cell stability in the dynamic simulation.

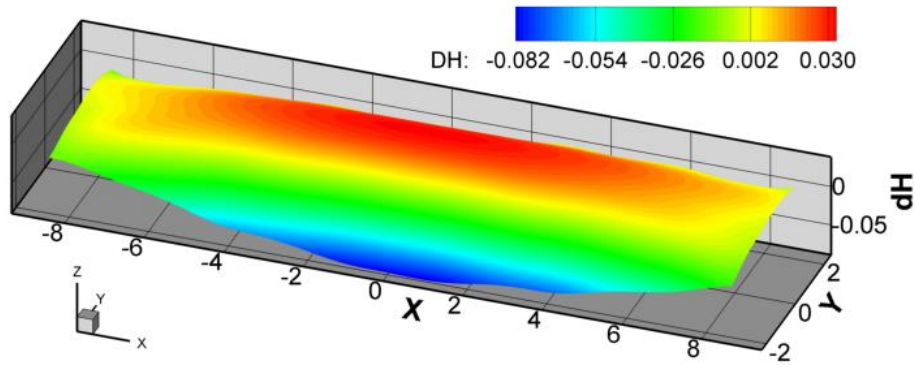


Figure 9: The resulting aluminium-electrolyte interface for the initial (flat) electric current distribution.

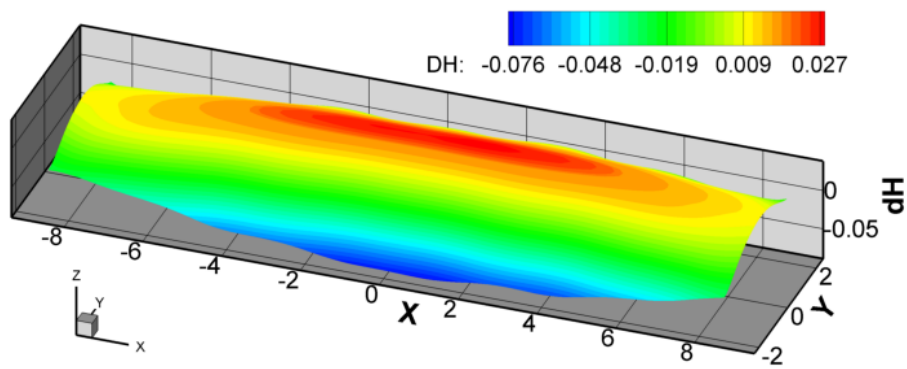


Figure 10: The resulting aluminium-electrolyte interface at the second time step after the electric current readjustment.

A time step of 0.25 s was used typically in the simulations. Waves take about 200 - 300 s to build and the damping sets in if the cell is stable, Figure 11. In an absolutely stable cell, this would be the time needed to damp the initial perturbation and to achieve a stationary interface position with the corresponding current distribution. Figure 11 shows an example of the damped oscillations. However, most often the cell waves stabilize about the quasi-stationary, low amplitude oscillation pattern, showing some cell noise typical for the most of commercial cells. The oscillation patterns beneath the first corner anode and the diagonally opposite far corner anode are shown in the top part of the Figure 11. The respective anode currents fluctuate in the same manner, the respective pictures can be created from the stored data using the supplied Tecplot layouts.

For the relatively symmetric circulation patterns, shown in the Figures 12-15, in the metal (and a different vortex pattern in the bath), the wave is slowly damped as it would be expected in a stable cell. In this instructive example the oscillations remain active for rather long time. This gives rise to the cell voltage oscillations of a magnitude about few mV, which are shown in the Figure 11. The potential drop oscillation is the result of the overall cell resistance change, caused by the non-uniform ACD changes during the wave motion. This type of the voltage noise is typically observed in all commercial cells. The Fourier spectrum for the oscillation indicates a dominant frequency located in between the third and fourth fundamental gravitational frequencies in the full spectrum of the normal gravity waves. As explained in [4], the MHD interaction is responsible for the shift from the purely hydrodynamic oscillation frequencies.

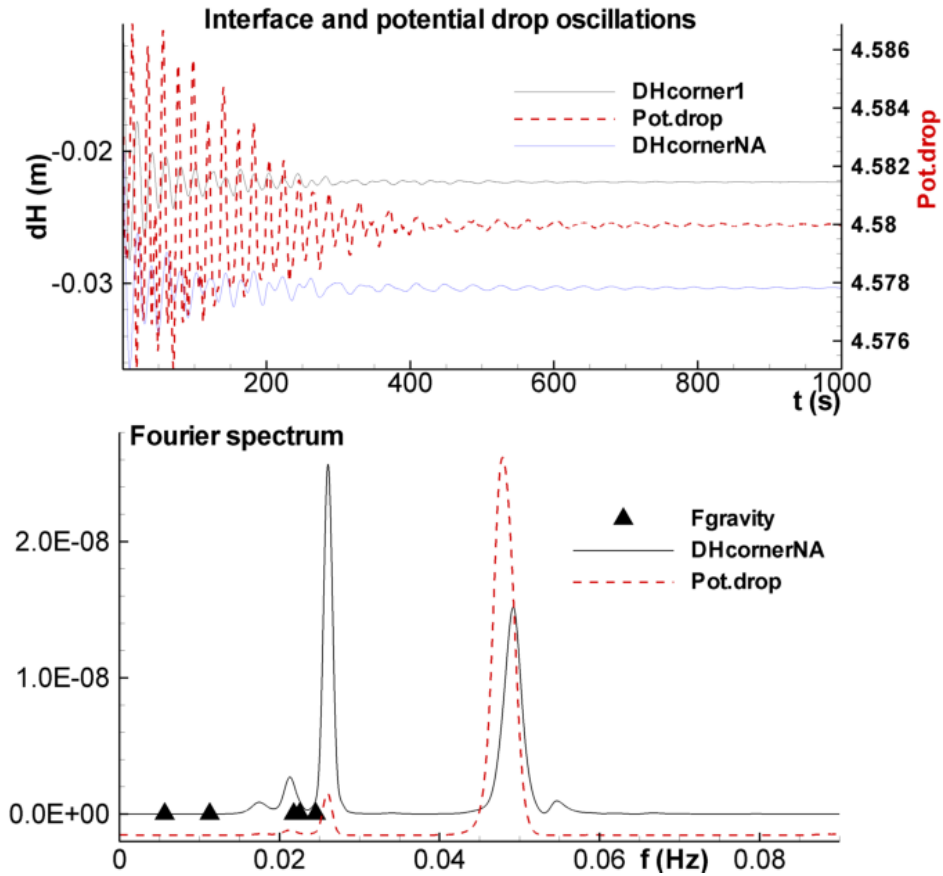


Figure 11: The computed oscillations in the 500 kA cell: top – interface position relative to the initial flat shape for the corner anode N1 and the diagonally opposite last anode NA, total cell voltage oscillation (V); bottom – Fourier power spectra for the same oscillations (the dominant and a secondary frequencies can be detected), triangles indicate the gravity frequencies for the fundamental gravity wave self oscillations for this two layer interface in the absence of electromagnetic interaction.

The re-circulating flow is predominantly horizontal and it develops in time with the ACD adjustment and the magnetic field change. The flow is turbulent for the typical conditions of the electrolysis cell. The MHD model presented here uses the 2-equation 'k- ω ', time dependent turbulence model which is solved simultaneously with other variables at each iteration. The velocity patterns and the effective turbulent viscosity distribution for a quasi-stationary regime at 500 s is shown in the Figures 13 and 15. The highly non-uniform distribution of the effective turbulent viscosity is shown by the color-filled contour lines. The regions of high turbulent viscosity are associated with enhanced turbulent heat and mass transport, which are important for predicting heat loss (ledge thickness) and the cell wall erosion.

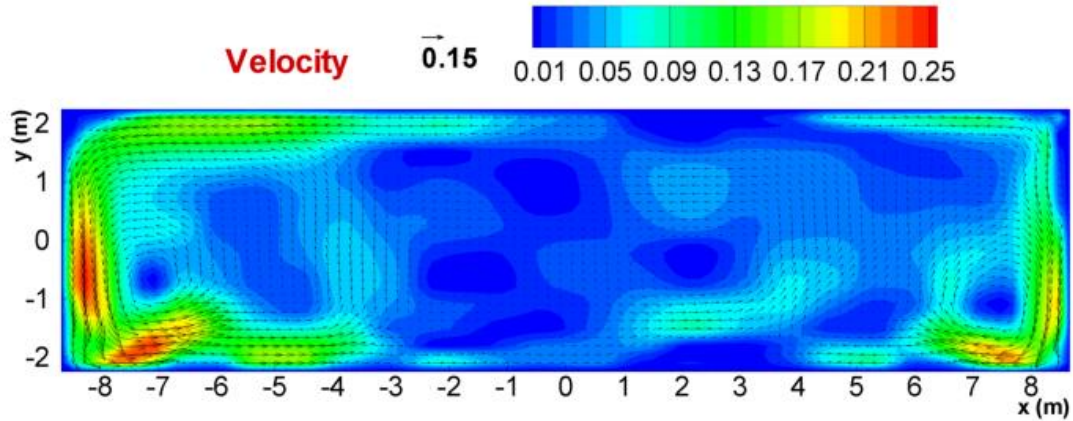


Figure 12. The quasi-stationary large scale horizontal recirculation velocity distribution in the liquid **aluminium**, the velocity magnitude is shown in flooded contour representation (see values in the top legend).

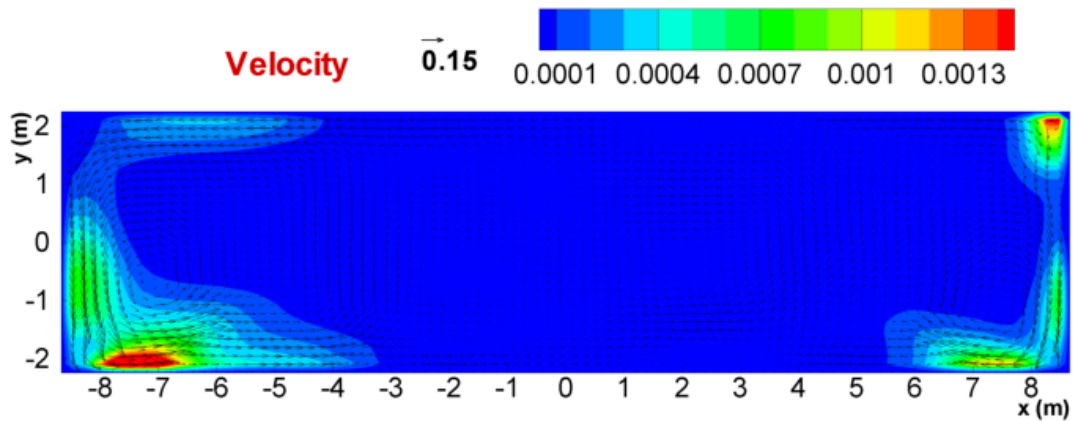


Figure 13. The quasi-stationary large scale horizontal recirculation velocity distribution in the liquid **aluminium** and the corresponding turbulent viscosity distribution shown in flooded contour representation (see values in the top legend).

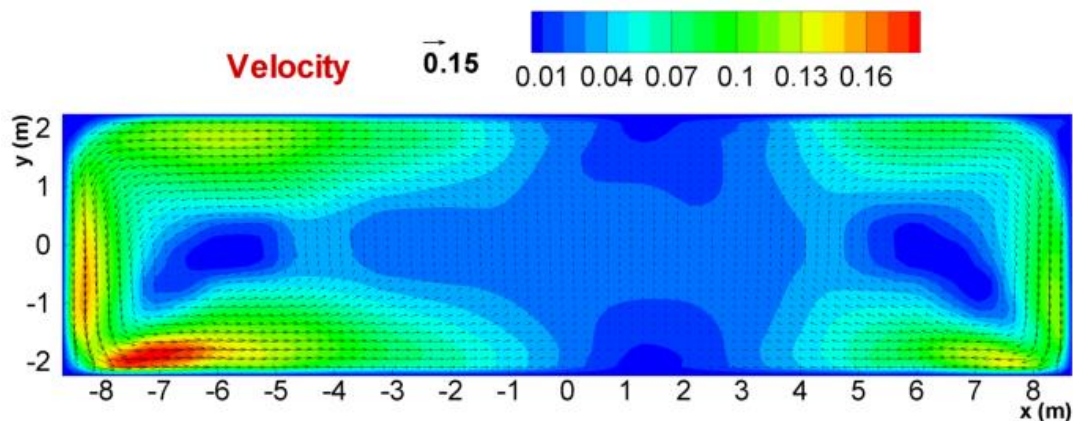


Figure 14. The quasi-stationary large scale horizontal recirculation velocity distribution in the liquid **electrolyte**, the velocity magnitude is shown in flooded contour representation (see values in the top legend).

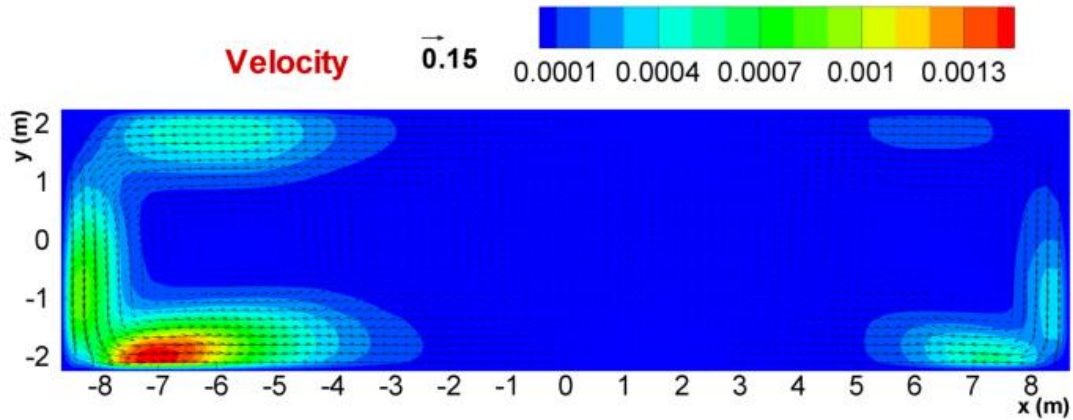


Figure 15. The quasi-stationary large scale horizontal recirculation velocity distribution in the liquid **electrolyte** and the corresponding turbulent viscosity distribution shown in flooded contour representation (see values in the top legend).

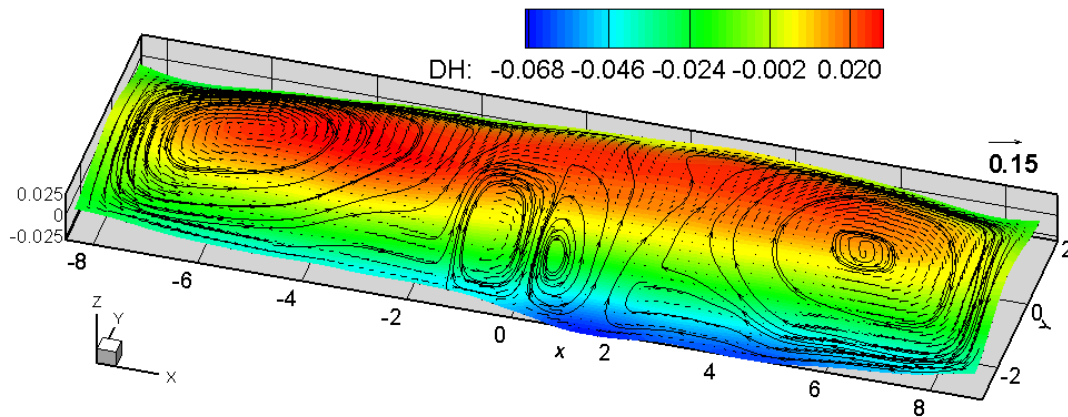


Figure 15a. The quasi-stationary large scale horizontal recirculation velocity distribution in the liquid **electrolyte** and the stationary dome shaped interface distribution shown in 3d and the flooded contours.

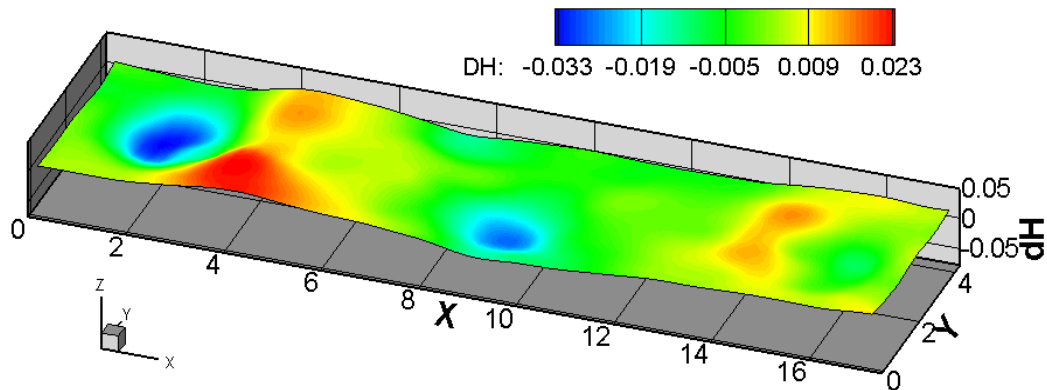


Figure 16. Metal-bath interface shape for 500 kA cell without the channel effect.

The coupling between pressure and velocities has some special effects on the metal-bath interface deformation. A large scale horizontal vortex can create a considerable free surface dip in its center. This is because the circulation pattern in the metal layer is different from the one in the electrolyte. The resulting pressure differences across the interface lead to the interface shape change in addition to the magnetic deformation, Figure 16. However these effects are not so obvious when the channel effect is invoked in the model by choosing the option to prescribe the cell bottom profile in the file 'BOTTOM', see Figures 9 and 10. The differences between the model results for the channel effect are illustrated in the Figure 17. The importance of recomputing the magnetic field from the time dependent electric current, oscillating with the interface, is shown in the Figure 17 as well. The parametric damping in this case helps to increase the cell stability. The instability type in the case without the channels is the classical rotating wave, as described in the theoretical papers [1-4]. The presence of the electrolyte channels changes the instability type, which resembles more a 'sloshing' wave constrained along the middle longitudinal line of the cell [8,9].

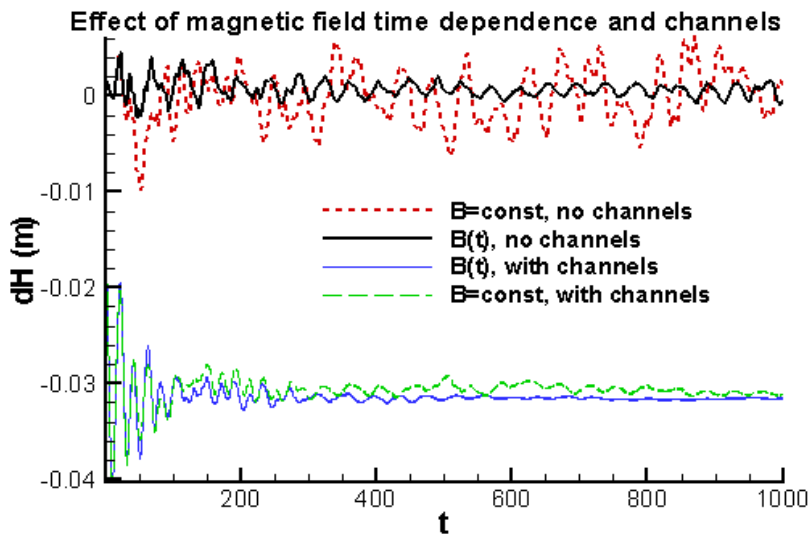


Figure 17. Different types of instability: 1) no channels, 2) with the channels, 3) if magnetic field modulation is included.

The other important effect included in the MHD model is the flow-induced electric current, resulting from the term $\sigma \mathbf{v} \times \mathbf{B}$ in the equation (5), where the high electrical conductivity σ makes this effect important for the liquid metal layer. This effect is included in the time dependent simulation process. It usually stabilizes the cell fluid dynamics because, according to the Lenz's law, the induced field always acts against the mechanical action causing it.

Various disturbances can be created using the MHD-VALDIS software, permitting to investigate the cell response with the dynamic simulation of the electromagnetic fields and the waves. Examples are shown in the Figures 18 and 19 for the electric current disturbances.

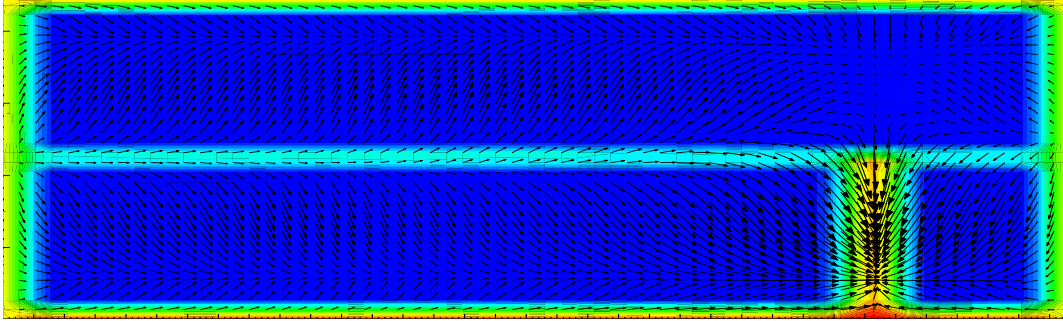


Figure 18. Typical disturbance: anode number 37 change giving the electric current distribution shown here.

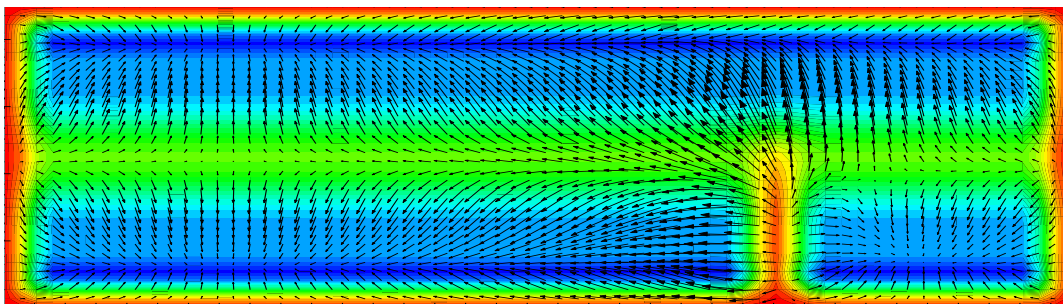


Figure 19. Typical disturbance: collector bar number 42 disconnected resulting in the electric current redistribution in the liquid aluminium.

References

1. V.Bojarevics et al. "Physical and mathematical modeling of MHD processes in an aluminium reduction cell". - In "*Liquid Metal Magnetohydrodynamics*" ed. by J.Lielpeteris, R.Moreau. "Kluwer Academic Publishers", Dordrecht / Boston / London (1989), p. 205.
2. V.Bojarevics. "MHD waves at the interface and the produced heat distribution in an aluminium electrolysis cell". - *Magnetohydrodynamics*, (1992) N 4, p. 47.
3. V.Bojarevics. "Interfacial MHD waves and associated heat distribution due to the dynamic electric current interaction in an aluminium electrolysis cell". - In "*Recent Advances in Heat Transfer*" ed. by B.Sunden, A.Zukauskas. Elsevier Science Publishers, (1992), p. 950.
4. Bojarevics and M.V. Romerio. "Long waves instability of liquid metal-electrolyte interface in aluminium electrolysis cells: a generalization of Sele's criterion". *Eur. J. Mech., B/Fluids*, Vol.13, No 1, (1994), p. 33-56.
5. V. Bojarevics, "Nonlinear waves with electromagnetic interaction in aluminium electrolysis cells." *Progr. Fluid Flow Res.: Turbulence and Applied MHD*, Eds. H.Branover and Y.Unger, AIAA, (1998), Chapter 58, p. 833-848.
6. V. Bojarevics and K. Pericleous. "Comparison of MHD models for aluminium reduction cells", *Light Metals 2006*, Ed. T.W. Galloway, TMS, 2006, p347-352.

7. V. Bojarevics and K. Pericleous. "Shallow water model for aluminium electrolysis cells with variable top and bottom", *Light Metals 2008*, Ed. David H. DeYoung, TMS, 2008, p. 403-408.
8. V. Bojarevics and K. Pericleous. "Solutions for the metal-bath interface in aluminium electrolysis cells", *Light Metals 2009*, Ed. G. Bearne, TMS, 2009, p. 569-574.
9. V. Bojarevics and K. Pericleous. Time Dependent MHD Models for Aluminium Reduction Cells. Proceedings Jim Evans Honorary Symposium, ed-s B.Q. Li, et al., Seattle, TMS, 2010, pp. 199-206.
10. V. Bojarevics, K. Pericleous, R.A. Harding and M. Wickins. "The Development and Validation of a Numerical Model of an Induction Skull Melting Furnace", *Metallurgical and Materials Transactions, B*, 2004, vol. 35B, p.785-803.
11. A.Bojarevics, V.Bojarevics, J.Gelfgat and K.Pericleous. "Liquid Metal Turbulent Flow Dynamics in a Cylindrical Container with Free Surface:Experiment and Numerical Analysis". *Magnetohydrodynamics*, 1999, vol. 35, N3, pp. 258-277.
12. D. C. Wilcox. *Turbulence Modelling for CFD*, 2nd ed. (DCW Industries, California, 1998).
13. M. Dupuis and V. Bojarevics. "Busbar sizing modeling tools: comparing an ANSYS® based 3D model with the versatile 1D model part of MHD-Valdis", *Light Metals 2006*, Ed. Alton T. Tabereaux, TMS, 2006, p341-346.
14. M. Dupuis, V. Bojarevics and J. Freibergs, "Demonstration Thermo-Electric and MHD Mathematical Models of a 500 kA Al Electrolysis cell", *Proceedings of the 42nd Conference on Light Metals*, CIM, (2003), 3-20.
15. M. Dupuis, V. Bojarevics and J. Freibergs, "Demonstration Thermo-Electric and MHD Mathematical Models of a 500 kA Al Electrolysis cell, Part 2", *Light Metals 2004*, Ed. Alton T. Tabereaux, TMS, 2004, p.453-459.
16. Freibergs J., "Optimization of MHD processes in an aluminium reduction cell," *Proc. Int. Colloq. 'Modelling Material Processing' Riga, Latvian University*, 1999, pp.86-91.
17. T. Tvedt and H. G. Nebell, "NEWBUS, a Simulation Program for Calculation of the Current Distribution in the Bus Bar System of Alumina Reduction Cells", *Light Metals, TMS*, (1988), 567-573.
18. M. Dupuis and V. Bojarevics, "Weakly coupled thermo-electric and MHD mathematical models of an aluminium electrolysis cell", *Light Metals 2005*, Ed. Halvor Kvande, TMS, 2005, p.449-454.
19. V.Bojarevics. A Fast computation method for three-dimensional electric current in a layered structure of an aluminum electrolysis cell. – In the 5h Biennial IEEE Conference on Electromagnetic Field Computation, 1992, p. WP39
20. Z. X. Feng. "The treatment of singularities in calculation of magnetic field by using integral method". *IEEE Magnetics*, 1985, MAG 21, N 6, 2207-2210.
21. Peter P. Silvester, Ronald L. Ferrari. 'Finite Elements for Electrical Engineers', Cambridge University Press, 1996, pages 239-241.
22. A.K. Rastogi and W. Rodi. Prediction of heat and mass transfer in open channels. *J. Hydraulics Division ASCE*, HY3 (1978), 397-420.
23. D.S. Severo, V. Gusberti, A.F. Schneider, E.C. Pinto and V. Potocnik, "Comparison of Various Methods for Modeling the Metal-Bath Interface". *In Proceedings of TMS Light Metals (2008)*, 413-418.
24. M.Dupuis and V.Bojarevics. "Retrofit of a 500 kA cell design into a 600 kA cell design", *International Aluminium Journal*, 2011, 87, N 1/2, pp. 52-55.
25. V. Bojarevics and A. Roy. "Bubble Transport by Electro-Magnetophoretic Forces at Anode Bottom of Aluminium Cells", TMS 140th Annual Meeting, *Light Metals 2011*, Ed. S. J. Lindsay, TMS, 2011, p. 549-554.
26. V. Bojarevics, A. Roy. "Effect of Magnetic Forces on Bubble Transport and MHD Stability of Aluminium Electrolysis Cells", *Magnetohydrodynamics*, 2012, Vol. 48, No. 1, pp. 125–136
27. Valdis Bojarevics, James W. Evans. "An Application of the Inverse Solution for Electric Current Distribution from Magnetic Field Measurements in Aluminium Electrolysis Cells", *Journal of Iron and Steel Research, International*, 2012, 19, 1-1, pp. 561-565.
28. M.Dupuis and V.Bojarevics. "Newest MHD-Valdis cell stability studies", *International Aluminium Journal*, 2014, 90, N 1/2, pp. 42-44.

29. M. Dupuis, V. Bojarevics. "Influence of the Cathode Surface Geometry on the Metal Pad Current Density", TMS Annual Meeting, Light Metals 2014, Ed. John Grandfield, TMS, 2014, p. 479-484.
30. V. Bojarevics, S. Sira. "MHD Stability for Irregular and Disturbed Aluminium Reduction Cells", TMS Annual Meeting, Light Metals 2014, Ed. John Grandfield, TMS, 2014, p. 685-690.
31. M. Dupuis, V. Bojarevics. "Nonlinear stability analysis of cells having different types of cathode surface geometry", TMS Annual Meeting, Light Metals 2015, Ed. M. Hyland, TMS, 2015, p. 821-826.
32. V. Bojarevics and J. Evans. "Mathematical modelling of Hall-Herault pot instability and verification of measurements of anode current distribution", TMS Annual Meeting, Light Metals 2015, Ed. M. Hyland, TMS, 2015, p. 783-788.
33. V. Bojarevics. "Effect of cathode collector copper inserts on the Hall-Hérault cell MHD stability", TMS Annual Meeting, Light Metals, Wiley, 2016, p. 933-938.
34. V. Bojarevics, A. Tucs. "MHD of Large Scale Liquid Metal Batteries", TMS Annual Meeting, Light Metals, Springer, 2017, p. 687-692.
35. V. Bojarevics, A. Tucs. Large Scale Liquid Metal Batteries, Magnetohydrodynamics Vol. 53 (2017), No. 4, pp. 677–685.
36. Tucs, A., Bojarevics, V., & Pericleous, K. Magnetohydrodynamic stability of large scale liquid metal batteries. Journal of Fluid Mechanics, (2018) 852, 453-483.
37. Tucs A., Bojarevics V., Pericleous K. Magneto-hydrodynamic stability of a liquid metal battery in discharge. EPL, 124 (2018)
38. V. Bojarevics, E. Radionov and Y. Tretiyakov, Anode bottom burnout shape and velocity field investigation in a high amperage electrolysis cell, Light Metals 2018, O. Martin (ed.), The Minerals, Metals & Materials Series, p. 551-556.

DATA INPUT AND OUTPUT

Data input is organised in several ASCII type text files, which is advantageous if there is a need to run under different to Windows operating system. The input data fields must be filled by the user in order to prescribe the particular electrolysis cell geometry, material parameters and the execution route. Other fields are used as comments intended to facilitate the inputs and to remind of some limitations. The program user must adhere strictly to the formatting of the files. The input is format sensitive similar to Fortran syntax. It is recommended to perform the data input while the 'insert' or 'overwrite' function for the keyboard is activated. The fixed space font, like 'Courier' must be used.

File 'MENU'

```
IN| MENU: EXPLANATIONS and COMMENTS
==|=====
2 | Anode base burnout: 0 "no", 1=4 time steps, >1=until N/dt (sec.), 99=all
20| Create data for TECPLOT files with N*dt frequency .GE.1 (0 - no)
0 | 0=Input from BUSNET only; 1=Input from BARSIN
0 | 'N' of anode to change at NTIME=3, 0 - no
0 | Recompute magnetic field at all time steps: Integer 1 means "yes", 0 - "no"
0 | 'N' of 2nd anode to change at NTIME=3, 0 - no
0 | 'N' of 3rd anode to change at NTIME=3, 0 - no
0 | 'N' of 4th anode to change at NTIME=3, 0 - no
0 | 0=keep velocity fixed after initial 20s; 1=full nonlinear dynamics; 2=fixed v & Hb
0 | 0=block bar graphical output if bar current < 10 A; 1=permit output
1 | 0=no fanning effect for current in electrolyte (use anode width); 1=permit fanning
==|=====
```

Inputs in the file 'MENU' determine the execution route. The left two columns starting with the 3rd line are intended for the user inputs.

If '1' is input for the anode base burnout option, then the program will adjust the bottom of the whole anode block to the constant ACD at the first time step. The adjustment then continues in a slow manner to the time average metal-bath interface shape, thus repeating in an accelerated manner the process in a real cell, where the anodes burn out non-uniformly according to the interface position. If this option is not desired, '0' input will eliminate the procedure.

The results of the calculations are output to the files suitable for the visual presentation with the graphical package Tecplot. The files are typically large, therefore we do not save the results at every time step. The option to create the Tecplot files at certain intervals is to be chosen on the fourth line. Typically we prefer about 5 seconds interval, which means the frequency of '20' for the time step 0.25 s (see file 'DATA').

When creating a new busbar arrangement from scratch, the input from the file 'BUSNET' is the only realistic possibility, chosen by the next input set as '0'. It is highly recommended to use this type of input even for the repeated bus generation inputs, because it guarantees the network generation as possible free of errors. The input from file 'BARSIN' is designed for the advanced users only, who wish to create non-standard bar arrangements, like e.g. shifted anodes, variable flexes, etc.

The anode change is a regular cell operation 'disturbance', which can be investigated for a given particular number of the anode. While creating a new cell design this is not activated by setting '0' in the corresponding position.

The file MENU can use the optional input as the last lines:

```
0 | 0=keep velocity fixed after initial 20s; 1=full nonlinear dynamics
```

The input '1' will recompute the full non-linear iteration for the velocity field at each time step during the full computational run. The input '0' will execute the full iterations for velocity solution for the first 20 seconds of the solution, then will freeze the final velocity field and will use this for the following time steps of the interface development. This input will not only save considerable time to solve the wave stability problem, but also will avoid the horizontal velocity vortex dynamic instability, which sometimes develops in hydrodynamic systems at high Reynolds numbers. Although this second instability of the velocity field is physically observable as a slow restructuring of the vortex structure, this effect is not what the classical MHD metal pad roll instability would predict and therefore will appear unexpected. If the 'classical' metal pad roll instability is the desired outcome, the option of the input '0' should be used.

The quasi-stationary velocity field will be calculated just 2 times at the beginning of the full wave analysis. The 3 times velocity calculation is reserved only for the case if the anode change is required in the MENU. This adjustment speeds up execution and adds robustness for the anode burnout effect estimate. Note that the anode burnout effect can be extended to more time steps using the larger than 1 input parameter in the respective MENU input.

If the preceding optional line is present, there could be 2 more lines added if required:

0 |0=block bar graphical output if bar current < 10 A; 1=permit output

This is useful when 'dummy' bars are used creating the end of line cell connections, not important for regular cells.

1 |0=no fanning effect for current in electrolyte (use anode width); 1=permit fanning

The 'fanning' effect in the electrolyte from the edges of the anode reduces slightly the effective electrical resistance of the cell, hence reducing also the potential drop by approximately 0.1 – 0.2 V.

File 'DATA'

```

DATA INPUT(w=16) | DATA: EXPLANATIONS and COMMENTS
===== | =====
4000 | Integer number of time steps (<20000) !4000
0.25 | Time step in (s) 0.125
17.34 | Cell cavity length (|x|, m) [at liquid metal top level] 17.34
4.49 | Cell cavity width (|y|, m) [at liquid metal top level]
500000. | Total electric current magnitude (A) 500000.
0.20 | Liquid aluminium average level (z, m) 0.20
0.040 | ACD, electrolyte thickness (z, m) 0.045
1.5947 | A(V) for overvoltage dU= A + B *'Current density' 1.6347 1.5947
0.00003815 | B(V*m**2/A) for overvoltage dU= A + B *'Current density' 0.0000187
74074. | Electrical conductivity:for cathode carbon (1/Om*m)
4000000. | for liquid aluminium (1/Om*m)
233. | for liquid electrolyte (1/Om*m) 210.
20450. | for anode carbon (1/Om*m) 21872.
0.000000265 | Resistivity for solid aluminium at 20 deg.C,Om*m
0.00429 | Resistivity temperature coefficient for solid aluminum
0.0000005 | Resistivity for cath. bars at 20 deg.C,Om*m

```

```

0.0062      |Resistivity temperature coefficient for cath. bars steel
0.000025   |Anode pin average contact Resistance, Om 0.000045
0.0000125  |Cathode bar average contact Resistance, Om '0.0000125'
210.       |Heat conductivity coefficient for aluminum busbars, W/(m*K)
45.        |Heat conductivity coefficient for cathode bars
6.         |C(W/K/m**2) for heat transfer coefficient to air = C(1+D*Tbar)
0.0064     |D(1/K) for heat transfer coefficient to air = C(1+D*Tbar)
300.      |Temperature of cathode bars (average), degC
900.      |Temperature of cathode carbon (average)
963.      |Temperature of electrolyte (average)
400.      |Temperature of anode pin 400.150.
25.       |Temperature for air at the cell
2300.     |Density for liquid aluminium (kg/m**3)
2075.     |           for           electrolyte 2066.
0.001     |Initial 'sloshing'wave perturbation C(1,0), max amplitude (m)
0.020     |Empirical bottom friction coefficient (nondimensional) 0.04
0.0000025 |Anode clamp average contact Resistance, Om 0.000025
0.00000125 |Cathode flex joint average contact Resistance, Om 0.0000125
0.0       |Initial 'sloshing'wave perturbation C(0,1), max amplitude (m) 0.005
0.0005    |ferromagnetic convergence criteria (>=0.0001)
0.05     |ferromagnetic mesh element max.size (m)
0        |ferromagnetic convergence max iteration N; 0 - no iteration 'magnetization.inp'
=====|=====

```

The user inputs start with the line 3, and the left 16 columns are designated for the input parameter values. The vertical line in column 17 is a delimiter, which must be kept untouched for the correct inputs.

The first number on the line 3 prescribes how many total number of time steps will be executed (must be an integer number without the decimal dot). This works in conjunction with the next input for the time step length in seconds. The smaller the time step, the more accurate is the numerical solution. However, the small time steps require larger total number of steps, therefore increasing the execution time. If the time step is too large, some non-linear and numerical instabilities can spoil your solution. From our experience the recommended length of the time step is 0.25 s for a typical electrolysis cell. Smaller amperage cells permit slightly larger time steps.

The cell cavity dimensions are the next two inputs. We observe the agreement that the x-coordinate is always along the longest cell side, and the y-coordinate along the short side. The coordinate center is in the middle of the cell and the z-coordinate starts at the carbon cathode bottom. For the correct description of the wave processes, **the cavity dimensions in the horizontal plane must be prescribed at the liquid metal average top level** (where the interface is located).

The cell total electric current is given in Amperes.

The metal level and the electrolyte thickness in the ACD is given in the SI units, m.

The following various material properties must be prescribed in the International Units (SI). Typical values for these are already supplied, however the user may change these according to the particular materials of the cell.

The electrochemical reaction overvoltage expression, used in this program, is in the simple linear form $dU = A + B * J$, where J (A/m^2) is the average vertical current density in the bath beneath the anodes, and the constants A and B are the user inputs corresponding to the chemical composition of the particular cell type. These will affect the total cell voltage and are responsible mostly for the reversible potential drop.

The electrical conductivities are used for the bulk materials used in the cell. These need to be given for the particular cell at operating temperatures.

The bus bar data is traditionally given for resistivity (inverse of the electrical conductivity). The temperature coefficient gives the linear variation of the resistivity with the temperature, which is used to iteratively adjust to the bus bar heating changes.

The contact resistance for the anode pins and cathode bars affects the local voltage drop and depends on the particular cell, therefore the average value of these are made as a user inputs.

‘Cathode flex joint average contact Resistance’

input from the DATA is corrected – it will be the default value if the file ‘Flexes’ is absent from the input.

The heat conductivity for the bus bar material is in W/(m*K).

The effective heat transfer coefficient to the surrounding air is an empirical input responsible for an average heat losses by convection and radiation to air (see the equation (3) for more explanations). This can be adjusted for a particular cell to achieve an experimentally measured temperature distribution in the bar network. Once set, it must be kept the same for all comparative studies of the particular design.

The temperatures for different internal parts of the cell can be set from the results of the thermoelectric model or from measured data. In this program they serve as a heat source in the thermal balance computed for the bus bars. The surrounding air temperature could affect the cell in dependence of the season and the geographical location.

The density values of the liquids are the typical ones used in simulations.

And finally, there is an option to input a sort of mechanical disturbance to the cell interface between the metal and bath in shape of the largest length gravity wave mode known as (1,0) or the ‘sloshing wave’: $C(N_x, N_y) = C(1,0) = a$ (the amplitude value in m). For a quasi-stationary case the value is $a=0$. For the stability analysis $a=0.005$ m is a recommended value for the DATA file input.

Usually there are no need to use this input because the initial transient electric current adjustment introduces sufficient perturbation. If investigating the very low ACD settings (say, below 30 - 35 mm) use the initial perturbation amplitude 0.001 m (not the 0.005 m as for large ACD) because this upsets the anode burnout correct calculation and adds more problems.

The empirical bottom friction coefficient represents the damping rate in addition to the one computed from the turbulence model. In simple linear theories this parameter historically was the only source of the dissipation limiting the wave growth and balancing the vortical electromagnetic force generating the horizontal flow. In the present model this parameter is given in the context of the depth averaged ‘shallow water’ representation of the 3-d fluid dynamics. The value is prescribed according to the bottom roughness. For more details see [22]. We recommend to use the values in the range from 0.02 (smooth bed) to 0.1 (rough).

Optional lines in the DATA file

```
DATA INPUT(w=16) | DATA: EXPLANATIONS and COMMENTS
=====|=====
8000          |Integer number of time steps (<20000) !4000
0.25         |Time step in (s) 0.125
17.34        |Cell cavity length (|x|, m) [at liquid metal top level] 17.34
4.49         |Cell cavity width (|y|, m) [at liquid metal top level]
500000.      |Total electric current magnitude (A) 500000.
0.20         |Liquid aluminium average level (z, m) 0.20
0.045        |ACD, electrolyte thickness (z, m) 0.045
1.5947       |A(V) for overvoltage dU= A + B *'Current density' 1.6347 1.5947
0.00003815  |B(V*m**2/A) for overvoltage dU= A + B *'Current density' 0.0000187
74074.       |Electrical conductivity:for cathode carbon (1/Om*m)
4000000.    |                for liquid aluminium (1/Om*m)
233.         |                for liquid electrolyte (1/Om*m) 210.
20450.       |                for anode carbon (1/Om*m) 21872.
0.0000000265|Resistivity for solid aluminium at 20 deg.C,Om*m
0.00429      |Resistivity temperature coefficient for solid aluminum
0.00000005  |Resistivity for cath. bars at 20 deg.C,Om*m
0.0062       |Resistivity temperature coefficient for cath. bars steel
0.000025     |Anode pin average contact Resistance, Om 0.000045
```

```

0.0000125 |Cathode bar average contact Resistance, Om '0.0000125'
210.      |Heat conductivity coefficient for aluminum busbars, W/(m*K)
45.       |Heat conductivity coefficient for cathode bars
6.        |C(W/K/m**2) for heat transfer coefficient to air = C(1+D*Tbar)
0.0064   |D(1/K) for heat transfer coefficient to air = C(1+D*Tbar)
300.     |Temperature of cathode bars (average), degC
900.     |Temperature of cathode carbon (average)
963.     |Temperature of electrolyte (average)
400.     |Temperature of anode pin 400.150.
25.      |Temperature for air at the cell
2300.    |Density for liquid aluminium (kg/m**3)
2075.    |          for          electrolyte 2066.
0.005    |Initial 'sloshing'wave perturbation C(1,0), max amplitude (m)
0.040    |Empirical bottom friction coefficient (nondimensional) 0.04
0.0000025 |Anode clamp average contact Resistance, Om 0.000025
0.00000125 |Cathode flex joint average contact Resistance, Om 0.0000125
0.0       |Initial 'sloshing'wave perturbation C(0,1), max amplitude (m) 0.005
0.0005   |ferromagnetic convergence criteria
0.05     |ferromagnetic mesh element max.size (m)
0         |ferromagnetic convergence max iteration N;0-no iteration 'magnetization.inp'
=====

```

Note the new optional lines in the DATA file at the end. The new features can be used adding optional lines in the existing input file DATA if required, the previous DATA files will be still accepted without these lines.

Possibility to add contact resistances in DATA for the collector bar to flex joint as well as the anode clamp (contact voltage drop between the anode busbar and the top of the anode stem).

The code is updated for more efficient ferromagnetic element non-linear properties solution. Users can input the desired mesh discretisation safe max resolution and the convergence accuracy in the file DATA as the optional lines at the end of the file:

```

0.0005   |ferromagnetic convergence criteria
0.05     |ferromagnetic mesh element max.size (m)
0         |ferromagnetic convergence max iteration N;0-no iteration 'magnetization.inp'

```

During the ferromagnetic iterations the file BFE.PLT is generated after each iteration, which permits to follow the convergence quality by viewing the respective graphical images. The convergence results are also output on the DOS screen as for example:

```

19 Magnetization curve points read from file MH
Ferr.iter 1 Err= 0.1918 kap.err= 0.1993 aver.kap=400.1565
Ferr.iter 2 Err= 0.0239 kap.err= 0.0672 aver.kap=466.3915
Ferr.iter 3 Err= 0.0064 kap.err= 0.0199 aver.kap=455.5856
Ferr.iter 4 Err= 0.0035 kap.err= 0.0077 aver.kap=449.8037
Ferr.iter 5 Err= 0.0025 kap.err= 0.0053 aver.kap=442.6490
Ferr.iter 6 Err= 0.0021 kap.err= 0.0045 aver.kap=436.3977
Ferr.iter 7 Err= 0.0020 kap.err= 0.0040 aver.kap=430.9161
Ferr.iter 8 Err= 0.0019 kap.err= 0.0036 aver.kap=426.2943
Ferr.iter 9 Err= 0.0018 kap.err= 0.0032 aver.kap=422.4320
Ferr.iter 10 Err= 0.0016 kap.err= 0.0029 aver.kap=419.2093
Ferr.iter 11 Err= 0.0015 kap.err= 0.0027 aver.kap=416.4967
Ferr.iter 12 Err= 0.0013 kap.err= 0.0025 aver.kap=414.1900
Ferr.iter 13 Err= 0.0012 kap.err= 0.0023 aver.kap=412.2195
Ferr.iter 14 Err= 0.0011 kap.err= 0.0021 aver.kap=410.5226

```

The last line of the DATA input permits to reset the number of iterations for the ferromagnetics to a new value instead of the default value of 20. If the last line will be absent, it will run with 20. The other new feature is activated if the Magnetization.inp file is present. The iterations will start with the field and magnetization values stored in this file. The number of elements generated from the Steelplates should be exactly the same, otherwise an error message will be output and the program stops.

If the parameter in the last line of DATA file for 'ferromagnetic convergence max iteration N' is set 0, then the magnetization will be used from the Magnetization.inp and no iterations will be performed. This is exactly as before, and the option is kept as default if the line in DATA is absent. However, if the iteration number is given, say, 10 or 30, then the iterations will run using the magnetization input as the initial values.

It does not mean that the iterations will converge immediately. In my tests it required 5 iterations to converge exactly to the same result as if using the default and running all iterations (in this case 16 were needed). Still it appears to be a large saving.

Unfortunately the iteration procedure is quite complex using a variable under relaxation parameters being adjusted for the best convergence from zero input. It would not be wise to modify the algorithm because then the basic case could suffer.

File 'BUSNET'

```

DATA INPUT (w=16) | BUSNET: EXPLANATIONS and COMMENTS
=====
500kA          !character, cell identification (max length 12)
=====CELL POSITION &ORIENTATION=====
2              !Integer,orientation:1 end-to-end(line current I in X);2 side-to-side(I in Y)
6              !Integer,number of cells represented in the same row: max 8
4              !Integer,cells in return row:max 6,0 line only,-1 nothing,-2,...,-6 cellonly
-50.           !X-position of next cell centre in cell-cavity longitudinal direction (m)
7.85          !Y-position of next cell centre in cell-cavity transverse direction (m) 6.85
105.          !cell centre distance to beginning of line (>0, m) 105. 4.75
105.          !cell centre distance to end of line (>0, m)
-0.1          !level of bars connecting to the return line, Z-level (m)
500.          !cut-out cell elements start (m) 3.7
500.          !cut-out cell elements end (m) 25.
0.            !cut-out return-line cell elements start (m) -10.9 4.5
0.            !cut-out return-line cell elements end (m) -4.75
=====CATHODE ARRANGEMENT=====
48            !Integer,number of cathode bars (total)
16.10         !interval (last)-(first) of cathode collector bar axes (X>0, m)
-0.45         !Z-level of cathode collector bars (central axis, m)
0.2           !collector bar starts at (|Y|>=0,m) from cell central axis(0.- connected)
2.9           !collector bar ends at (|Y|>0, m) from the cell central axis
0.28          !collector bar thickness1 (|X|>0, m) [compound for double bars]
0.22          !collector bar thickness2 (|Z|>0, m)
0.30          !collector flex thickness1 (|X|>0, m)
0.10          !collector flex thickness2 (|Z|>0, m)
0.20          !Ledge width at Y+ wall, at bottom, including ram paste (m) |file Ledge.txt|
0.20          !Ledge width at Y- wall, at bottom, including ram paste (m) |overrides this|
0.25          !Ledge width at X+ wall, at bottom, including ram paste (m) |file Ledge.txt|
0.25          !Ledge width at X- wall, at bottom, including ram paste (m) |overrides this|

```

```

0.0          !distance between double collector bar axes in a cathode block
=====ANODE ARRANGEMENT=====
40          !Integer,number of anode stems (total per cell)
5           !Integer,number anode pins (per anode; min=1, max=4 snagl.row; 5:2*2, 6:3*2)
15.96      !interval (last)-(first) of anode stem axes (X>0, m)
2.1        !Z-level of anode bus bar (bridge) centre (m)
1.84       !?interval between anode bridge bar axes (|Y|>0, m) 2.10
0.86       !Anode horizontal X-size (>0,m)
1.95       !Anode horizontal Y-size (>0,m)
0.19       !Average Y-gap between preb.anodes (>0,m) [=0 for Soderberg]
0.72       !lower Z-level where anode pins end (average) (m)
0.92       !Z-level where anode pins connect to stem (average) (m)
0.30       !Anode bridge bar thickness1 (|X|,|Y|>0, m)
0.50       !Anode bridge bar thickness2 (|Z|>0, m)
0.16       !Anode stem thickness1 (|X|>0, m)
0.16       !Anode stem thickness2 (|Y|>0, m)
0.155      !Anode pin thickness1 (|X|>0, m)
0.155      !Anode pin thickness2 (|Y|>0, m)
0.16       !Anode pin yoke thickness1 (|X|>0, m)
0.16       !Anode pin yoke thickness2 (|Y|>0, m)
=====BUS-BAR ARRANGEMENT=====
|SECTIONS OF CURRENT PATH TO NEXT CELL STARTING FROM CATHODE BARS|CROS.SECT.:in orientation
|---X---|---Y---|---Z---|=====|-----|=====|-----|=====|Thc1|Thc2| either X Y
|-6.15 ! 3.0 ! -0.85 !| Section| 1 !...to...| 4 ! bars | .2 ! .25! or X Z
|-8.33 ! 3.0 ! ! !| | | | | .2 ! .25! or Y Z
|-7.05 ! 3.0 ! ! !| Bar numbering starts at | .2 ! .25! (can be at
angle)
| ! ! -1.10 ! min X, max Y corner | .25! .2 !
| ! 3.33 ! ! ! and goes in growing order along X | .25! .2 !
| ! ! 1.00 ! ! ! | .25! .2 !
|-7.05 ! 4.80 ! 2.1 ! ! | .25! .2 !
|-7.14 ! 6.93 ! 2.1 ! ! | .25! .2 !
|-7.98 ! ! ! ! ! | .3 ! .5 !
|-8.46 ! ! ! ! ! | .3 ! .5 !
| ! 8.77 ! ! ! Last point at end of anode bridge | .3 ! .5 !
|-7.98 ! ! ! ! ! | .3 ! .5 !
|---X---|---Y---|---Z---|=====|-----|=====|-----|=====|Thc1|Thc2|
|-3.26 ! 3.0 ! -0.85 !| Section| 5 !...to...| 8 ! bars | .2 ! .25!
|-5.44 ! 3.0 ! ! !| | | | | .2 ! .25!
|-4.26 ! 3.0 ! ! !| | | | | .2 ! .25!
| ! ! -1.10 ! ! ! | .25! .2 !
| ! 3.33 ! ! ! ! | .25! .2 !
| ! ! 1.00 ! ! ! | .25! .2 !
| ! 4.80 ! 2.1 ! ! ! | .25! .2 !
| ! 6.93 ! 2.1 ! ! ! | .25! .2 !
| ! 8.77 ! 2.1 ! Last point at end of anode bridge | .2 ! .5 !
|---X---|---Y---|---Z---|=====|-----|=====|-----|=====|Thc1|Thc2|
|-0.36 ! 3.0 ! -0.85 !| Section| 9 !...to...| 12 ! bars | .2 ! .25!
|-2.54 ! 3.0 ! ! !| | | | | .2 ! .25!
|-1.26 ! 3.0 ! ! !| | | | | .2 ! .25!
| ! ! -1.10 ! ! ! | .25! .2 !
| ! 3.33 ! ! ! ! | .25! .2 !
| ! ! 1.00 ! ! ! | .25! .2 !
| ! 4.80 ! 2.1 ! ! ! | .25! .2 !
| ! 6.93 ! 2.1 ! ! ! | .25! .2 !
| ! 8.77 ! 2.1 ! Last point at end of anode bridge | .2 ! .5 !
|---X---|---Y---|---Z---|=====|-----|=====|-----|=====|Thc1|Thc2|
| 0.36 ! 3.0 ! -0.85 !| Section| 13 !...to...| 16 ! bars | .2 ! .25!
| 2.54 ! 3.0 ! ! !| | | | | .2 ! .25!
| 1.26 ! 3.0 ! ! !| | | | | .2 ! .25!
| ! ! -1.10 ! ! ! | .25! .2 !
| ! 3.33 ! ! ! ! | .25! .2 !
| ! ! 1.00 ! ! ! | .25! .2 !

```

	!	4.80	!	2.1	!							.25!	.2	!					
	!	6.93	!	2.1	!							.25!	.2	!					
	!	8.77	!	2.1	!							.2	!	.5	!				
	----	X----	----	Y----	----	Z----	=====	-----	=====	-----	=====	Thc1	Thc2						
	3.26	!	3.0	!	-.85	!	Section	17	!...	to...		20	!	bars		.2	!	.25!	
	5.44	!	3.0	!		!						.2	!	.25!					
	4.26	!	3.0	!		!						.2	!	.25!					
		!		!	-1.10	!						.25!	.2	!					
		!	3.33	!		!						.25!	.2	!					
		!		!	1.00	!						.25!	.2	!					
		!	4.80	!	2.1	!						.25!	.2	!					
		!	6.93	!	2.1	!						.25!	.2	!					
		!	8.77	!	2.1	!						.2	!	.5	!				
	----	X----	----	Y----	----	Z----	=====	-----	=====	-----	=====	Thc1	Thc2						
	6.15	!	3.0	!	-.85	!	Section	21	!...	to...		24	!	bars		.2	!	.25!	
	8.33	!	3.0	!		!						.2	!	.25!					
	7.05	!	3.0	!		!						.2	!	.25!					
		!		!	-1.10	!						.25!	.2	!					
		!	3.33	!		!						.25!	.2	!					
		!		!	1.00	!						.25!	.2	!					
	7.05	!	4.80	!	2.1	!						.25!	.2	!					
	7.14	!	6.93	!	2.1	!						.25!	.2	!					
	7.98	!		!		!						.3	!	.5	!				
	8.46	!		!		!						.3	!	.5	!				
		!	8.77	!		!						.3	!	.5	!				
	7.98	!		!		!						.3	!	.5	!				
	----	X----	----	Y----	----	Z----	=====	-----	=====	-----	=====	Thc1	Thc2						
	-6.65	!	-3.0	!	-.85	!	Section	25	!...	to...		27	!	bars		.3	!	.4	!
	-8.05	!	-3.0	!		!						.3	!	.4	!				
		!		!	-1.10	!						.35!	.3	!					
	-9.33	!		!		!						.35!	.3	!					
		!	3.63	!	-0.90	!						.35!	.3	!					
	-7.05	!		!		!						.35!	.3	!					
		!		!	.80	!						.35!	.3	!					
	-7.05	!	5.0	!	1.90	!						.35!	.3	!					
	-7.14	!	6.93	!	2.1	!						.35!	.3	!					
	----	X----	----	Y----	----	Z----	=====	-----	=====	-----	=====	Thc1	Thc2						
	-5.95	!	-3.0	!	-.85	!	Section	28	!...	to...		28	!	bars		.3	!	.2	!
	-6.05	!	-3.7	!		!						.3	!	.2	!				
	-8.05	!		!		!						.3	!	.2	!				
	-8.05	!	-3.0	!		!						.3	!	.2	!				
	----	X----	----	Y----	----	Z----	=====	-----	=====	-----	=====	Thc1	Thc2						
	-3.26	!	-3.0	!	-.85	!	Section	29	!...	to...		32	!	bars		.3	!	.4	!
	-5.44	!	-3.0	!		!						.3	!	.4	!				
	-5.20	!	-3.0	!		!						.3	!	.4	!				
		!		!	-1.40	!						.5	!	.3	!				
	-9.83	!		!		!						.5	!	.3	!				
		!	3.63	!	-1.20	!						.5	!	.3	!				
	-4.26	!		!		!						.5	!	.3	!				
		!		!	.80	!						.5	!	.3	!				
		!	5.0	!	1.90	!						.5	!	.3	!				
		!	6.93	!	2.1	!						.5	!	.3	!				
	----	X----	----	Y----	----	Z----	=====	-----	=====	-----	=====	Thc1	Thc2						
	-0.36	!	-3.0	!	-.85	!	Section	33	!...	to...		36	!	bars		.3	!	.5	!
	-2.54	!	-3.0	!		!						.3	!	.5	!				
	-2.30	!	-3.0	!		!						.3	!	.5	!				
		!		!	-1.70	!						.5	!	.3	!				
	-9.33	!		!		!						.5	!	.3	!				
		!	3.63	!	-1.50	!						.5	!	.3	!				
	-1.26	!		!	-1.70	!						.5	!	.3	!				
		!		!	.80	!						.5	!	.3	!				
		!	5.0	!	1.90	!						.5	!	.3	!				
		!	6.93	!	2.1	!						.5	!	.3	!				

```

|----X---|----Y---|----Z---| |=====|-----|=====|-----|=====|Thc1|Thc2|
| 0.36 ! -3.0 ! -.85 ! | Section| 37 !...to...| 40 ! bars | .3 ! .5 !
| 2.54 ! -3.0 ! ! | | | | | .3 ! .5 !
| 0.80 ! -3.0 ! ! | | | | | .3 ! .5 !
| ! ! -2.00 ! | | | | | .6 ! .3 !
| -9.83 ! ! ! | | | | | .6 ! .3 !
| ! 3.63 ! -1.80 ! | | | | | .6 ! .3 !
| 1.26 ! ! -2.20 ! | | | | | .6 ! .3 !
| ! ! .80 ! | | | | | .6 ! .3 !
| ! 5.0 ! 1.90 ! Last point at end of anode bridge | .6 ! .3 !
| ! 6.93 ! 2.1 ! | | | | | .6 ! .3 !
|----X---|----Y---|----Z---| |=====|-----|=====|-----|=====|Thc1|Thc2|
| 3.26 ! -3.0 ! -.85 ! | Section| 41 !...to...| 44 ! bars | .2 ! .4 !
| 5.44 ! -3.0 ! ! | | | | | .2 ! .4 !
| 4.50 ! -3.0 ! ! | | | | | .5 ! .3 !
| ! ! -1.50 ! | | | | | .5 ! .3 !
| 9.83 ! -3. ! ! | | | | | .5 ! .3 !
| ! 3.63 ! -1.10 ! | | | | | .5 ! .3 !
| 4.26 ! ! -1.10 ! | | | | | .5 ! .3 !
| ! ! .80 ! | | | | | .5 ! .3 !
| ! 5.0 ! 1.90 ! Last point at end of anode bridge | .5 ! .3 !
| ! 6.93 ! 2.1 ! | | | | | .5 ! .3 !
|----X---|----Y---|----Z---| |=====|-----|=====|-----|=====|Thc1|Thc2|
| 6.15 ! -3.0 ! -.85 ! | Section| 45 !...to...| 48 ! bars | .3 ! .4 !
| 8.33 ! -3.0 ! ! | | | | | .3 ! .4 !
| 8.10 ! ! ! | | | | | .3 ! .4 !
| ! ! -1.20 ! | | | | | .4 ! .3 !
| 9.33 ! -3. ! ! | | | | | .4 ! .3 !
| ! 3.63 ! -0.80 ! | | | | | .4 ! .3 !
| 7.05 ! ! ! | | | | | .3 ! .4 !
| ! ! .80 ! | | | | | .4 ! .3 !
| 7.05 ! 5.0 ! 1.90 ! Last point at end of anode bridge | .4 ! .3 !
| 7.14 ! 6.93 ! 2.1 ! | | | | | .4 ! .3 !
|-----|-----|-----| |-----|-----|-----|-----|-----|
| Current-carrying bars,optional (connected to network if Current=0) |
|---X1---|---Y1---|---Z1---| |---X2---|---Y2---|---Z2---| |Current |Thc1|Thc2|
|-20.0 ! -2.0 ! -2.0 ! | -20.0 ! 2.0 ! -2.0 ! | 0.1 !0.50!0.30!
|-----|-----|-----| |-----|-----|-----| |-----|-----|

```

The file 'BUSNET' is the largest and the most important input of the data for the cell arrangement in the row and the whole busbar network design.

The specific data input starts at the third line of the file with a character information label describing the current project. In this case it is: `New500` .

In the first part of 'BUSNET' the input manner is very similar to 'DATA', where the first 16 columns are used for the input.

Line number 5 offers to define the type of the cell: ('2') corresponds to side-to-side, or ('1') – to end-to-end type. Note, that these and similar inputs are integer numbers (without a decimal point). This determines also the coordinate orientation: always the longer cell side along x. Thus, side-to-side cells will have y-axis along the line current *I* and x-axis pointing to the right, see Figure 6.

The next two rows prescribe how many cells will be represented in the present simulation. The cells are numbered according to the Figure 12, starting with the test cell (1) where the full hydrodynamics are computed. The maximum currently implemented is 6 cells in the main row. In principle this number can be increased, but for optimum execution time we choose 6 or less. For the return row there is an option to eliminate its effect completely (for tests) by setting the parameter '-1', or to represent it as a single current line: '0' (the last option may turn out to be very good approximation in order to save some computational time). The maximum number of the cells in the return row presently can be set as 4. The rest of the two lines will be simulated by the long supply bars (see for example Figure 6).

The x- and y-positions of the next cell centre will determine how the cell structure is continued periodically. For the side-to-side cells x-position indicates where the return row is located, and the y-position – how close the cells are positioned in the main row. Note, that the y-position in this case must be complying with the sections inputs for the anode ring position (see later the second part of the 'BUSNET').

The next two lines give an option to prescribe the position of the test cell along the main line. This can be used to model the cells close to the end of line.

The level of bars connecting to the return line will prescribe the position of these bars.

Then follows the information regarding the cathode arrangement, starting with the total number of the collector bars per cell. It must be an even number. If there are double bars per cathode block, then it is safer to account for these as blended together. The user can experiment with these settings, just bearing in mind that the interval between the bars will be regular.

The interval length between the first and the last collector bars along the same side will determine the positioning of the equidistant bars in the cathode.

z-level of cathode collector bars will prescribe the position of the central axis of this bar.

The collector bar will start at the prescribed distance from the central axis, and will continue to the given end point. These settings will affect the current distribution at the bottom of liquid metal.

The collector bar thickness is prescribed first for the horizontal dimension, second - for the vertical.

The same input follows for the collector flex thickness.

Finally, there is an option to prescribe a uniform ledge width along each side of the cavity. This ledge in the model includes the ramming paste and the non-conducting layer of the ledge on the cell bottom. The given 'ledge width' in the model is the electrically insulating strip along the perimeter of the cell cavity. The external boundary is at the cell cavity end dimension (as given in 'DATA'). The file 'Ledge.txt' is an optional input which will override these parameters, if such detailed information is available (see below).

The anode arrangement follows similar rules. The first input is again the total number of anode stems per cell (integer number). Note, that this formulation permits also the input for Soderberg type of cells (the anode size is respectively larger).

The anode pin number per anode permits to use the following option how each anode stem is branching to the pins: 1 – will use a single pin in the centre of anode, 2 – two equally spaced pins, 3 – three equally spaced pins, 4 – four equally spaced pins in single row, 5 – will place four pins in two rows, 6 – six pins in two rows. This arrangement meets the majority of practical design versions, yet considerably simplifies the user input effort.

The interval length for the last - first anode stem positions will prescribe the positioning of all the anode stems at equidistant positions along the cell length.

The anode bridge level (for its central axis) and the interval between the opposite bridge sides are given.

The anode horizontal dimensions are given both for the pre-bake type, and the Soderberg type, which will be recognised by the given anode size at this stage.

The y-gap between the pre-bake anodes defines the central channel width. It is zero for the Soderberg.

The other inputs prescribe the dimensions of the anode pins, yoke, stems and the bridge bar.

The Part 2 of the 'BUSNET' prescribes the electrically insulated path of the connected bars from the test cell to the next cell given by the crucial node points (see Figure 20 for the overall view). Each section contains certain number of the collector bars numbered in the growing order as shown in Figure 20 (starting in the left downstream corner: min x, max y coordinates). The numbering proceeds along the x-direction, then similarly along the upstream side. The first and the second lines for each section contain the coordinates for the cathode bar start and end points for that particular section. The respective cathode collector bars within the indicated number range will be automatically connected to this bar via flexes of previously given cross-section dimensions. The arrangement of the sections and the bar numbering are shown in Figure 21. The following lines prescribe the coordinates of the node points for the connected bars in their path to the risers and ending at the anode bridge. In the second part of 'BUSNET', prescribing

the SECTIONS OF CURRENT PATH..., the empty fields mean that the program will repeat the same value of the coordinate as the last given above in the same section (see the example file). Bars can be oriented at arbitrary angles. Their thickness defines the respective cross-section normal to the length given by the input coordinates for the bar central axis connection nodes. If the coordinates of any bar end-points coincide, there is electrical connection, otherwise the sections will go isolated to the anode bridge bars as prescribed in the section path. The rule of the electrical connection is valid not only for the same section, but also for all the network bars. In this way electrical connections between the various sections can be optionally given. The max number of points in a single section is 200.

Additional electrical connections between the nodes, e.g., given in the SECTIONS list, can be arranged using the part 'Current-carrying bars...' (at the end of the file). This part of the bar data permits also to prescribe the bar current (optionally). If the current value is set equal to 0 (zero), the program will attempt to connect this bar to the general network and to compute the current in it from the respective equations (1) constructed for the whole circuit. If the current in the 'Current-carrying bars...' is given as non-zero, these bars will be used to construct an independent electrical circuit, as for example for the 'booster' loops or lines in order to modify the magnetic field.

The more nodes will be input in the section path, the more accurate the representation of the curves, etc. The last node point in each section is recommended to position at the desired location on the anode bridge, otherwise the connection to the nearest anode ring bar will be created automatically.

The anode crossbar can be created without any duplication of the bars in the anode bridge structure. As a guide the following procedure is suggested:

- 1) Finish the riser at the upstream anode bridge bar: in the example below that would be at x,y,z:
 | -7.8 ! 6.005 ! 2.655
- 2) Create in the 'additional bars' a connection at the upstream side and the cross-bar starting at the anode rod position closest to the cross-bar, then the bar itself, and the connection at the downstream side to the closest anode rod (symmetrically as at the upstream side):

```
| -8.97 ! 6.005 ! 2.655 !| -8.503 ! 6.005 ! 2.655 !| 0. | .20! .55!
| -8.503 ! 6.005 ! 2.655 !| -8.503 ! 7.595 ! 2.655 !| 0. | .35! .33!
| -8.97 ! 7.595 ! 2.655 !| -8.503 ! 7.595 ! 2.655 !| 0. | .20! .55!
```

- 3) The missing connections between the riser and the cross-bar will be created automatically.
- 4) Do not try to duplicate the connection path further from the first connection of the riser at the upstream side – that is the main problem that you are trying to create bars which overlap the existing connections, leading to false duplicate bars!
- 5) Check the current distribution using FI.plt which is best suited for the current path visualization.

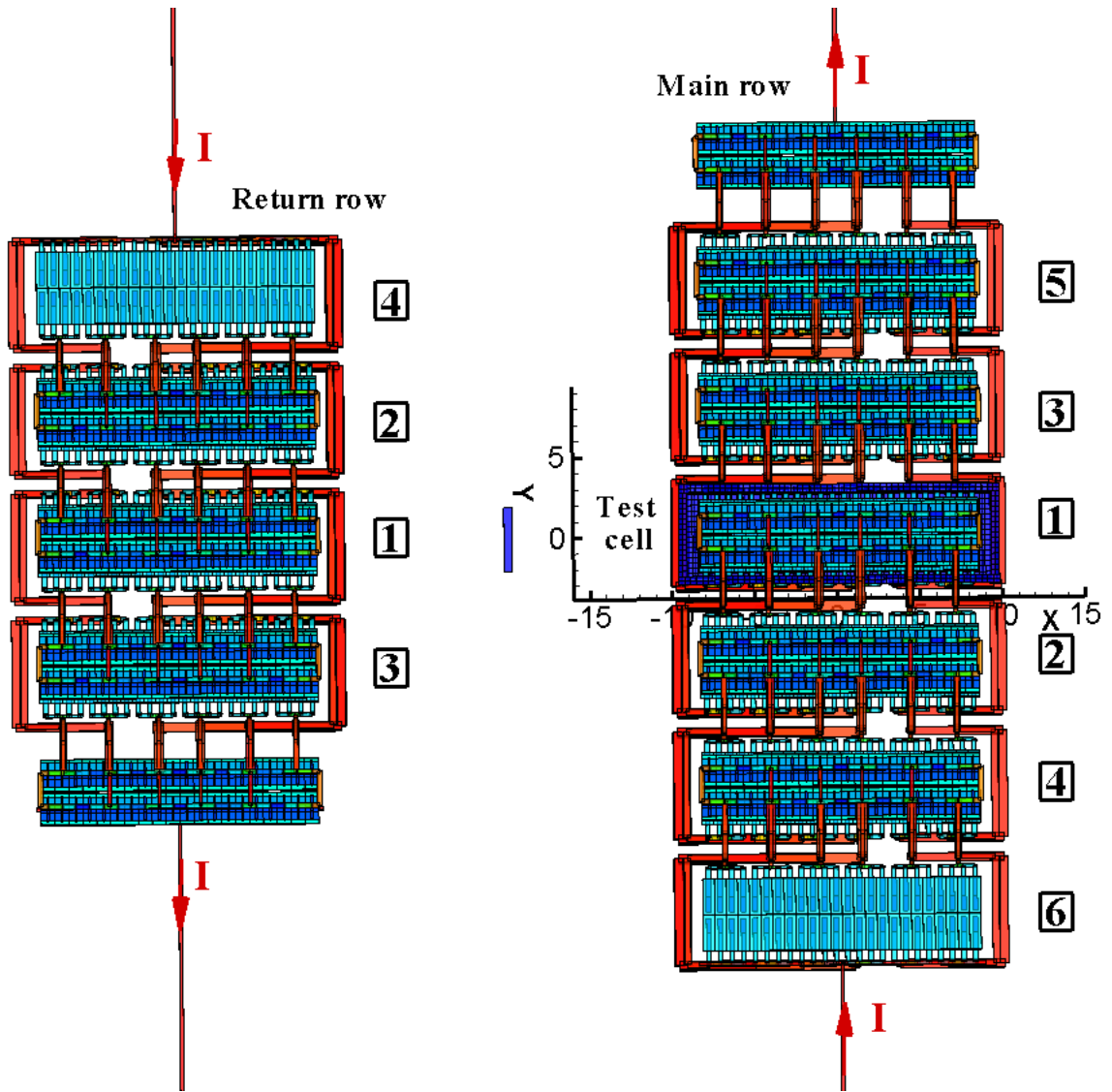


Figure 20. The arrangement of the cells, coordinates, line current I direction, and the sequence of the cells in the file 'BUSNET'.

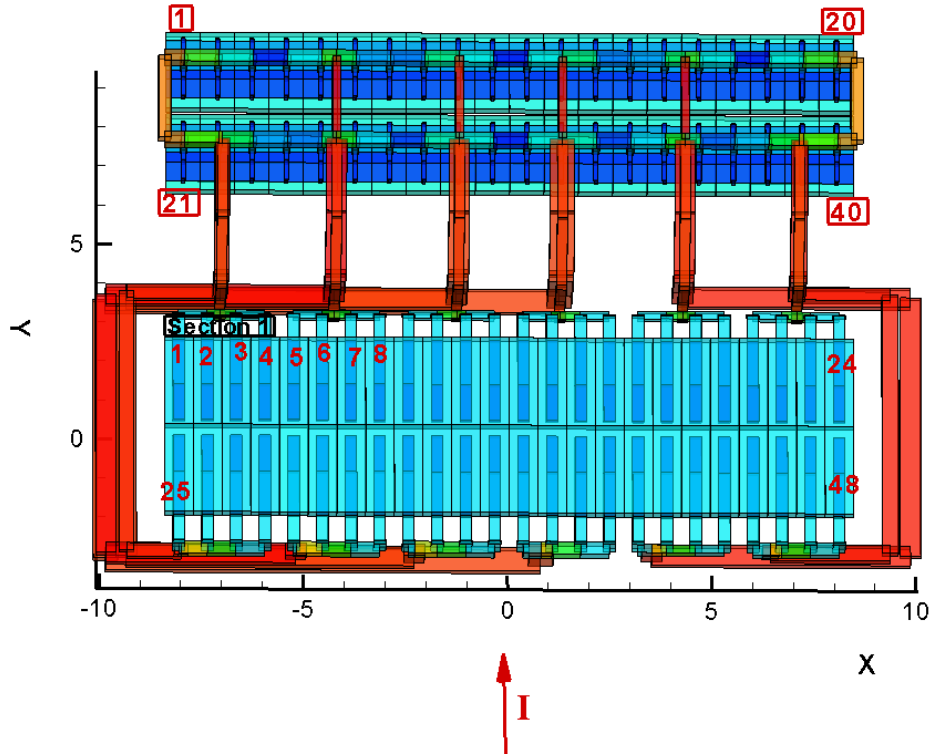


Figure 21. The arrangement of coordinates, numbering of the cathode collector bars in the sections, the anodes and the current I direction in the file 'BUSNET'.

Individual heat transfer coefficient and ambient temperature for each bar

The update of the program permits to use the old style 'BUSNET' or optionally the new format containing 2 additional columns. The indicator for the new format is the character 'Htr' appearing before the sections input start in the header line:

```
|SECTIONS OF CURRENT PATH TO NEXT CELL STARTING FROM CATHODE BARS|CROS.SECT| HtrC| Tair|CROS.SECT:
```

If the 'Htr' parameter appears before the sections input, the two columns permitting input of the Heat Transfer coefficient D (instead of the one given in 'DATA') will be used to read the optional inputs of the individual heat transfer coefficients (format F5.x) and the environment air temperature T (format I5 or F5.x) for selected bar to adjust temperatures according to measurements or ANSYS results. If the number in the column is empty or equals 0. , then the default value given in DATA will be used. This is an example:

```
|          ! 3.110 !          !          | .275! .775!          !          |
|          !          ! 0.680 ! Riser#2      | .275! .775!          !          |
| -2.235 ! 3.914 ! 2.386 !          | .275! .775!          ! 400 !
```

In this example case 'blowing' 400 deg C air at the riser #2 increases its temperature and the electrical resistance grows, the resulting current drops by approximately 10 kA in this riser, being redirected to other risers, and the cell could be destabilized, leading to the MHD wave appearance.

Obviously, this input works for the bars created in the 'SECTIONS' input and the 'Current-carrying bars' if the input 'Current' = 0. (this indicates that the bar is connected in the network to compute the current distribution).

The update does not include the option for the cathode flexes and the anode stems because these elements are not created explicitly as individual items within the 'BUSNET' input, rather being generated automatically.

Model busbar of a stopped pot or damaged busbar on a pot (one local pot).

These features are realized using the new input options in the file **BUSNET** shown as additional optional lines:

```
DATA INPUT(w=16) | BUSNET: EXPLANATIONS and COMMENTS
=====
500kA          !character, cell identification (max length 12)
=====CELL POSITION & ORIENTATION=====
2              !Integer,orientation:1 end-to-end(line current I in X);2 side-to-side(I in Y)
8              !Integer,number of cells represented in the same row: max 8
6              !cells in return row: max 6, 0 line only,-1 nothing,|-2,..,-6|cells only
-50.           !X-position of next cell centre in cell-cavity longitudinal direction (m)
7.85           !Y-position of next cell centre in cell-cavity transverse direction (m) 6.85
105.           !cell centre distance to beginning of line (>0, m) 105. 4.75
105.           !cell centre distance to end of line (>0, m) 105. 4.5
-0.85          !level of bars connecting to the return line, Z-level (m)
-10.9          !cut-out cell elements start (m) -10.9
-4.75          !cut-out cell elements end (m) -4.75
0.             !cut-out return-line cell elements start (m) -10.9
0.             !cut-out return-line cell elements end (m) -4.75
=====CATHODE ARRANGEMENT=====
48             !Integer,number of cathode bars (total)
.....
```

The resulting busbar arrangement is shown in the Figure 22. The new connection between the preceding and the test cell should be created using the additional bar input at the end of the file **BUSNET** according to the specific engineering options for the cut-out cell by-pass. The Figure 22 shows the resulting magnetic field in the test cell at the liquid metal level.

The option is implemented for the side-by-side and the end-to-end cells.

Additional options in **BUSNET** are available for the return line cells by prescribing the respective inputs:

```
6              ! cells in return row: max 6, 0 line only, -1 nothing,|-2,..,-6|cells only
```

or alternatively if the line current connecting bars should be removed as:

```
-6            ! cells in return row: max 6, 0 line only, -1 nothing,|-2,..,-6|cells only
```

The total number of the cells in the main line is up to 8, and in the return row – up to 6 cells are permitted. This feature is implemented for the side-by-side and the end-to-end cells. The return line cut-out features can be controlled separately.

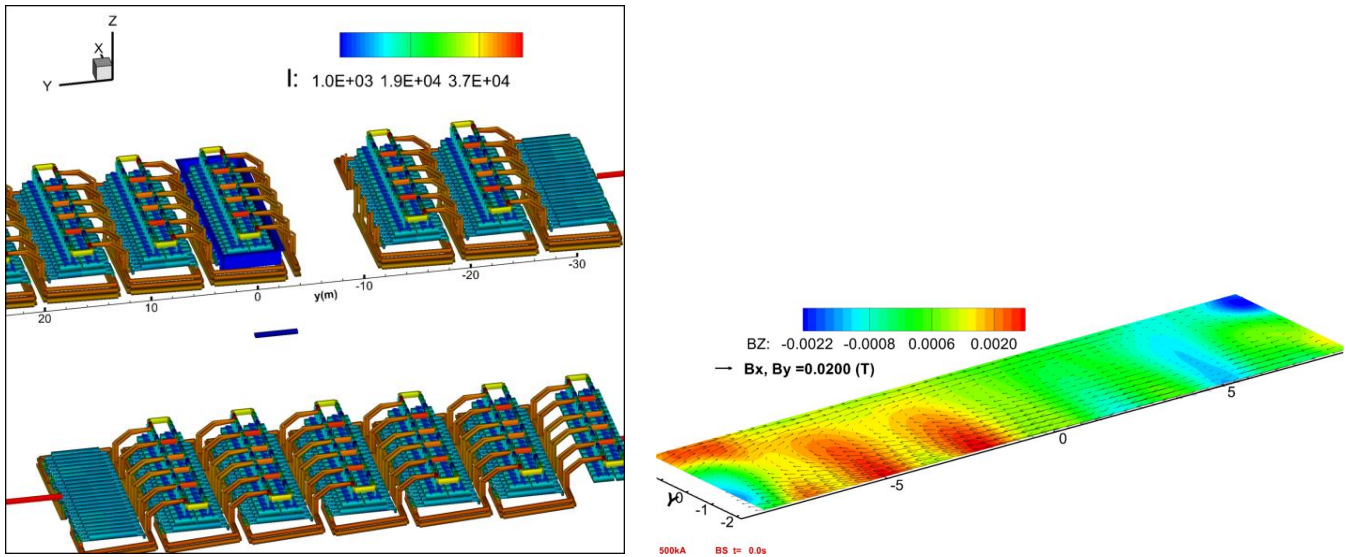


Figure 22. The effect of the cut-out cell on the magnetic field.

Possibility to create a special busbar system representing the pot exiting the row at the end of a row and at the passageway

For the end pot at the exit of the pot row, the cathode busbars are not connected to the anode risers and the anode busbar of the inexistent next pot, but to the end of the crossover between pot rows. At the passageway the exiting pot busbar is connected to anode busbar far away. These special end or passageway busbars should be generated in the **BUSNET** file so that the program will know that this busbar network applies only to one pot and is not to be repeated for the upstream and downstream pots. The program includes option to create end of line cells with different supply path to optimize the magnetic field and electric current in these cells. This is a complicated add-on, requiring the special know-how input. In fact the 3 separate cell busbar connections are now computed in the line positioning: the test cell, upstream and downstream cells. The solutions are output to BARSIN, BARSIN1, BARSIN2 and BARSOT, BARSOUT2.

If the cell is a regular one in the middle, with periodic continuation – the results are not changing from the previous.

These features can be used with the file **BUSNET** prescribing the newly created combination of the ‘cut-out’ and the ‘end of line’ definition combined with the return row definition using the negative number of the cells:

```

DATA INPUT(w=16) | BUSNET: EXPLANATIONS and COMMENTS
=====
500kA          !character, cell identification (max length 12)
=====CELL POSITION & ORIENTATION=====
2              !Integer,orientation:1 end-to-end(line current I in X);2 side-to-side(I in Y)
8              !Integer,number of cells represented in the same row: max 8
6              ! cells in return row: max 6, 0 line only, -1 nothing,|-2,...,-6|cells only
-50.          !X-position of next cell centre in cell-cavity longitudinal direction (m)

```

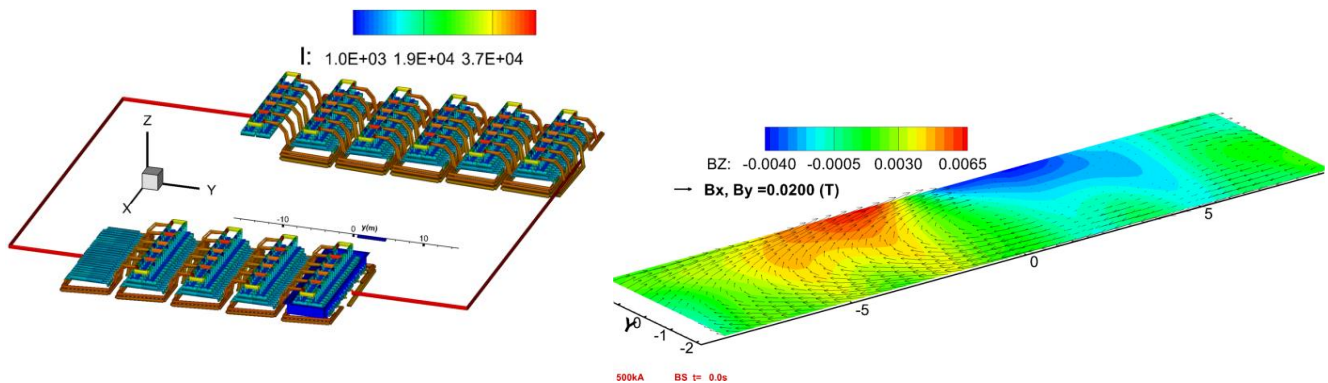
```

7.85      !Y-position of next cell centre in cell-cavity transverse direction (m) 6.85
45.       !cell centre distance to beginning of line (>0, m) 105. 4.75
20.       !cell centre distance to end of line (>0, m) 105. 4.5
-0.85    !level of bars connecting to the return line, Z-level (m)
3.7      !cut-out cell elements start (m) -10.9 4.5
25.      !cut-out cell elements end (m) -4.75
0.       !cut-out return-line cell elements start (m) -10.9 4.5
0.       !cut-out return-line cell elements end (m) -4.75

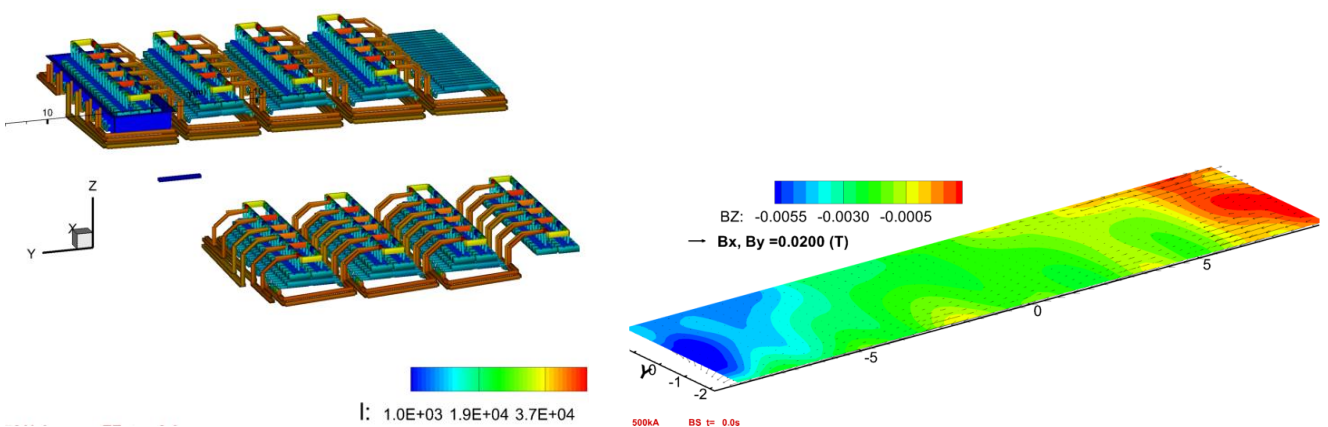
```

Examples shown in the Figure 23 are for the case of line connection preserved. The case without a line connection – in the Figure 24. The latter will require the connections to be created using the ‘additional bars’ feature at the end of the file **BUSNET** leading to optimized end line connections as for instance shown in the Figure 25.

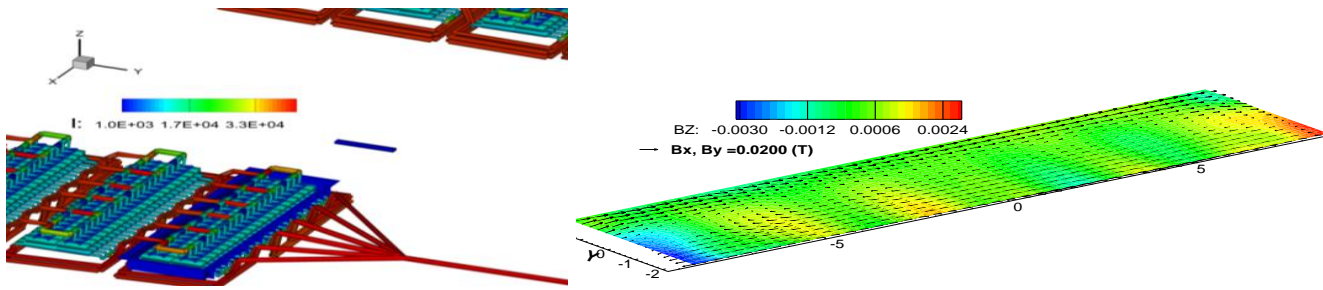
The magnetic field z-component in this case (Figure 25) is below the values of a typical mid-line cell, leading to a stable interface dynamics (Figure 26).



Figures 23. The effects of the end of line cell when the line bus is preserved.



Figures 24. The effects of the end of line cell when the line bus is removed.



Figures 25. The optimized compensating bus arrangement and the magnetic field at the liquid metal for the end of line cell.

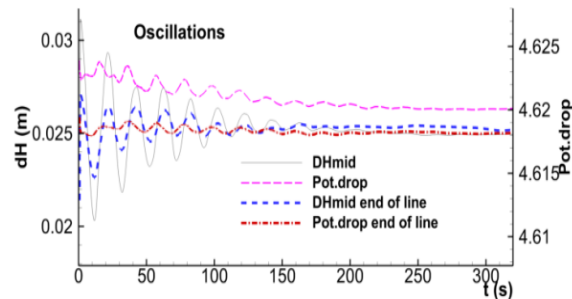


Figure 26. Effect of the optimized compensating bus arrangement on the wave behavior in comparison with the stable mid line cell.

The case shown in the pictures is optimised both for the electric current balance and the magnetic field, which leads to the MHD stable cell at the line entry. In order to create the correct electrical network the ‘Additional bars’ are used with the following settings for the respective value of the Current:

- 1.0 is for connections to the cell N 1 which is the test cell itself. It is to be used when the test cell is the last in the line and the downstream bars need to be cut.
- 2.0 is for connections to the cell N 2 which is the upstream cell before the test cell. This needs to be cut to model the first cell in the line.
- Both will be connected to the electrical network ending with the one equipotential point where the full line current enters or leaves. This last bar could be any size, even a symbolic very tiny one where all previous bars are joined.
- Current 0.0 additional bars will be added to all periodically replicated regular cells.

When using the cut out and additional bars the file RESULTS will contain messages about 1neighbour bars.

- these messages are useful while creating the connections from the initial standard case. They are kept to pinpoint to possible lost connections. There is an option in the MENU:
- 0 |0=block bar graphical output if bar current < 10 A; 1=permit output
- Try setting it to 1 and you will see all those disconnected bars, not useful after the arrangement is finished, therefore use option 0 afterwards.

The main point to pay attention is the order how the additional bars are input, see the comment at end of BUSNET:

- downstream bars: last (.) must be the outermost
- upstream bars: 1-st (.) must be the outermost

File 'Steelplates'

The file 'Steelplates' allows the user to input the ferromagnetic steel construction elements. For the input simplicity it is arranged as a collection of rectangular plates oriented along the Cartesian coordinate axes. The number of rectangular plates can be very large (up to 10000), and additionally each plate is divided in elements, the number for which is chosen by the user (last three columns). The sloped or inclined parts of the cell structure can be easily represented by the step-like arrangement of smaller size plates. The rectangular element (of variable sizes) discretisation permits to apply a particular technique for the nonlinear magnetization equation set, which is easy to invert for the solution. Therefore the iterations for the nonlinear solution converge relatively fast in comparison to other problem statements. The larger the number of the plates and the element divisions, the more accurately the geometry will be represented. Typically 10 000 – 40 000 elements can be successfully used to obtain an initial converging solution in few minutes of PC time. The larger number of the elements will slow down the execution time. After the initial state convergence is achieved, the required solution at the following time steps is close to the initial, and normally takes a fraction of a second to update the magnetic field from steel elements.

In order to avoid inconsistencies in the steelplates meshing leading to huge errors in the magnetic field, there is a built in a safeguard against numerically unstable mesh division. At the first input of the plate the division along the longest dimension should be not less than 90 elements (the first line input). Then for all other divisions this is imposed as the maximum size of the element. This results in uniformly discretised steel plates. However user can always prescribe even finer mesh, if the available RAM permits up to 4 000 000 elements in total. Eventually this simplifies input, permitting course elements division, which is automatically refined. However, still some caution is recommended.

N	x1, m	y1, m	z1, m	x2, m	y2, m	z2, m	Nx(elem)	Ny(elem)	Nz(elem)	Comments
1	-9.20	-2.60	-0.80	9.20	2.60	-0.79	54	16	1	bottom
2	-9.21	-2.60	-0.80	-9.20	2.60	0.80	1	16	8	box
3	9.20	-2.60	-0.80	9.21	2.60	0.80	1	16	8	
4	-9.20	-2.61	-0.80	9.20	-2.60	0.80	54	1	8	
5	-9.20	2.60	-0.80	9.20	2.61	0.80	54	1	8	
6	-9.70	-3.10	0.80	9.70	-2.60	0.81	54	2	1	deck
7	-9.70	2.60	0.80	9.70	3.10	0.81	54	2	1	
8	-9.70	-2.60	0.80	-9.20	2.60	0.81	2	16	1	
9	9.20	-2.60	0.80	9.70	2.60	0.81	2	16	1	
10	-8.71	-2.90	-1.10	-8.70	2.90	-0.80	1	16	2	bott.r.
11	-7.71	-2.90	-1.10	-7.70	2.90	-0.80	1	16	2	
12	-6.71	-2.90	-1.10	-6.70	2.90	-0.80	1	16	2	
13	-5.71	-2.90	-1.10	-5.70	2.90	-0.80	1	16	2	
14	-4.71	-2.90	-1.10	-4.70	2.90	-0.80	1	16	2	
15	-3.71	-2.90	-1.10	-3.70	2.90	-0.80	1	16	2	
16	-2.71	-2.90	-1.10	-2.70	2.90	-0.80	1	16	2	
17	-1.71	-2.90	-1.10	-1.70	2.90	-0.80	1	16	2	
18	-0.71	-2.90	-1.10	-0.70	2.90	-0.80	1	16	2	
19	0.70	-2.90	-1.10	0.71	2.90	-0.80	1	16	2	
21	1.70	-2.90	-1.10	1.71	2.90	-0.80	1	16	2	
22	2.70	-2.90	-1.10	2.71	2.90	-0.80	1	16	2	
23	3.70	-2.90	-1.10	3.71	2.90	-0.80	1	16	2	
24	4.70	-2.90	-1.10	4.71	2.90	-0.80	1	16	2	
25	5.70	-2.90	-1.10	5.71	2.90	-0.80	1	16	2	
26	6.70	-2.90	-1.10	6.71	2.90	-0.80	1	16	2	
27	7.70	-2.90	-1.10	7.71	2.90	-0.80	1	16	2	
28	8.70	-2.90	-1.10	8.71	2.90	-0.80	1	16	2	
30	-8.71	-2.90	-0.80	-8.70	-2.60	0.80	1	2	6	side.r.
31	-7.71	-2.90	-0.80	-7.70	-2.60	0.80	1	2	6	
32	-6.71	-2.90	-0.80	-6.70	-2.60	0.80	1	2	6	
33	-5.71	-2.90	-0.80	-5.70	-2.60	0.80	1	2	6	
34	-4.71	-2.90	-0.80	-4.70	-2.60	0.80	1	2	6	
35	-3.71	-2.90	-0.80	-3.70	-2.60	0.80	1	2	6	
36	-2.71	-2.90	-0.80	-2.70	-2.60	0.80	1	2	6	
37	-1.71	-2.90	-0.80	-1.70	-2.60	0.80	1	2	6	
38	-0.71	-2.90	-0.80	-0.70	-2.60	0.80	1	2	6	

39	0.70	-2.90	-0.80	0.71	-2.60	0.80	1	2	6	
40	1.70	-2.90	-0.80	1.71	-2.60	0.80	1	2	6	
41	2.70	-2.90	-0.80	2.71	-2.60	0.80	1	2	6	
42	3.70	-2.90	-0.80	3.71	-2.60	0.80	1	2	6	
43	4.70	-2.90	-0.80	4.71	-2.60	0.80	1	2	6	
44	5.70	-2.90	-0.80	5.71	-2.60	0.80	1	2	6	
45	6.70	-2.90	-0.80	6.71	-2.60	0.80	1	2	6	
46	7.70	-2.90	-0.80	7.71	-2.60	0.80	1	2	6	
47	8.70	-2.90	-0.80	8.71	-2.60	0.80	1	2	6	
48	-8.71	2.60	-0.80	-8.70	2.90	0.80	1	2	6	side.r.
49	-7.71	2.60	-0.80	-7.70	2.90	0.80	1	2	6	
50	-6.71	2.60	-0.80	-6.70	2.90	0.80	1	2	6	
51	-5.71	2.60	-0.80	-5.70	2.90	0.80	1	2	6	
52	-4.71	2.60	-0.80	-4.70	2.90	0.80	1	2	6	
53	-3.71	2.60	-0.80	-3.70	2.90	0.80	1	2	6	
54	-2.71	2.60	-0.80	-2.70	2.90	0.80	1	2	6	
55	-1.71	2.60	-0.80	-1.70	2.90	0.80	1	2	6	
56	-0.71	2.60	-0.80	-0.70	2.90	0.80	1	2	6	
57	0.70	2.60	-0.80	0.71	2.90	0.80	1	2	6	
58	1.70	2.60	-0.80	1.71	2.90	0.80	1	2	6	
59	2.70	2.60	-0.80	2.71	2.90	0.80	1	2	6	
60	3.70	2.60	-0.80	3.71	2.90	0.80	1	2	6	
61	4.70	2.60	-0.80	4.71	2.90	0.80	1	2	6	
62	5.70	2.60	-0.80	5.71	2.90	0.80	1	2	6	
63	6.70	2.60	-0.80	6.71	2.90	0.80	1	2	6	
64	7.70	2.60	-0.80	7.71	2.90	0.80	1	2	6	
65	8.70	2.60	-0.80	8.71	2.90	0.80	1	2	6	side.r.

Steel element generation using only one quarter of the shell input

(other quarters are generated automatically by mirror flipping in cases when the steel is symmetric in both horizontal axes)

This feature is implemented as shown in the following 'steelplates' input file (Example 1):

N	x1, m	y1, m	z1, m	x2, m	y2, m	z2, m	Nx(elem)	Ny(elem)	Nz(elem)	Comments
1	0.	0.	-0.80	9.20	2.60	-0.79	27	8	1	bottom lcm
2	9.20	0.	-0.80	9.21	2.60	0.80	1	8	8	box
4	0.	2.60	-0.80	9.20	2.61	0.80	27	1	8	
6	0.	2.60	0.80	9.70	3.10	0.81	27	2	1	deck
8	9.20	0.	0.80	9.70	2.60	0.81	2	16	1	
Q										
10	-8.71	-2.90	-1.10	-8.70	2.90	-0.80	1	16	2	bott.r.
R	1.0						17			
30	-8.71	-2.90	-0.80	-8.70	-2.60	0.80	1	2	6	side.r.
R	1.0						17			
48	-8.71	2.60	-0.80	-8.70	2.90	0.80	1	2	6	side.r.
R	1.0						17			

In the preceding new style input file 'steelplates' the first lines until the one containing the letter Q in the first position (Q-marker line) are used to create the first quarter ($X > 0, Y > 0$) of the steel plates. Then the input Q tells to create a mirror image of the previous plates to the other 3 quarters.

The input lines before the marker 'Q' should be used to create only the plates defined for the positive values of the coordinates, otherwise an error message will be generated and the program will terminate. After the Q-marker line the input of arbitrary additional plates can be used.

The feature with 'R' in the first position of a line can be used to repeat the preceding line in order to create the number of plates required times with the given shift in x, y or/and z coordinates.

The R marker can be used before the Q marked line if the shifts are limited within the positive values of the x and y coordinates.

After the Q marked line, there is no restriction in using the marker R.

The following 2 inputs for the 'steelplates' will generate the same input as the Example 1:

Example 2. Without 'Q' reflection:

N	x1, m	y1, m	z1, m	x2, m	y2, m	z2, m	Nx(elem)	Ny(elem)	Nz(elem)	Comments
1	-9.20	-2.60	-0.80	9.20	2.60	-0.79	54	16	1	bottom lcm
2	-9.21	-2.60	-0.80	-9.20	2.60	0.80	1	16	8	box
R	18.41						1			rep.prev.Nx times,shift x1
4	-9.20	-2.61	-0.80	9.20	-2.60	0.80	54	1	8	
R		5.21					1			rep.prev.Nx times,shift y1
6	-9.70	-3.10	0.80	9.70	-2.60	0.81	54	2	1	deck
R		5.70					1			rep.prev.Nx times,shift y1
8	-9.70	-2.60	0.80	-9.20	2.60	0.81	2	16	1	
R	18.90						1			rep.prev.Nx times,shift x1
10	-8.71	-2.90	-1.10	-8.70	2.90	-0.80	1	16	2	bott.r.
R	1.0						17			
30	-8.71	-2.90	-0.80	-8.70	-2.60	0.80	1	2	6	side.r.
R	1.0						17			
48	-8.71	2.60	-0.80	-8.70	2.90	0.80	1	2	6	side.r.
R	1.0						17			

Example 3. Normal old style using all plates input (see above).

The discretization in elements of the 'steelplates' now uses the dynamic memory allocation for the storage, permitting the maximum of 4 million elements in total. However, the execution time will increase proportionally to the number of elements. We recommend to use less to retain a practically usable application run times. After the ferromagnetic solution is obtained the program generates automatically a new file 'Magnetization.dat' in the working directory. If this file is renamed as 'Magnetization.inp' and retained in the directory when a new run of the program is initiated, the magnetization values stored in the file will be used, avoiding the new lengthy iteration process. At all cases the steel elements are generated from the file 'steelplates' input. The total number of the steel elements should be exactly equal to the total element number stored in the 'Magnetization.dat', otherwise the error message is output and the program stops.

Instead of using an integer number of division for meshing (in x, y or z directions), the actual mesh size (in meters units) in each direction can be optionally prescribed in the same file 'steelplates', while preserving the number of divisions option to maintain compatibility with older version. The input of desirable mesh size will be imposed after reading the input file columns | Nx or dx| Ny or dy| Nz or dz| depending on the input:

if (Nx or dx) < 1, the decimal value of the dx will be used;

if (Nx or dx) >= 1, the integer value of the number will be used.

The inputs act similarly for the Ny and Nz inputs. The inputs are independent in all the directions, for instance, there could be Nx and dy input for the same plate. As a safeguard, the full plate will have at least one element in each direction. If the input discretization is too crude, the other safeguard will prevent the mesh size to exceed the default value = (max X – min X) / 200.

The option of the full quarter of the steel structure mirror reflection to remaining 3 quarters is retained. This action is initiated if the character 'Q' appears in the first column directly after the lines describing the first quadrant structure of the steel plates. The parameter 'Q' is permitted only once in the 'steelplates' input.

The other option of repeating the previous line of input using the character 'R' in the first column directly in the line following, is available both for the first quadrant input lines, and for the input lines following the first quadrant input. If the parameter 'R' appears in the first column, the previous line input will be repeated Nx times, using the shift of dx=x1, and/or dy=y1, and/or dz=z1. The parameter 'R' may appear as many times as needed after the preceding line being a regular input line.

The following input shows an example of the mixed input for the 'steelplates':

N	x1, m	y1, m	z1, m	x2, m	y2, m	z2, m	Nx or dx	Ny or dy	Nz or dz	M-type
16	4.044	2.255	0.053	4.038	2.315	0.247	1	1	1	1
Q										
1	4.851	-2.501	-1.080	4.839	-2.001	-0.920	0.01	0.01	0.01	1
R	0.012						1			
2	4.851	-2.501	-0.920	4.839	-2.001	-0.760	1	1	1	2
3	4.851	-2.001	-1.080	4.839	-1.501	-0.920	1	1	1	3
4	4.851	-2.001	-0.920	4.839	-1.501	-0.760	1	1	1	1

Restart using 'Magnetization.inp' as the initial approximation

In order to use the restart option using 'Magnetization.inp' as the initial approximation the new additional lines in the DATA file are required at the end of the file. An example of the DATA file last lines is given below, with the new additional lines in red:

```

...
0.005 |Initial 'sloshing'wave perturbation C(1,0), max amplitude (m)
0.06 |Empirical bottom friction coefficient (nondimensional) 0.075 0.04
0.000025 |Anode clamp average contact Resistance, Om 0.000025
0.0000125 |Cathode flex joint average contact Resistance, Om 0.0000125
0.0 |Initial 'sloshing'wave perturbation C(0,1), max amplitude (m) 0.005
0.0005 |ferromagnetic convergence criteria
0.05 |ferromagnetic mesh element max.size (m)
30 |ferromagnetic convergence max iteration N; 0 - no iteration 'magnetization.inp'
=====

```

Note, that all additional lines after the standard last line for the 'Empirical bottom friction' must be included to activate the Magnetization restart.

The new input permits to reset the number of iterations for the ferromagnetics to a new value, instead of the default value of 20. If the last line will be absent, it will run with 20.

The restart iteration feature is activated if the previously generated 'Magnetization.dat' file is renamed to 'Magnetization.inp' and it is included in the working directory. The iterations will start with the field and magnetization values stored in this file. The number of elements generated from the 'Steelplates' should be exactly the same, otherwise an error message will be output and the program stops.

If the parameter in the last line of DATA file for 'ferromagnetic convergence max iteration N' is set as 0, then the magnetization of the steel elements will be set as given in the file 'Magnetization.inp' and no iterations will be performed. This works exactly as in the previous versions, and the option should work in the same way as the default when the additional lines in DATA are absent. However, if the iteration number is given, say, 10 or 30, then the iterations will run using the magnetization input as the initial values.

It does not mean necessarily that the iterations will converge immediately. In a typical test it required 5 iterations to converge exactly to the same result as if running all iterations (in this case 16 iterations were needed). However, if the currents in the bus bar are not significantly different, the iterations will converge immediately. There is a safeguard to run at least 2 iterations due to the over-relaxation parameter used to start the iteration process in general case. Sometimes the reduced value of the 'ferromagnetic convergence criteria' is recommended to achieve a longer iteration process, say instead of the value 0.0005 a smaller value (e.g. 0.0004) can be entered. However there is a limitation that 'ferromagnetic convergence criteria' is ≥ 0.0001 .

Possible sources for incorrect performance of the restart option:

- not all optional lines included in the DATA file, say, one of the following is missing:

```

0.000025 |Anode clamp average contact Resistance, Om 0.000025
0.0000125 |Cathode flex joint average contact Resistance, Om 0.0000125

```

```

0.0      |Initial 'sloshing'wave perturbation C(0,1), max amplitude (m) 0.005
0.0005  |ferromagnetic convergence criteria
0.05    |ferromagnetic mesh element max.size (m)
0       |ferromagnetic convergence max iteration N; 0 - no iteration 'magnetization.inp'

```

- the number of elements generated from the Steelplates is extremely large. This formally has a limit of 4 million, however the test example is using '133308 ferromagnetic elements created'. In principle the convergence criteria could be reduced further because the average norm is defined in the program as $DFE=DFE/3/NBE/HMAX$! FEH solution error
- in this case reduce the 'ferromagnetic convergence criteria' significantly below 0.0005 , say to 0.00004 or even less if the iterations are formally converging in two iterations. However there is a limitation that 'ferromagnetic convergence criteria' is ≥ 0.0001 .

File 'MH'

The steel structure magnetic properties depend on the particular type of steel used. The file 'MH' is designed to give a user the possibility to input his own curve of the magnetization dependence on the magnetic field M(H) in A/m units. However, the supplied curve is reliable data obtained by directly measuring the M(H) curve for the samples taken from working reduction cell. The program uses a spline interpolation between the given points in the table.

```

N | M,A/m | H,A/m | Comments:
-----
1 | 16000. | 8. | |M and H in SI units (A/m), !
2 | 32000. | 16. | |H in growing order;
3 | 80000. | 40. | |minimum 5, maximum 100 points
4 |160000. | 80. | |
5 |480000. | 400. | |
6 |800000. | 800. | |
7 |1280000. |4000. | |
8 |1400000. |8000. | |
9 |1500000. |40000. | |
10 |1520000. |80000. | |

```

Multiple M-H curves

The option of multiple magnetization M(H) properties curves is implemented using the two files for input: 'MH' and 'steelplates'. The file 'MH' is supplemented with the two optional columns to input new M(H) data. The program permits input of up to 20 different magnetization M(H) curves supplied in the file 'MH'. The new input format maintains an option to use the old style 'MH' input file. The new format 'MH' input is given in the example below:

File 'MH' as used for the test cell '500 kA'

```

N | M,A/m | H,A/m | M2,A/m | M3...M20 columns; H in growing order, (5 - 100) points
4 |M(H):1 |-----2-----3-----4-----5-----6-----7-----8-----
1 | 1591.5 | 10. | 1591.5 | 1591.5 | 1591.5 | 1591.5 | 1591.5 | 1591.5 | 1591.5 |
2 | 13528.2 | 78. | 13528.2 | 13528.2 | 13528.2 | 13528.2 | 13528.2 | 13528.2 | 13528.2 |
3 | 20292.3 | 100. | 20292.3 | 20292.3 | 20292.3 | 20292.3 | 20292.3 | 20292.3 | 20292.3 |
4 | 31035. | 150. | 31035. | 31035. | 31035. | 31035. | 31035. | 31035. | 31035. |
5 | 40585. | 195. | 40585. | 40585. | 40585. | 40585. | 40585. | 40585. | 40585. |
6 | 151197. | 400. | 151197. | 151197. | 151197. | 151197. | 151197. | 151197. | 151197. |
7 | 223613. | 500. | 223613. | 223613. | 223613. | 223613. | 223613. | 223613. | 223613. |
8 | 477465. | 830. | 477465. | 477465. | 477465. | 477465. | 477465. | 477465. | 477465. |
9 | 580916. | 1000. | 580916. | 580916. | 580916. | 580916. | 580916. | 580916. | 580916. |
10 | 795775. | 1470. | 795775. | 795775. | 795775. | 795775. | 795775. | 795775. | 795775. |

```

11	962887.	2000.	962887.	962887.	962887.	962887.	962887.	962887.	962887.	962887.
12	1066338.	2500.	1066338.	1066338.	1066338.	1066338.	1066338.	1066338.	1066338.	1066338.
13	1145916.	3000.	1145916.	1145916.	1145916.	1145916.	1145916.	1145916.	1145916.	1145916.
14	1225493.	4000.	1225493.	1225493.	1225493.	1225493.	1225493.	1225493.	1225493.	1225493.
15	1273240.	4800.	1273240.	1273240.	1273240.	1273240.	1273240.	1273240.	1273240.	1273240.
16	1368733.	7200.	1368733.	1368733.	1368733.	1368733.	1368733.	1368733.	1368733.	1368733.
17	1432395.	10000.	1432395.	1432395.	1432395.	1432395.	1432395.	1432395.	1432395.	1432395.
18	1591549.	23000.	1591549.	1591549.	1591549.	1591549.	1591549.	1591549.	1591549.	1591549.
19	1710916.	50000.	1710916.	1710916.	1710916.	1710916.	1710916.	1710916.	1710916.	1710916.

If the data in M2, and/or Mn columns is absent, only the default M(H) data will be used, applying the appropriate spline interpolation when creating the new iterative runs.

The meaningful input starts at the 2nd line where an integer (1 – 20) gives an optional number of input columns for M values corresponding to the single H (A/m) values in the ferromagnetic plate. In the example above only 4 columns of M values will be used. The properties given in the numbered columns will be applied to the ferromagnetic elements created from the input file ‘Steelplates’ where the last column indicates the corresponding number of the M(H) curve created from the ‘MH’ input:

File ‘Steelplates’ as used for the test cell ‘500 kA’

N	x1, m	y1, m	z1, m	x2, m	y2, m	z2, m	Nx or dx	Ny or dy	Nz or dz	M-type
1	-9.20	-2.60	-0.80	9.20	2.60	-0.79	54	16	1	4
2	-9.21	-2.60	-0.80	-9.20	2.60	0.80	1	16	8	1
R	18.41						1			1
4	-9.20	-2.61	-0.80	9.20	-2.60	0.80	54	1	8	1
R		5.21					1			1
6	-9.70	-3.10	0.80	9.70	-2.60	0.81	54	2	1	1
R		5.70					1			1
8	-9.70	-2.60	0.80	-9.20	2.60	0.81	2	16	1	1
R	18.90						1			1
10	-8.71	-2.90	-1.10	-8.70	2.90	-0.80	1	16	2	1
R	1.0						17			1
30	-8.71	-2.90	-0.80	-8.70	-2.60	0.80	1	2	6	2
R	1.0						17			2
48	-8.71	2.60	-0.80	-8.70	2.90	0.80	1	2	6	3
R	1.0						17			3

The ‘Q’ and ‘R’ directives will preserve the previous lines inputs for the M(H) curves. If required the number of M-type columns input can be increased, however restricted in the present implementation to 20 curves. The new update of the program is supposed to be compatible with the old types of input files ‘MH’ and ‘Steelplates’. If the last column in ‘Steelplates’ is absent, then the first column of the M(H) will be used for all ferromagnetic elements. If the number given in the ‘M-type’ column exceeds the total number of the M(H) property columns, the M-type is set = 1.

Individual flex contact resistance

A new option to assign individual cathode flexes with different length/design option is introduced using a new separate file 'Flexes.txt' containing inputs in 3 columns: 1st is the number of collector bar; 2nd is the contact resistance in Om, 3rd – the length of the flex in m:

N	ContRes Om	Length m
1	0.	1.
2	0.00000125	0.
3	0.	0.
4	0.	0.
5	0.	0.

The image created from the FE.PLT or FF.PLT will appear as before for the automatically generated flexes geometrically connecting along the shortest path the end of collector bars and the cathode bars created in the 'BUSNET' as the sections. However in the resistance calculations the prescribed length for each bar will be used as in the file 'Flexes.txt'. If the zero value is given or the input field is empty, then the average contact resistance from DATA.dat will be used. The total number of the flexes should match the one given in the 'BUSNET'.

Force_out.plt

The files 'Force_out.plt' and 'BS.PLT' are continued to be output at the time steps when the Tecplot outputs are requested using the input in MENU:

```
20|Create data for TECPLOT files with N*dt frequency .GE.1 (0 - no)
```

Summary of the outputs stored in the files:

- 1) for the flat interface dH=0, Time=0,
- 2) for the initial quasi-stationary dH without the effect of velocities, Time=0.2s,
- 3) for the initial quasi-stationary dH with the effect of velocities, Time=0.5s,
- 4) then at the intervals requested in the MENU.

The format used to output in these files is the 'Point' type suitable for the Excel spread sheet analysis. The size of the files increases significantly using this format, if compared to the old type using the 'Duplicate' and 'Block' format for the time steps following the first one in the 'Point' type.

File 'Ledge.txt'

This file is created as the text output from the MS Excel table where the ledge can be input from the Thermolectric solution or as measured at the plant. If this file is present in the working directory, the data will override the uniform ledge inputs from 'BUSNET'. The first line in 'Ledge.txt' tells the total number of input points. The following lines each contain the number of the input point, x, y, z - coordinates of the ledge edge, assuming the coordinate origin in the centre of the cell. The z-coordinate is ignored. The points should run around the cell perimeter, covering as uniformly as possible the whole length. The ledge position is affecting the electric current distribution on the cell bottom and can be seen from Figure 4 (file JA.PLT).

```
496
1 0.0000 1.9251 0.8800
2 0.0557 1.9251 0.8800
```

3	0.1113	1.9251	0.8800
4	0.2530	1.9251	0.8800
5	0.3542	1.9251	0.8800
6	0.4554	1.9251	0.8800
7	0.5971	1.9251	0.8800
8	0.6527	1.9251	0.8800
9	0.7084	1.9251	0.8800
10	0.7641	1.9251	0.8800
11	0.8197	1.9251	0.8800
12	0.9614	1.9251	0.8800
13	1.0626	1.9251	0.8800
14	1.1638	1.9251	0.8800
15	1.3055	1.9251	0.8800
16	1.3611	1.9263	0.8800
17	1.4168	1.9275	0.8800
18	1.4725	1.9286	0.8800
19	1.5281	1.9303	0.8800
20	1.6698	1.9317	0.8800
21	1.7710	1.9342	0.8800
22	1.8722	1.9352	0.8800
23	2.0139	1.9361	0.8800
24	2.0695	1.9367	0.8800
25	2.1252	1.9368	0.8800
26	2.1809	1.9368	0.8800
27	2.2365	1.9367	0.8800
28	2.3782	1.9360	0.8800
29	2.4794	1.9349	0.8800
30	2.5806	1.9329	0.8800
31	2.7223	1.9314	0.8800
32	2.7779	1.9290	0.8800
33	2.8336	1.9281	0.8800
34	2.8893	1.9269	0.8800
35	2.9449	1.9252	0.8800
36	3.0866	1.9251	0.8800
37	3.1878	1.9251	0.8800
38	3.2890	1.9251	0.8800
39	3.4307	1.9251	0.8800
40	3.4863	1.9251	0.8800
41	3.5420	1.9251	0.8800
42	3.5977	1.9251	0.8800
43	3.6533	1.9251	0.8800
44	3.7950	1.9251	0.8800
45	3.8962	1.9251	0.8800
46	3.9974	1.9251	0.8800
47	4.1391	1.9251	0.8800
48	4.1947	1.9251	0.8800
49	4.2504	1.9251	0.8800
50	4.3061	1.9251	0.8800
51	4.3617	1.9251	0.8800
52	4.5034	1.9251	0.8800
53	4.6046	1.9251	0.8800
54	4.7058	1.9251	0.8800
55	4.8475	1.9251	0.8800
56	4.9031	1.9251	0.8800
57	4.9588	1.9251	0.8800
58	5.0145	1.9251	0.8800
59	5.0701	1.9251	0.8800
60	5.2118	1.9251	0.8800
61	5.3130	1.9251	0.8800
62	5.4142	1.9251	0.8800
63	5.5559	1.9251	0.8800
64	5.6115	1.9274	0.8800
65	5.6672	1.9284	0.8800
66	5.7229	1.9296	0.8800
67	5.7785	1.9312	0.8800
68	5.9202	1.9326	0.8800
69	6.0214	1.9348	0.8800
70	6.1226	1.9357	0.8800
71	6.2643	1.9364	0.8800
72	6.3199	1.9366	0.8800
73	6.3756	1.9366	0.8800

```

74 6.4313      1.9364 0.8800
75 6.4869      1.9361 0.8800
76 6.6286      1.9350 0.8800
77 6.7298      1.9338 0.8800
78 6.8310      1.9316 0.8800
79 6.9727      1.9298 0.8800
80 7.0283      1.9272 0.8800
81 7.0840      1.9260 0.8800
82 7.1397      1.9251 0.8800
83 7.1953      1.9251 0.8800
84 7.3370      1.9251 0.8800
85 7.4382      1.9251 0.8800
86 7.5394      1.9251 0.8800
87 7.6811      1.9251 0.8800
88 7.7367      1.9251 0.8800
89 7.7924      1.9251 0.8800
90 7.8481      1.9251 0.8800
91 7.9037      1.9251 0.8800
92 8.0454      1.9251 0.8800
93 8.1466      1.9251 0.8800
94 8.2478      1.9251 0.8800
95 8.3895      1.9251 0.8800
96 8.3915      1.9249 0.8800

```

File 'BARSIN'

This file is created automatically after the input from 'BUSNET' and it contains all the bars carrying electrical current. It is useful if additional connections are desired via the input from 'Current-carrying bars ...' in 'BUSNET'. The exact node position, required to achieve the electrical contact within the network, can be found from the 'BARSIN'.

For advanced users, the file 'BARSIN' gives extra opportunities to create more complicated bar designs (e.g., nonuniformly spaced anodes, collector bars, variable flexes, etc). In this case the file 'MENU' gives an option to create the network input from the previously created file 'BARSIN' ('BUSNET' is required as well). However, we can not guarantee that the user variation of the file BARSIN will be compatible with the automatic design requirements. This will be always the case with the input from 'BUSNET' only.

New500

N	X1	Y1	Z1	X2	Y2	Z2	Thc1	Thc2	Rho	TCo	Description
1	-8.070	1.122	0.000	-8.070	1.122	-0.450	0.70	2.24	.14E-04		Cath.carb. 1
2	-7.368	1.122	0.000	-7.368	1.122	-0.450	0.70	2.24	.14E-04		Cath.carb. 2
3	-6.667	1.122	0.000	-6.667	1.122	-0.450	0.70	2.24	.14E-04		Cath.carb. 3
4	-5.965	1.122	0.000	-5.965	1.122	-0.450	0.70	2.24	.14E-04		Cath.carb. 4
5	-5.263	1.122	0.000	-5.263	1.122	-0.450	0.70	2.24	.14E-04		Cath.carb. 5
6	-4.561	1.122	0.000	-4.561	1.122	-0.450	0.70	2.24	.14E-04		Cath.carb. 6
7	-3.860	1.122	0.000	-3.860	1.122	-0.450	0.70	2.24	.14E-04		Cath.carb. 7
8	-3.158	1.122	0.000	-3.158	1.122	-0.450	0.70	2.24	.14E-04		Cath.carb. 8
9	-2.456	1.122	0.000	-2.456	1.122	-0.450	0.70	2.24	.14E-04		Cath.carb. 9
10	-1.754	1.122	0.000	-1.754	1.122	-0.450	0.70	2.24	.14E-04		Cath.carb.10
11	-1.053	1.122	0.000	-1.053	1.122	-0.450	0.70	2.24	.14E-04		Cath.carb.11
12	-0.351	1.122	0.000	-0.351	1.122	-0.450	0.70	2.24	.14E-04		Cath.carb.12
13	0.351	1.122	0.000	0.351	1.122	-0.450	0.70	2.24	.14E-04		Cath.carb.13
14	1.053	1.122	0.000	1.053	1.122	-0.450	0.70	2.24	.14E-04		Cath.carb.14
15	1.754	1.122	0.000	1.754	1.122	-0.450	0.70	2.24	.14E-04		Cath.carb.15
16	2.456	1.122	0.000	2.456	1.122	-0.450	0.70	2.24	.14E-04		Cath.carb.16
17	3.158	1.122	0.000	3.158	1.122	-0.450	0.70	2.24	.14E-04		Cath.carb.17
18	3.860	1.122	0.000	3.860	1.122	-0.450	0.70	2.24	.14E-04		Cath.carb.18
19	4.561	1.122	0.000	4.561	1.122	-0.450	0.70	2.24	.14E-04		Cath.carb.19
20	5.263	1.122	0.000	5.263	1.122	-0.450	0.70	2.24	.14E-04		Cath.carb.20
21	5.965	1.122	0.000	5.965	1.122	-0.450	0.70	2.24	.14E-04		Cath.carb.21
22	6.667	1.122	0.000	6.667	1.122	-0.450	0.70	2.24	.14E-04		Cath.carb.22
23	7.368	1.122	0.000	7.368	1.122	-0.450	0.70	2.24	.14E-04		Cath.carb.23
24	8.070	1.122	0.000	8.070	1.122	-0.450	0.70	2.24	.14E-04		Cath.carb.24
25	-8.070	-1.122	0.000	-8.070	-1.122	-0.450	0.70	2.24	.14E-04		Cath.carb.25
26	-7.368	-1.122	0.000	-7.368	-1.122	-0.450	0.70	2.24	.14E-04		Cath.carb.26

27	-6.667	-1.122	0.000	-6.667	-1.122	-0.450	0.70	2.24	.14E-04	Cath.carb.27
28	-5.965	-1.122	0.000	-5.965	-1.122	-0.450	0.70	2.24	.14E-04	Cath.carb.28
29	-5.263	-1.122	0.000	-5.263	-1.122	-0.450	0.70	2.24	.14E-04	Cath.carb.29
30	-4.561	-1.122	0.000	-4.561	-1.122	-0.450	0.70	2.24	.14E-04	Cath.carb.30
31	-3.860	-1.122	0.000	-3.860	-1.122	-0.450	0.70	2.24	.14E-04	Cath.carb.31
32	-3.158	-1.122	0.000	-3.158	-1.122	-0.450	0.70	2.24	.14E-04	Cath.carb.32
33	-2.456	-1.122	0.000	-2.456	-1.122	-0.450	0.70	2.24	.14E-04	Cath.carb.33
34	-1.754	-1.122	0.000	-1.754	-1.122	-0.450	0.70	2.24	.14E-04	Cath.carb.34
35	-1.053	-1.122	0.000	-1.053	-1.122	-0.450	0.70	2.24	.14E-04	Cath.carb.35
36	-0.351	-1.122	0.000	-0.351	-1.122	-0.450	0.70	2.24	.14E-04	Cath.carb.36
37	0.351	-1.122	0.000	0.351	-1.122	-0.450	0.70	2.24	.14E-04	Cath.carb.37
38	1.053	-1.122	0.000	1.053	-1.122	-0.450	0.70	2.24	.14E-04	Cath.carb.38
39	1.754	-1.122	0.000	1.754	-1.122	-0.450	0.70	2.24	.14E-04	Cath.carb.39
40	2.456	-1.122	0.000	2.456	-1.122	-0.450	0.70	2.24	.14E-04	Cath.carb.40
41	3.158	-1.122	0.000	3.158	-1.122	-0.450	0.70	2.24	.14E-04	Cath.carb.41
42	3.860	-1.122	0.000	3.860	-1.122	-0.450	0.70	2.24	.14E-04	Cath.carb.42
43	4.561	-1.122	0.000	4.561	-1.122	-0.450	0.70	2.24	.14E-04	Cath.carb.43
44	5.263	-1.122	0.000	5.263	-1.122	-0.450	0.70	2.24	.14E-04	Cath.carb.44
45	5.965	-1.122	0.000	5.965	-1.122	-0.450	0.70	2.24	.14E-04	Cath.carb.45
46	6.667	-1.122	0.000	6.667	-1.122	-0.450	0.70	2.24	.14E-04	Cath.carb.46
47	7.368	-1.122	0.000	7.368	-1.122	-0.450	0.70	2.24	.14E-04	Cath.carb.47
48	8.070	-1.122	0.000	8.070	-1.122	-0.450	0.70	2.24	.14E-04	Cath.carb.48
49	-8.070	1.122	-0.450	-8.070	0.200	-0.450	0.28	0.22	.11E-05 200	Cath.inbar 1
50	-7.368	1.122	-0.450	-7.368	0.200	-0.450	0.28	0.22	.11E-05 200	Cath.inbar 2
51	-6.667	1.122	-0.450	-6.667	0.200	-0.450	0.28	0.22	.11E-05 200	Cath.inbar 3
52	-5.965	1.122	-0.450	-5.965	0.200	-0.450	0.28	0.22	.11E-05 200	Cath.inbar 4
53	-5.263	1.122	-0.450	-5.263	0.200	-0.450	0.28	0.22	.11E-05 200	Cath.inbar 5
54	-4.561	1.122	-0.450	-4.561	0.200	-0.450	0.28	0.22	.11E-05 200	Cath.inbar 6
55	-3.860	1.122	-0.450	-3.860	0.200	-0.450	0.28	0.22	.11E-05 200	Cath.inbar 7
56	-3.158	1.122	-0.450	-3.158	0.200	-0.450	0.28	0.22	.11E-05 200	Cath.inbar 8
57	-2.456	1.122	-0.450	-2.456	0.200	-0.450	0.28	0.22	.11E-05 200	Cath.inbar 9
58	-1.754	1.122	-0.450	-1.754	0.200	-0.450	0.28	0.22	.11E-05 200	Cath.inbar10
59	-1.053	1.122	-0.450	-1.053	0.200	-0.450	0.28	0.22	.11E-05 200	Cath.inbar11
60	-0.351	1.122	-0.450	-0.351	0.200	-0.450	0.28	0.22	.11E-05 200	Cath.inbar12
61	0.351	1.122	-0.450	0.351	0.200	-0.450	0.28	0.22	.11E-05 200	Cath.inbar13
62	1.053	1.122	-0.450	1.053	0.200	-0.450	0.28	0.22	.11E-05 200	Cath.inbar14
63	1.754	1.122	-0.450	1.754	0.200	-0.450	0.28	0.22	.11E-05 200	Cath.inbar15
64	2.456	1.122	-0.450	2.456	0.200	-0.450	0.28	0.22	.11E-05 200	Cath.inbar16
65	3.158	1.122	-0.450	3.158	0.200	-0.450	0.28	0.22	.11E-05 200	Cath.inbar17
66	3.860	1.122	-0.450	3.860	0.200	-0.450	0.28	0.22	.11E-05 200	Cath.inbar18
67	4.561	1.122	-0.450	4.561	0.200	-0.450	0.28	0.22	.11E-05 200	Cath.inbar19
68	5.263	1.122	-0.450	5.263	0.200	-0.450	0.28	0.22	.11E-05 200	Cath.inbar20
69	5.965	1.122	-0.450	5.965	0.200	-0.450	0.28	0.22	.11E-05 200	Cath.inbar21
70	6.667	1.122	-0.450	6.667	0.200	-0.450	0.28	0.22	.11E-05 200	Cath.inbar22
71	7.368	1.122	-0.450	7.368	0.200	-0.450	0.28	0.22	.11E-05 200	Cath.inbar23
72	8.070	1.122	-0.450	8.070	0.200	-0.450	0.28	0.22	.11E-05 200	Cath.inbar24
73	-8.070	-1.122	-0.450	-8.070	-0.200	-0.450	0.28	0.22	.11E-05 200	Cath.inbar25
74	-7.368	-1.122	-0.450	-7.368	-0.200	-0.450	0.28	0.22	.11E-05 200	Cath.inbar26
75	-6.667	-1.122	-0.450	-6.667	-0.200	-0.450	0.28	0.22	.11E-05 200	Cath.inbar27
76	-5.965	-1.122	-0.450	-5.965	-0.200	-0.450	0.28	0.22	.11E-05 200	Cath.inbar28
77	-5.263	-1.122	-0.450	-5.263	-0.200	-0.450	0.28	0.22	.11E-05 200	Cath.inbar29
78	-4.561	-1.122	-0.450	-4.561	-0.200	-0.450	0.28	0.22	.11E-05 200	Cath.inbar30
79	-3.860	-1.122	-0.450	-3.860	-0.200	-0.450	0.28	0.22	.11E-05 200	Cath.inbar31
80	-3.158	-1.122	-0.450	-3.158	-0.200	-0.450	0.28	0.22	.11E-05 200	Cath.inbar32
81	-2.456	-1.122	-0.450	-2.456	-0.200	-0.450	0.28	0.22	.11E-05 200	Cath.inbar33
82	-1.754	-1.122	-0.450	-1.754	-0.200	-0.450	0.28	0.22	.11E-05 200	Cath.inbar34
83	-1.053	-1.122	-0.450	-1.053	-0.200	-0.450	0.28	0.22	.11E-05 200	Cath.inbar35
84	-0.351	-1.122	-0.450	-0.351	-0.200	-0.450	0.28	0.22	.11E-05 200	Cath.inbar36
85	0.351	-1.122	-0.450	0.351	-0.200	-0.450	0.28	0.22	.11E-05 200	Cath.inbar37
86	1.053	-1.122	-0.450	1.053	-0.200	-0.450	0.28	0.22	.11E-05 200	Cath.inbar38
87	1.754	-1.122	-0.450	1.754	-0.200	-0.450	0.28	0.22	.11E-05 200	Cath.inbar39
88	2.456	-1.122	-0.450	2.456	-0.200	-0.450	0.28	0.22	.11E-05 200	Cath.inbar40
89	3.158	-1.122	-0.450	3.158	-0.200	-0.450	0.28	0.22	.11E-05 200	Cath.inbar41
90	3.860	-1.122	-0.450	3.860	-0.200	-0.450	0.28	0.22	.11E-05 200	Cath.inbar42
91	4.561	-1.122	-0.450	4.561	-0.200	-0.450	0.28	0.22	.11E-05 200	Cath.inbar43
92	5.263	-1.122	-0.450	5.263	-0.200	-0.450	0.28	0.22	.11E-05 200	Cath.inbar44
93	5.965	-1.122	-0.450	5.965	-0.200	-0.450	0.28	0.22	.11E-05 200	Cath.inbar45
94	6.667	-1.122	-0.450	6.667	-0.200	-0.450	0.28	0.22	.11E-05 200	Cath.inbar46
95	7.368	-1.122	-0.450	7.368	-0.200	-0.450	0.28	0.22	.11E-05 200	Cath.inbar47
96	8.070	-1.122	-0.450	8.070	-0.200	-0.450	0.28	0.22	.11E-05 200	Cath.inbar48

1065	-7.980	8.900	0.234	-7.980	8.900	0.183	0.84	1.95	.43E-02	Electro	1
1066	-7.140	8.900	0.237	-7.140	8.900	0.187	0.84	1.95	.43E-02	Electro	2
1067	-6.300	8.900	0.239	-6.300	8.900	0.192	0.84	1.95	.43E-02	Electro	3
1068	-5.460	8.900	0.242	-5.460	8.900	0.197	0.84	1.95	.43E-02	Electro	4
1069	-4.620	8.900	0.244	-4.620	8.900	0.200	0.84	1.95	.43E-02	Electro	5
1070	-3.780	8.900	0.245	-3.780	8.900	0.201	0.84	1.95	.43E-02	Electro	6
1071	-2.940	8.900	0.245	-2.940	8.900	0.202	0.84	1.95	.43E-02	Electro	7
1072	-2.100	8.900	0.246	-2.100	8.900	0.202	0.84	1.95	.43E-02	Electro	8
1073	-1.260	8.900	0.246	-1.260	8.900	0.202	0.84	1.95	.43E-02	Electro	9
1074	-0.420	8.900	0.247	-0.420	8.900	0.202	0.84	1.95	.43E-02	Electro	10
1075	0.420	8.900	0.248	0.420	8.900	0.202	0.84	1.95	.43E-02	Electro	11
1076	1.260	8.900	0.250	1.260	8.900	0.204	0.84	1.95	.43E-02	Electro	12
1077	2.100	8.900	0.249	2.100	8.900	0.204	0.84	1.95	.43E-02	Electro	13
1078	2.940	8.900	0.249	2.940	8.900	0.203	0.84	1.95	.43E-02	Electro	14
1079	3.780	8.900	0.249	3.780	8.900	0.203	0.84	1.95	.43E-02	Electro	15
1080	4.620	8.900	0.248	4.620	8.900	0.202	0.84	1.95	.43E-02	Electro	16
1081	5.460	8.900	0.247	5.460	8.900	0.201	0.84	1.95	.43E-02	Electro	17
1082	6.300	8.900	0.247	6.300	8.900	0.201	0.84	1.95	.43E-02	Electro	18
1083	7.140	8.900	0.247	7.140	8.900	0.202	0.84	1.95	.43E-02	Electro	19
1084	7.980	8.900	0.245	7.980	8.900	0.200	0.84	1.95	.43E-02	Electro	20
1085	-7.980	6.800	0.238	-7.980	6.800	0.191	0.84	1.95	.43E-02	Electro	21
1086	-7.140	6.800	0.242	-7.140	6.800	0.196	0.84	1.95	.43E-02	Electro	22
1087	-6.300	6.800	0.249	-6.300	6.800	0.203	0.84	1.95	.43E-02	Electro	23
1088	-5.460	6.800	0.253	-5.460	6.800	0.209	0.84	1.95	.43E-02	Electro	24
1089	-4.620	6.800	0.253	-4.620	6.800	0.209	0.84	1.95	.43E-02	Electro	25
1090	-3.780	6.800	0.252	-3.780	6.800	0.208	0.84	1.95	.43E-02	Electro	26
1091	-2.940	6.800	0.252	-2.940	6.800	0.208	0.84	1.95	.43E-02	Electro	27
1092	-2.100	6.800	0.251	-2.100	6.800	0.207	0.84	1.95	.43E-02	Electro	28
1093	-1.260	6.800	0.248	-1.260	6.800	0.205	0.84	1.95	.43E-02	Electro	29
1094	-0.420	6.800	0.248	-0.420	6.800	0.205	0.84	1.95	.43E-02	Electro	30
1095	0.420	6.800	0.247	0.420	6.800	0.205	0.84	1.95	.43E-02	Electro	31
1096	1.260	6.800	0.247	1.260	6.800	0.204	0.84	1.95	.43E-02	Electro	32
1097	2.100	6.800	0.247	2.100	6.800	0.204	0.84	1.95	.43E-02	Electro	33
1098	2.940	6.800	0.247	2.940	6.800	0.203	0.84	1.95	.43E-02	Electro	34
1099	3.780	6.800	0.246	3.780	6.800	0.201	0.84	1.95	.43E-02	Electro	35
1100	4.620	6.800	0.244	4.620	6.800	0.199	0.84	1.95	.43E-02	Electro	36
1101	5.460	6.800	0.243	5.460	6.800	0.198	0.84	1.95	.43E-02	Electro	37
1102	6.300	6.800	0.240	6.300	6.800	0.194	0.84	1.95	.43E-02	Electro	38
1103	7.140	6.800	0.236	7.140	6.800	0.190	0.84	1.95	.43E-02	Electro	39
1104	7.980	6.800	0.233	7.980	6.800	0.188	0.84	1.95	.43E-02	Electro	40

N | X1 | Y1 | Z1 | X2 | Y2 | Z2 | Thc1|Thc2| Rho |TCo|Description |

File 'BARSOUT'

The numbering of bars in the 'BARSOUT' file is exactly the same as in the 'BARSIN'. This file is created at the last time step of the program execution and gives the current, voltage and temperature distributions. At the end of file the upstream, downstream current balance is given for electrical design tests. Note, the user can run the program just for, say, 3-5 time steps in total (prescribed in DATA), and the electrical design info will be available.

New500

N	Current A	Deviat. A	Voltage V	Resist.Om	Length m	Sect.m*m	T Co	Description
1	0.1017E+05	0.2434E+03	0.3923E-01	.3856E-05	0.4500	1.5754	700	Cath.carb. 1
2	0.1029E+05	0.1238E+03	0.3969E-01	.3856E-05	0.4500	1.5754	700	Cath.carb. 2
3	0.1026E+05	0.1601E+03	0.3955E-01	.3856E-05	0.4500	1.5754	700	Cath.carb. 3
4	0.1010E+05	0.3137E+03	0.3896E-01	.3856E-05	0.4500	1.5754	700	Cath.carb. 4
5	0.1020E+05	0.2179E+03	0.3933E-01	.3856E-05	0.4500	1.5754	700	Cath.carb. 5
6	0.1033E+05	0.8471E+02	0.3984E-01	.3856E-05	0.4500	1.5754	700	Cath.carb. 6
7	0.1030E+05	0.1198E+03	0.3971E-01	.3856E-05	0.4500	1.5754	700	Cath.carb. 7
8	0.1016E+05	0.2557E+03	0.3918E-01	.3856E-05	0.4500	1.5754	700	Cath.carb. 8
9	0.1017E+05	0.2484E+03	0.3921E-01	.3856E-05	0.4500	1.5754	700	Cath.carb. 9
10	0.1031E+05	0.1059E+03	0.3976E-01	.3856E-05	0.4500	1.5754	700	Cath.carb.10
11	0.1041E+05	0.5212E+01	0.4015E-01	.3856E-05	0.4500	1.5754	700	Cath.carb.11
12	0.1027E+05	0.1452E+03	0.3961E-01	.3856E-05	0.4500	1.5754	700	Cath.carb.12
13	0.1028E+05	0.1380E+03	0.3964E-01	.3856E-05	0.4500	1.5754	700	Cath.carb.13
14	0.1042E+05	-.3438E+00	0.4017E-01	.3856E-05	0.4500	1.5754	700	Cath.carb.14
15	0.1032E+05	0.1010E+03	0.3978E-01	.3856E-05	0.4500	1.5754	700	Cath.carb.15
16	0.1017E+05	0.2432E+03	0.3923E-01	.3856E-05	0.4500	1.5754	700	Cath.carb.16
17	0.1014E+05	0.2744E+03	0.3911E-01	.3856E-05	0.4500	1.5754	700	Cath.carb.17
18	0.1028E+05	0.1317E+03	0.3966E-01	.3856E-05	0.4500	1.5754	700	Cath.carb.18
19	0.1034E+05	0.7524E+02	0.3988E-01	.3856E-05	0.4500	1.5754	700	Cath.carb.19
20	0.1021E+05	0.2088E+03	0.3936E-01	.3856E-05	0.4500	1.5754	700	Cath.carb.20
21	0.1002E+05	0.3921E+03	0.3866E-01	.3856E-05	0.4500	1.5754	700	Cath.carb.21
22	0.1019E+05	0.2272E+03	0.3929E-01	.3856E-05	0.4500	1.5754	700	Cath.carb.22
23	0.1024E+05	0.1768E+03	0.3949E-01	.3856E-05	0.4500	1.5754	700	Cath.carb.23
24	0.1012E+05	0.3014E+03	0.3901E-01	.3856E-05	0.4500	1.5754	700	Cath.carb.24
25	0.1072E+05	-.3048E+03	0.4134E-01	.3856E-05	0.4500	1.5754	700	Cath.carb.25
26	0.1060E+05	-.1832E+03	0.4087E-01	.3856E-05	0.4500	1.5754	700	Cath.carb.26
27	0.1047E+05	-.5830E+02	0.4039E-01	.3856E-05	0.4500	1.5754	700	Cath.carb.27
28	0.1039E+05	0.2555E+02	0.4007E-01	.3856E-05	0.4500	1.5754	700	Cath.carb.28
29	0.1108E+05	-.6587E+03	0.4271E-01	.3856E-05	0.4500	1.5754	700	Cath.carb.29
30	0.1097E+05	-.5527E+03	0.4230E-01	.3856E-05	0.4500	1.5754	700	Cath.carb.30
31	0.1086E+05	-.4401E+03	0.4187E-01	.3856E-05	0.4500	1.5754	700	Cath.carb.31
32	0.1078E+05	-.3592E+03	0.4155E-01	.3856E-05	0.4500	1.5754	700	Cath.carb.32
33	0.1042E+05	-.3955E+01	0.4018E-01	.3856E-05	0.4500	1.5754	700	Cath.carb.33
34	0.1037E+05	0.4632E+02	0.3999E-01	.3856E-05	0.4500	1.5754	700	Cath.carb.34
35	0.1028E+05	0.1355E+03	0.3965E-01	.3856E-05	0.4500	1.5754	700	Cath.carb.35
36	0.1021E+05	0.2070E+03	0.3937E-01	.3856E-05	0.4500	1.5754	700	Cath.carb.36
37	0.1040E+05	0.2109E+02	0.4009E-01	.3856E-05	0.4500	1.5754	700	Cath.carb.37
38	0.1041E+05	0.7279E+01	0.4014E-01	.3856E-05	0.4500	1.5754	700	Cath.carb.38
39	0.1032E+05	0.1007E+03	0.3978E-01	.3856E-05	0.4500	1.5754	700	Cath.carb.39
40	0.1024E+05	0.1788E+03	0.3948E-01	.3856E-05	0.4500	1.5754	700	Cath.carb.40
41	0.1081E+05	-.3934E+03	0.4169E-01	.3856E-05	0.4500	1.5754	700	Cath.carb.41
42	0.1077E+05	-.3531E+03	0.4153E-01	.3856E-05	0.4500	1.5754	700	Cath.carb.42
43	0.1062E+05	-.2050E+03	0.4096E-01	.3856E-05	0.4500	1.5754	700	Cath.carb.43
44	0.1051E+05	-.9625E+02	0.4054E-01	.3856E-05	0.4500	1.5754	700	Cath.carb.44
45	0.1081E+05	-.3971E+03	0.4170E-01	.3856E-05	0.4500	1.5754	700	Cath.carb.45
46	0.1083E+05	-.4138E+03	0.4176E-01	.3856E-05	0.4500	1.5754	700	Cath.carb.46
47	0.1075E+05	-.3289E+03	0.4144E-01	.3856E-05	0.4500	1.5754	700	Cath.carb.47
48	0.1068E+05	-.2672E+03	0.4120E-01	.3856E-05	0.4500	1.5754	700	Cath.carb.48
1065	0.1126E+05	0.1243E+04	0.1510E+01	.1341E-03	0.0512	1.6380	963	Electrolyt 1
1066	0.1148E+05	0.1019E+04	0.1498E+01	.1305E-03	0.0498	1.6380	963	Electrolyt 2
1067	0.1188E+05	0.6166E+03	0.1481E+01	.1246E-03	0.0476	1.6380	963	Electrolyt 3
1068	0.1227E+05	0.2259E+03	0.1465E+01	.1194E-03	0.0456	1.6380	963	Electrolyt 4
1069	0.1254E+05	-.4485E+02	0.1457E+01	.1161E-03	0.0443	1.6380	963	Electrolyt 5
1070	0.1264E+05	-.1443E+03	0.1452E+01	.1148E-03	0.0438	1.6380	963	Electrolyt 6
1071	0.1269E+05	-.1939E+03	0.1449E+01	.1141E-03	0.0436	1.6380	963	Electrolyt 7
1072	0.1265E+05	-.1475E+03	0.1452E+01	.1148E-03	0.0438	1.6380	963	Electrolyt 8

1073	0.1247E+05	0.2993E+02	0.1463E+01	.1173E-03	0.0448	1.6380	963	Electro	9
1074	0.1233E+05	0.1733E+03	0.1467E+01	.1190E-03	0.0454	1.6380	963	Electro	10
1075	0.1225E+05	0.2544E+03	0.1472E+01	.1202E-03	0.0459	1.6380	963	Electro	11
1076	0.1234E+05	0.1586E+03	0.1471E+01	.1192E-03	0.0455	1.6380	963	Electro	12
1077	0.1226E+05	0.2397E+03	0.1471E+01	.1200E-03	0.0458	1.6380	963	Electro	13
1078	0.1223E+05	0.2673E+03	0.1471E+01	.1203E-03	0.0459	1.6380	963	Electro	14
1079	0.1221E+05	0.2908E+03	0.1473E+01	.1207E-03	0.0461	1.6380	963	Electro	15
1080	0.1217E+05	0.3302E+03	0.1474E+01	.1211E-03	0.0462	1.6380	963	Electro	16
1081	0.1214E+05	0.3589E+03	0.1473E+01	.1213E-03	0.0463	1.6380	963	Electro	17
1082	0.1224E+05	0.2561E+03	0.1468E+01	.1199E-03	0.0458	1.6380	963	Electro	18
1083	0.1238E+05	0.1227E+03	0.1464E+01	.1183E-03	0.0451	1.6380	963	Electro	19
1084	0.1243E+05	0.7111E+02	0.1464E+01	.1178E-03	0.0450	1.6380	963	Electro	20
1085	0.1232E+05	0.1781E+03	0.1495E+01	.1214E-03	0.0463	1.6380	963	Electro	21
1086	0.1244E+05	0.6439E+02	0.1499E+01	.1205E-03	0.0460	1.6380	963	Electro	22
1087	0.1262E+05	-.1225E+03	0.1492E+01	.1182E-03	0.0451	1.6380	963	Electro	23
1088	0.1284E+05	-.3411E+03	0.1485E+01	.1156E-03	0.0441	1.6380	963	Electro	24
1089	0.1287E+05	-.3658E+03	0.1485E+01	.1154E-03	0.0441	1.6380	963	Electro	25
1090	0.1281E+05	-.3105E+03	0.1486E+01	.1160E-03	0.0443	1.6380	963	Electro	26
1091	0.1286E+05	-.3585E+03	0.1482E+01	.1153E-03	0.0440	1.6380	963	Electro	27
1092	0.1296E+05	-.4632E+03	0.1478E+01	.1140E-03	0.0435	1.6380	963	Electro	28
1093	0.1307E+05	-.5679E+03	0.1474E+01	.1128E-03	0.0430	1.6380	963	Electro	29
1094	0.1313E+05	-.6267E+03	0.1470E+01	.1119E-03	0.0427	1.6380	963	Electro	30
1095	0.1322E+05	-.7240E+03	0.1464E+01	.1107E-03	0.0423	1.6380	963	Electro	31
1096	0.1322E+05	-.7244E+03	0.1465E+01	.1108E-03	0.0423	1.6380	963	Electro	32
1097	0.1301E+05	-.5073E+03	0.1471E+01	.1131E-03	0.0432	1.6380	963	Electro	33
1098	0.1287E+05	-.3659E+03	0.1476E+01	.1147E-03	0.0438	1.6380	963	Electro	34
1099	0.1274E+05	-.2445E+03	0.1482E+01	.1163E-03	0.0444	1.6380	963	Electro	35
1100	0.1261E+05	-.1050E+03	0.1488E+01	.1180E-03	0.0450	1.6380	963	Electro	36
1101	0.1247E+05	0.2537E+02	0.1491E+01	.1195E-03	0.0456	1.6380	963	Electro	37
1102	0.1226E+05	0.2410E+03	0.1478E+01	.1205E-03	0.0460	1.6380	963	Electro	38
1103	0.1231E+05	0.1889E+03	0.1476E+01	.1199E-03	0.0458	1.6380	963	Electro	39
1104	0.1249E+05	0.6181E+01	0.1462E+01	.1170E-03	0.0447	1.6380	963	Electro	40

N |Current A |Deviat. A |Voltage V |Resist.Om|Length m|Sect.m*m|T Co|Description |

4.324 = potential drop (ohmic+polarization)

170556.69 (A) = total cathodic upstream current (50.16%)
169443.31 (A) = total cathodic downstream current (49.84%)
171258.14 (A) = total anodic upstream current (50.37%)
168741.86 (A) = total anodic downstream current (49.63%)

File 'Results'

This file is a replica of the screen info showing the program performance during the run time. The initial outputs help detect possible input errors and the most important initial settings. Watch for outputs for the potential drop, number of ferromagnetic iterations, interface DH and velocities, which all indicate the program performance depending on the specific input data.

```
Reading MENU
Read MENU
Read DATA Cf
Read DATA C01
Read DATA ferr. mesh max.size
read mesh for on-demand dH output = F
LBOTTOM= T
      5 *          13 bottom position read
G-wave: KF1W=      0.00033 KF2W=      0.00148
                                           T=      0.000 (s)
liquid Al mass (t) & volume(m**3)=      35.8140      15.5713
*** DH ***
      -0.0050  -0.0033  -0.0017   0.0000   0.0017   0.0033   0.0050
*****
+++++++      4444444  33333  222222  11111  0000000  -----*
+++++++      4444444  33333  222222  11111  0000000  -----*
+++++++      4444444  33333  222222  11111  0000000  -----*
+++++++      4444444  33333  222222  11111  0000000  -----*
+++++++      4444444  33333  222222  11111  0000000  -----*
+++++++      4444444  33333  222222  11111  0000000  -----*
+++++++      4444444  33333  222222  11111  0000000  -----*
+++++++      4444444  33333  222222  11111  0000000  -----*
+++++++      4444444  33333  222222  11111  0000000  -----*
+++++++      4444444  33333  222222  11111  0000000  -----*
+++++++      4444444  33333  222222  11111  0000000  -----*
+++++++      4444444  33333  222222  11111  0000000  -----*
+++++++      4444444  33333  222222  11111  0000000  -----*
+++++++      4444444  33333  222222  11111  0000000  -----*
*****
LBDEM= F
      105.00000      105.00000      cut-out in-line interval
      105.00000      105.00000      cut-out return-line interval
500kA
      744 = NTC1
      1464 = NTC22=NTC2
      1512 = NTC3
      1560 = NTC4
After input from BUSNET:
Total number of bars generated = 2315
Total number of NONZERO bars left = 2302
Total number of NONEQUAL bars left = 2294
maxminDH2= 0.0000000000000000E+000 0.0000000000000000E+000
2414=total number of bars per cell created
NLSTEM, NT-3*NA-NAPT = 1814 1814
      1431 X1 points for potential
      1482 =MT total number of nodes
      4.252 = Total potential drop between cells (ohmic+polarization)
      4.419 = Total potential drop between cells (ohmic+polarization)
      4.398 = Total potential drop between cells (ohmic+polarization)
      4.402 = Total potential drop between cells (ohmic+polarization)
      4.402 = potential drop
average y+ ledge 0.223801828325303
average y- ledge 0.223801828325303
```


Restart using 'Magnetization.inp' as the initial approximation for the ferromagnetic parts magnetic fields

In order to use the restart option using 'Magnetization.inp' as the initial approximation the new additional lines in the DATA file are required at the end of the file. An example of the DATA file last lines is given below, with the new additional lines in red:

```
...
0.005      |Initial 'sloshing'wave perturbation C(1,0), max amplitude (m)
0.040      |Empirical bottom friction coefficient (nondimensional)
0.0000025  |Anode clamp average contact Resistance, Om
0.00000125 |Cathode flex joint average contact Resistance, Om
0.0        |Initial 'sloshing'wave perturbation C(0,1), max amplitude (m), 0.005
0.0005     |ferromagnetic convergence criteria (>=0.0001)
0.05       |ferromagnetic mesh element max.size (m)
30         |ferromagnetic convergence max iteration N; 0 - no iteration 'magnetization.inp'
=====|=====
```

Note, that all additional lines after the standard last line for the 'Empirical bottom friction' must be included to activate the Magnetization restart.

The new input permits to reset the number of iterations for the ferromagnetics to a new value, instead of the default value of 20. If the last line will be absent, it will run with 20.

The restart iteration feature is activated if the previously generated 'Magnetization.dat' file is renamed to 'Magnetization.inp' and it is included in the working directory. The iterations will start with the field and magnetization values stored in this file. The number of elements generated from the 'Steelplates' should be exactly the same, otherwise an error message will be output and the program stops.

If the parameter in the last line of DATA file for 'ferromagnetic convergence max iteration N' is set as 0, then the magnetization of the steel elements will be set as given in the file 'Magnetization.inp' and no iterations will be performed. This works exactly as in the previous versions, and the option should work in the same way as the default when the additional lines in DATA are absent.

However, if the iteration number is given, say, 10 or 30, then the iterations will run using the magnetization input as the initial values. Note that the output of the steel plate magnetization in the iterated solutions is created after each iteration, file BFE.PLT, which permits to follow the visual appearance of the steel magnetic properties in iterations.

It does not mean necessarily that the iterations will converge immediately. In a typical test it required 2 iterations to converge exactly to the same result as if running all iterations (in this case 14 iterations were needed). However, if the currents in the bus bar are not significantly different, the iterations will converge immediately. There is a safeguard to run at least 2 iterations due to the over-relaxation parameter used to start the iteration process in general case. Sometimes a reduced value of the 'ferromagnetic convergence criteria' is recommended to achieve a longer iteration process, say instead of the value 0.0005 a smaller value (e.g. 0.0004) can be entered. However there is a limitation that 'ferromagnetic convergence criteria' is ≥ 0.0001 .

The graphical presentation of the magnetic field in the liquid metal can be reconstructed from the file BS.PLT, to compare the vertical component B_z at the upstream line along x-coordinate between the cases 1 and 2:

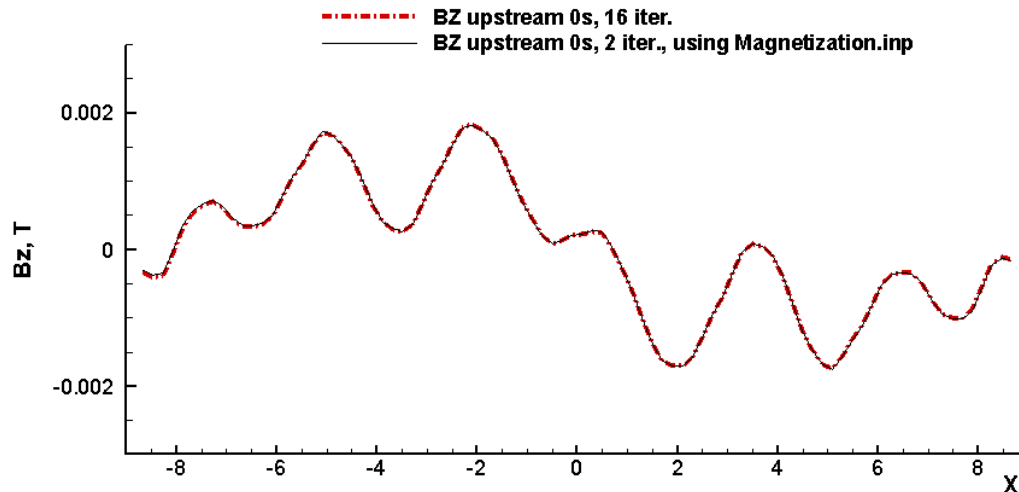


Figure. The comparison of the case 1 (full convergence in 16 iterations) and the restart case 2 (2 iterations).

Possible sources for incorrect performance of the restart option

- not all optional lines included in the DATA file, say, one of the following is missing:

```
0.0000025 |Anode clamp average contact Resistance, 0m
0.00000125 |Cathode flex joint average contact Resistance, 0m
0.0       |Initial 'sloshing'wave perturbation C(0,1), max amplitude (m)
0.0005   |ferromagnetic convergence criteria (>=0.0001)
0.05     |ferromagnetic mesh element max.size (m)
30       |ferromagnetic convergence max iteration N; 0 - no iteration 'magnetization.inp'
```

- the number of elements generated from the Steelplates is extremely large. This formally has a limit of 4 million, however the test example is using '103306 ferromagnetic elements created'. In principle the convergence criteria could be reduced further because the average norm is defined in the program as $DFE = DFE / 3 / NBE / HMAX$! FEH solution error
- in this case the 'ferromagnetic convergence criteria' can be reduced below 0.0005, say to 0.0004 or even less if the iterations are formally converging in two iterations. However there is a limitation that 'ferromagnetic convergence criteria' should be ≥ 0.0001 .

User defined magnetic field outputs

There are two new output files BOUT.PLT and BOUT_Xgraph.PLT giving the magnetic field on a user requested grid specified in the file MESH.B (.TXT or .DAT extensions are permitted). The file MESH.B, for example:

```
'NX,NY,NZ=' 80 30 1      ! mesh dimensions (number of nodes)
'Xmin,Xmax=' -6.9 6.9
'Ymin,Ymax=' -1.95 1.95
'Zmin,Zmax=' 0. 0.
```

specifies a 3d mesh on which to compute the magnetic field. By positioning the z-level at the liquid metal average height, say 0.20 m, the field output will be on this level of the unperturbed metal surface. BOUT.PLT gives the 3d field components and the magnitude at each node point, see the template Bout_DX.lpk for example and the Figure 27. Additional possibilities are demonstrated in the Figures 28

and 29 showing the detailed magnetic field at the level just below the anode bus. The file BOUT is created only for the first time step and contains the ASCII format data which can be used either with the Tecplot or Excel (after deleting the first 3 rows).

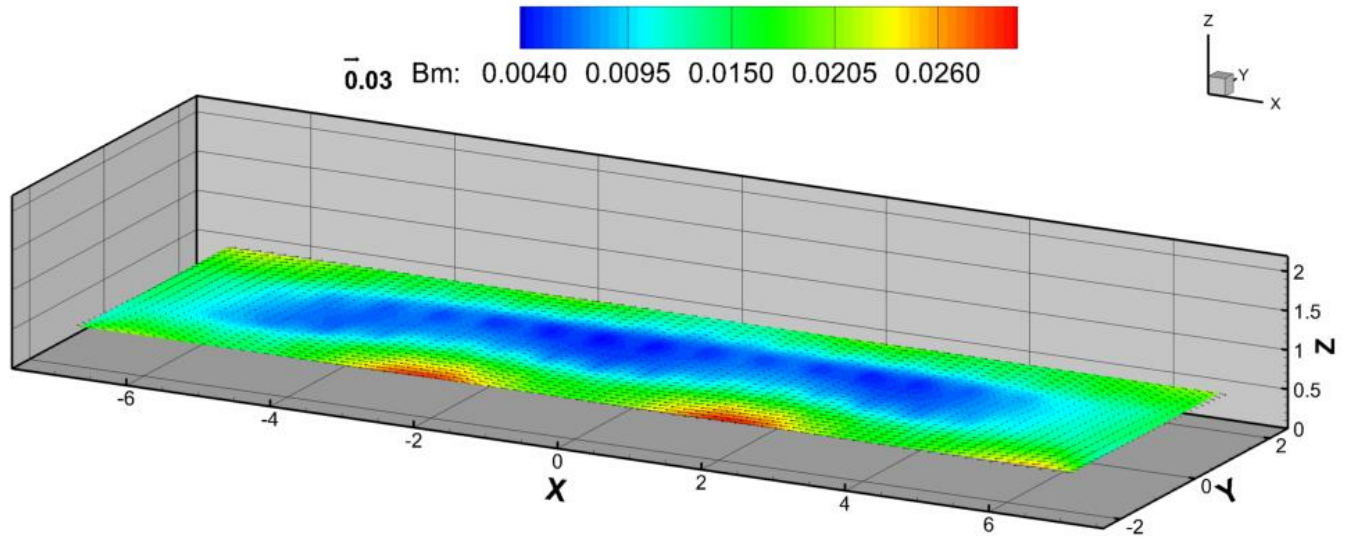


Figure 27. The magnetic field created from BOUT.PLT in one layer at the metal height.

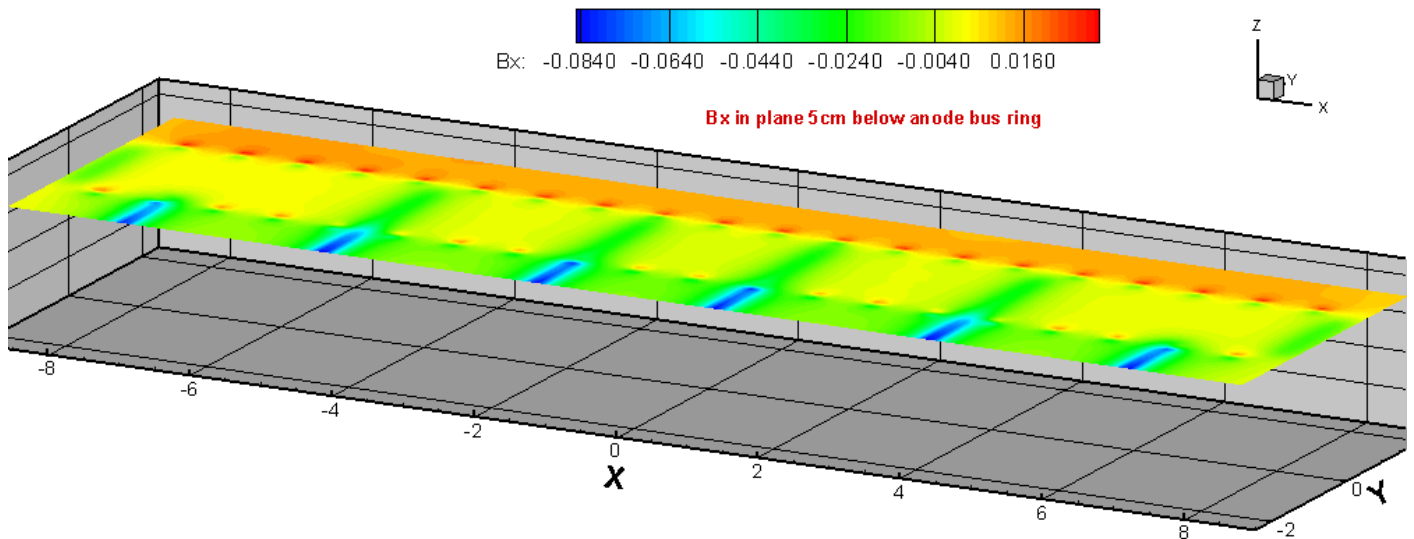


Figure 28. Magnetic field Bx as computed below anode bus ring: anode rod and riser presence is clearly visible.

The additional file BOUT_Xgraph.PLT is intended to present the magnetic field distribution along the length of the cell (x-coordinate) in the two end lines of the mesh created from MESHb. This is useful for instance in presenting the field variation along the long channels at both sides of the cell. The template Bout_xedges_DX.lpk is created for this purpose to use in the Tecplot, Figure 30.

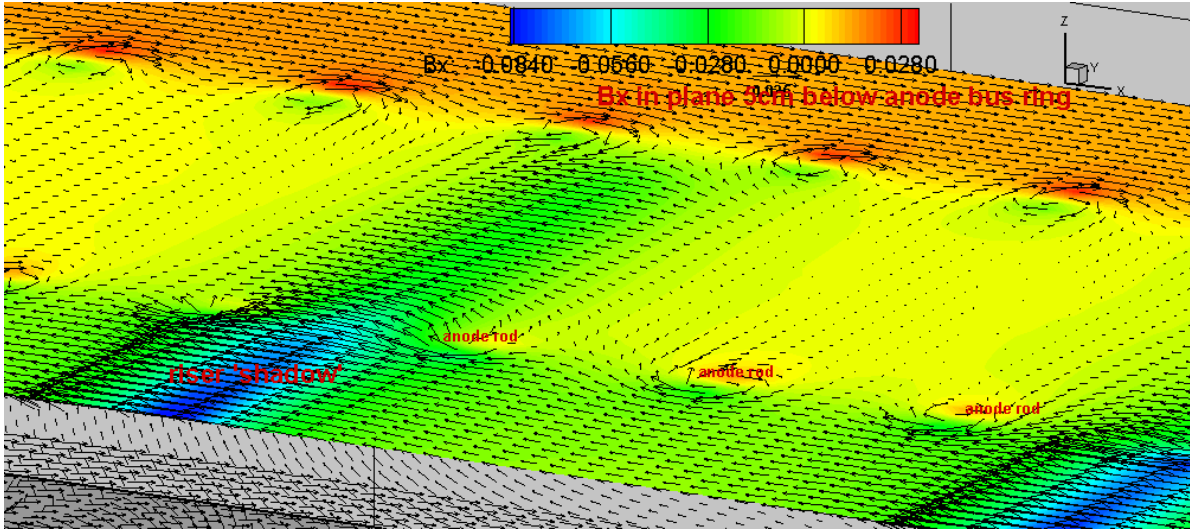


Figure 29. Magnetic field below anode bus: zoom-in view showing detail around individual anode rods.

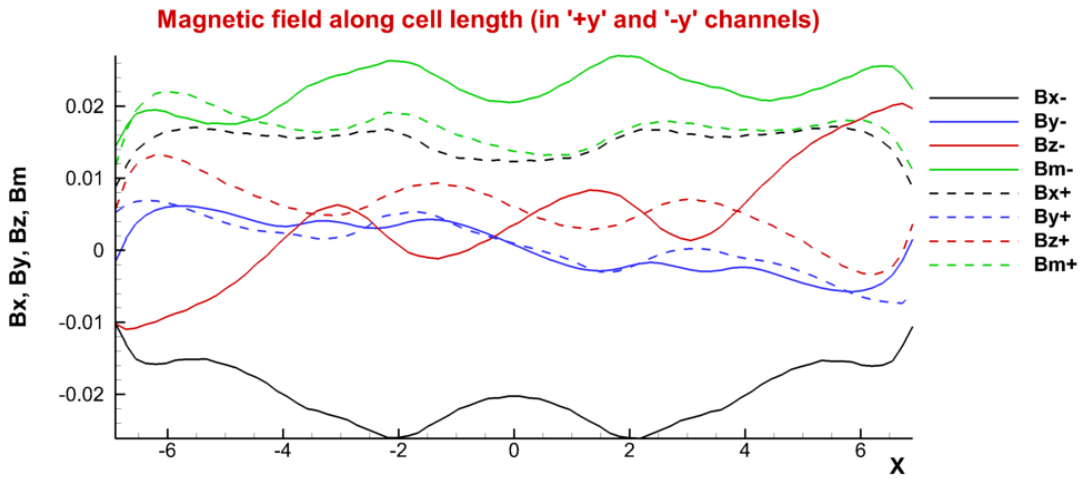


Figure 30. The magnetic field created from BOUT_Xgraph.PLT showing the distribution as line graphs along the channels at the metal height.

THE OUTPUTS OF THE MODEL INCLUDE THE FOLLOWING ITEMS:

1. The electric current distribution and the bus bar network presentation can be visualized by using the files FE.PLT(test cell only) and FF.PLT(complete set of all cells in the simulation). These must be loaded in the Tecplot after the supplied packaged layout FE.LPK for previous test runs have been opened. Then in the 'File menu' choose 'Load Data File'; from 'View' dialog choose 'Data Fit' to fit the actual geometry.

1a. Outputs FI.PLT and FFI.PLT permit additionally the option to show arrows for the direction of current in every element in a busbar (an arrow in the center of every element), Figure 31.

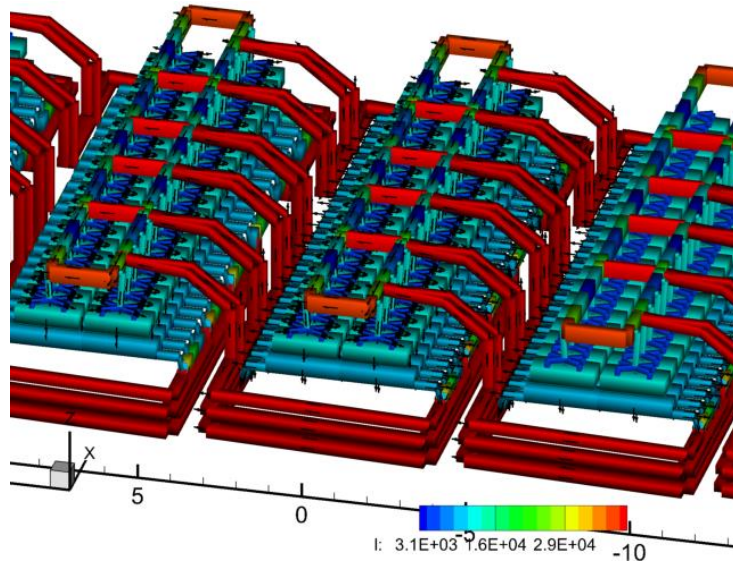


Figure 31. The current directions shown in the bus-bars by arrows.

1b. Output FB.PLT permits the option to show the bus-bar arrangement only without any cell elements, see the example in the Figure 32.

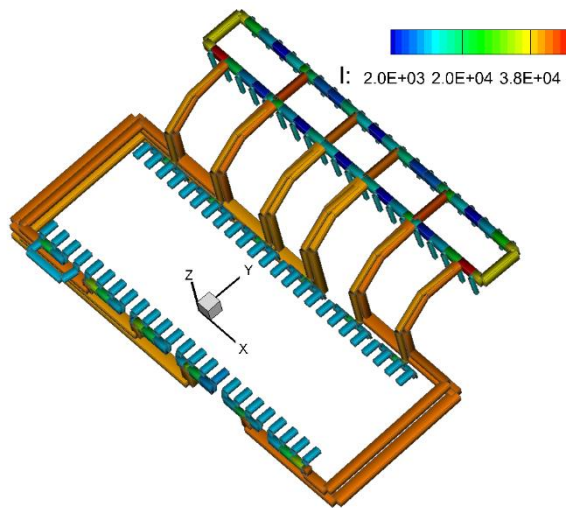


Figure 32. The current in the bus-bars only.

1c. Current densities and potentials in the bus network

A new Tecplot output file FD.PLT is created containing the new independent variable 'DI' for the current density, see the figure 33.

BARSOUT and BARSIN file formats have been adjusted: 3 decimal figures for the variables THICK1, THICK2, RHO, and 4 decimal figures for the area 'Sect. m*m'. 'Current A' has 7 decimal figures. The new column 'CurrD A/m^2' is added for the current density.

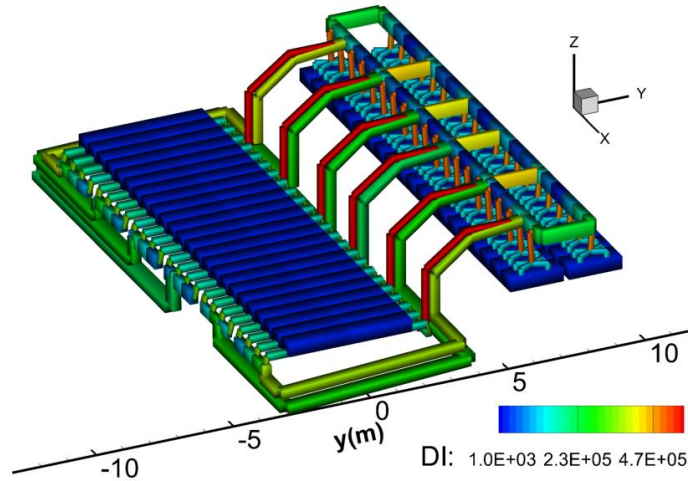


Figure 33. Current densities in the bus network available with the new output file FD.LT

The new output file 'JZb_dH1.dat' contains ASCII output for the x, y, current density at bottom, interface height in the table format without headers. The data are created after the 1st time step only.

There are two new outputs for the electric current distribution over the cathode collectors IC.PLT and the anodes IA.PLT for all time steps. The first zone stores data for the flat interface, the second – for initial stationary deformation, and the following sequence for all time steps. By choosing the zone in Tecplot, the respective current distribution can be viewed. The example of the results is shown in Figure 34.

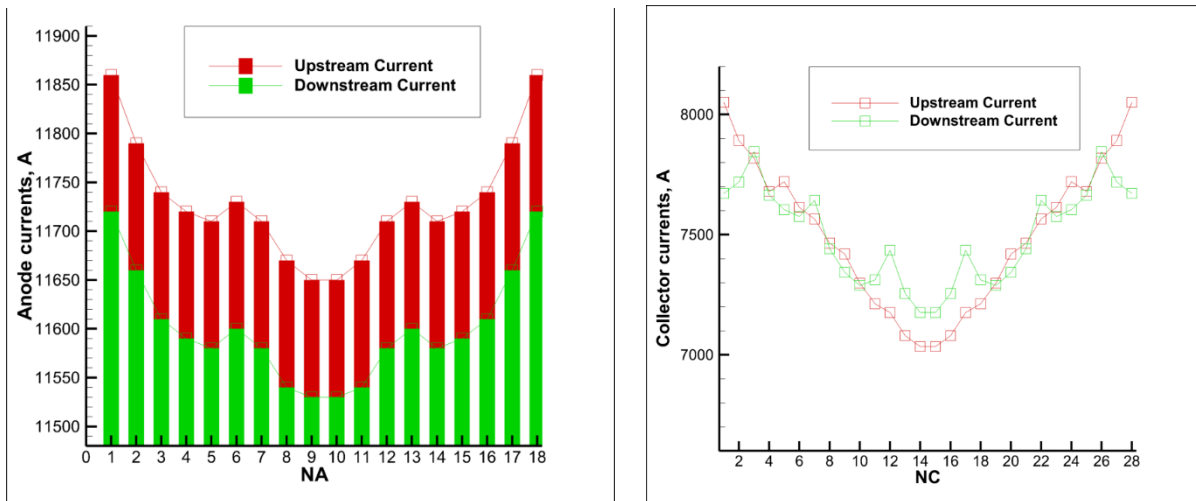


Figure 34. The electric current distribution over the anode rods and the cathode collectors provided in the files IA.PLT, IC.PLT

The files 'dHanodes.dat' and 'lanodes.dat' provide the interface height and anode currents under the centres of all anodes for all time steps of the simulation. The respective Fourier spectra generation for all of these is prohibitive in time cost, therefore this is available only for the selected locations as previously. However, the time development of the respective quantity is now available from the new output files. These can be opened in Tecplot, which will automatically generate the graph for the first independent variable (anode N1), then in the 'Zone style' box it is possible to choose any or multiple variables giving the time dependence of the oscillations for comparison.

The output files FE.PLT and FF.PLT now contain the second independent variable representing the absolute value of the potential in the network of the busbars denoted DI (for compatibility purposes with older templates). The potential is given for the bar exit point. This is useful when analysing the potential drop between arbitrary elements in the full network using the probing tool in the Tecplot window: by clicking on any desired network element the variable values are shown.

The second option is provided with the modification of the BARSOUT file containing now in the 4th column the value of the absolute value of the electric potential at the exit point of the respective bar. This is in addition to the 5th column data showing the voltage drop along the length of the same bar. Due to the parallel nature of multiple electrical connections this method is the most reliable in our opinion.

2. For the current distribution in the liquid bath and liquid aluminium use the results file JA.PLT.
3. The total magnetic field in the liquid bath and liquid aluminium at the level of liquid metal top is stored in BS.PLT. BI.PLT stores only the part of magnetic field created by the electric currents in the fluid itself. BB.PLT – stores the total magnetic field at the bottom of liquid metal.
4. The turbulent velocity fields, interpolated to the fine mesh used for the electric current calculation, in the bath and liquid aluminium: VE.PLT and VA.PLT
5. The turbulent viscosity distribution in the bath and liquid aluminium: VE.PLT and VA.PLT, if the turbulence model is active.
6. The time development of the waves at the interface between the electrolyte and aluminium calculated dynamically for the non linear electromagnetically induced fully coupled flow, including the respective modification of the magnetic and electric fields: DH.PLT . Animated movies can be created in Tecplot.
7. The graphs for the interface time dependence at fixed x,y positions (and the respective anode currents) can be created from the file HT.PLT . The growth of the waves indicate the instability of the cell depending on the design parameters.
8. The cell time dependent behavior in long term can be analyzed by the supplied Fourier spectral analysis for the interface (or current) at two critical locations, and the respective cell voltage noise analysis (the file OM.PLT). The file OG.PLT contains the normal gravity wave mode frequencies.
9. The anode burnout option can be activated, to estimate the anode bottom non uniform adjustment to the liquid interface static and time average change. The final shape of the anode bottom is represented in the file DA.PLT, while the intermediate profiles are available in 3-d representation in the file HB.PLT. The file HB.PLT contains also the visual representation of the bottom profile if 'BOTTOM' is available.
10. The motion and the magnetic field induced electric currents (important for large amperage cells) are stored in the file JI.PLT

11. BFE.PLT gives the magnetization and the magnetic field in the steel structure.
12. JQ.PLT gives the time averaged Joule heat in the liquid bath.